ERDC TR-01-17

Construction Engineering Research Laboratory

US Army Corps of Engineers®
Engineer Research and Development Center

Seismic Testing of a 1/20 Scale Model of Koyna Dam

James Wilcoski, Robert L. Hall, Enrique E. Matheu, James B. Gambill, and Mostafiz R. Chowdhury

November 2001

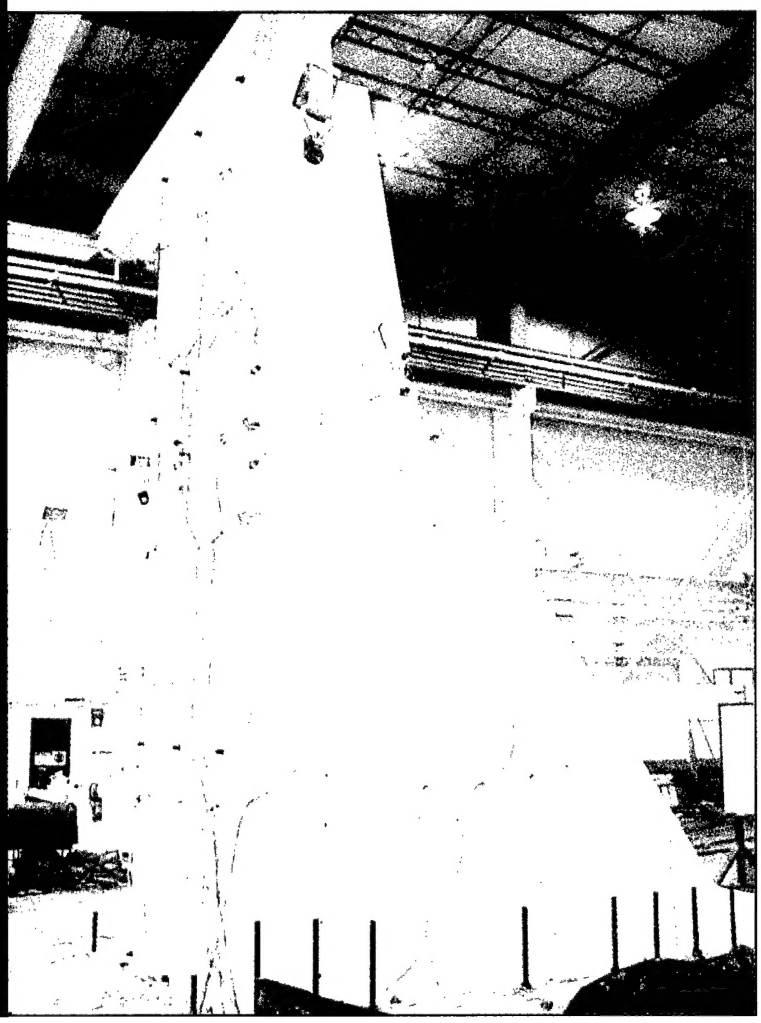

ERDC TR-01-17

Construction Engineering Research Laboratory

US Army Corps of Engineers®
Engineer Research and Development Center

Seismic Testing of a 1/20 Scale Model of Koyna Dam

James Wilcoski, Robert L. Hall, Enrique E. Matheu, James B. Gambill, and Mostafiz R. Chowdhury

November 2001

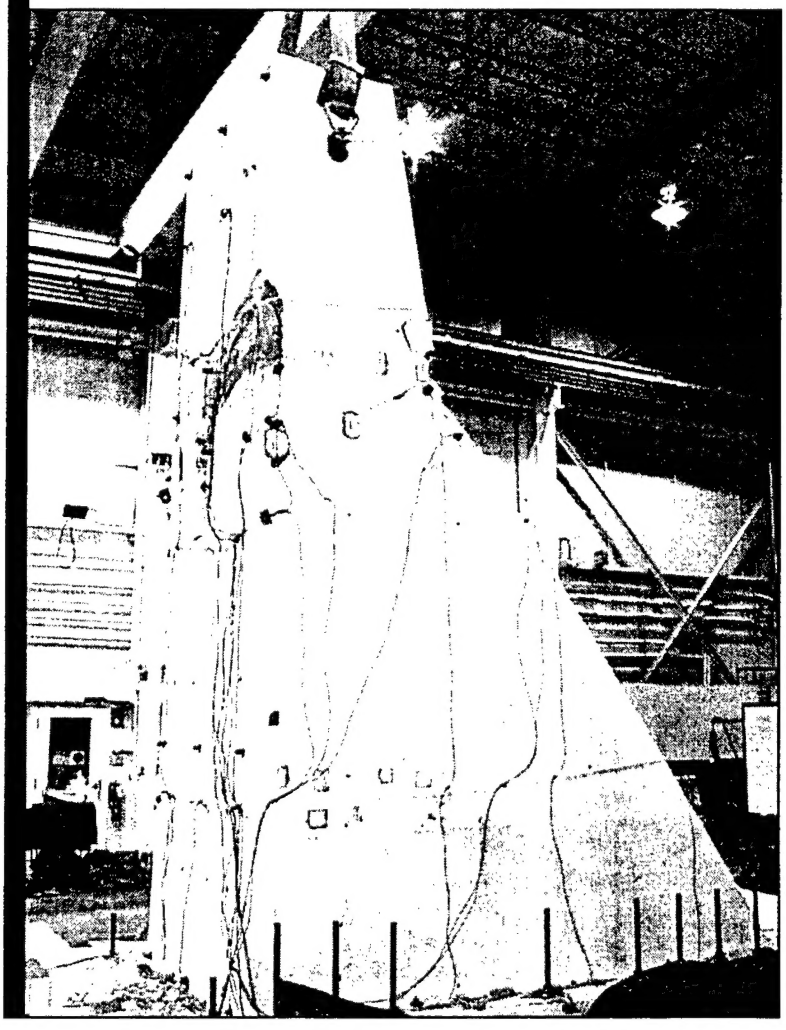

Foreword

This study was conducted for U.S. Army Corps of Engineers, Engineering Research and Development Center (ERDC), Construction Engineering Research Laboratory (CERL) and the Geotechnical and Structures Laboratory (GSL) in support of the Army Civil Works Earthquake Engineering Research Program. The work supports the GSL work units, "Validation of Dynamic Nonlinear Analysis Methods for Concrete Dams," work unit 33013 and "Time Domain Solutions for Non-Linear Problems of Concrete Dams," work unit 33011. The technical monitor was Bruce C. Riley, CECW-EW. Funding was provided by GSL under Military Interdepartmental Purchase Requests (MIPR) W81EWF92045594 and W81EWF92442674. Further funding was provided under direct-funded Civil Works Appropriation 96X3121, General Investigations, Program 387, Earthquake Engineering.

The authors express appreciation to Billy D. Neeley, CEERD-GM-C, who led the development of the dam mix design, guided the batching process, provided quality control during casting, guided surface treatment for proper curing, and tested cylinders and core samples. Julius Hufmeyer of Charter Landings Construction built the complex formwork used to cast the model. Jim Gledhill of Cimbar Performance Minerals coordinated the acquisition and delivery of the barite. James S. Acheson and Richard J. Plimpton of Prairie Group managed the batching process for Prairie Central. Mike Duce, Duce Construction, provided pumping services for the unique fluid mix. Finally, Kenny Warner of Farmers Ag Services supported the core sampling, demolition, and disposal of the model.

The work was performed by the Materials and Structures Branch (CF-M) of the Facilities Division (CF), Construction Engineering Research Laboratory (CERL). The GSL Principal Investigator was Robert L. Hall and the CERL Principal Investigator was James Wilcoski. The technical editor was Gordon L. Cohen, Information Technology Laboratory. Martin J. Savoie is Chief, CEERD-CF-M, and L. Michael Golish is Chief, CEERD-CF. The Technical Director for this work unit was Dr. Paul A. Howdyshell, CEERD-CV-ZT, and the Director of CERL is Dr. Alan W. Moore.

CERL is an element of the Engineer Research and Development Center (ERDC), U.S. Army Corps of Engineers. The Commander and Executive Director of ERDC is COL John W. Morris III, EN, and the Director is Dr. James R. Houston.

Contents

List of Figures and Tables

Figures

Tables

1 Introduction

Background

On 11 December 1967, the 103 m high Koyna mass concrete dam in India was seriously damaged by a magnitude 6.5 earthquake. The damage began with a crack at the change in geometry at the downstream slope, which subsequently spread through the entire cross-section. This event was unique because the Koyna Dam is the only concrete dam that has suffered significant damage due to ground shaking, and accelerometers at the site recorded the time histories of the entire event. The Koyna Dam failure is considered a classic problem for experimental studies and to validate numerical procedures for predicting the seismic response of concrete gravity dams.

The University of California at Berkeley previously conducted shake table tests of the Koyna Dam using a 1/150-scale model,[1] and the Bureau of Reclamation, U.S. Department of Interior, has conducted shake table tests using a 1/50-scale model.[2, 3] Scaling material properties to provide appropriate modeling of the damage and failure mechanisms in these types of small-scale models is always difficult and complex. Unfortunately, the small-scale model tests referenced above did not provide the amount of comprehensive data required for the systematic validation of nonlinear numerical procedures.

The Engineer Research and Development Center (ERDC) Geotechnical and Structures Laboratory (GSL) has conducted extensive linear and nonlinear analyses of concrete gravity dams as part of its mission for the U.S. Army Corps of Engineers. To further develop its analytical models, GSL tested a 1/20-scale

---

[1] Niwa, A., and R. W. Clough (1980). "Shaking Table Research on Concrete Dam Models", Technical Report UCB/EERC 80-05, Earthquake Engineering Research Center, University of California, Berkeley, CA.

[2] Harris, D. W., N. Snorteland, T. Dolen, and F. Travers (1999). "Shaking Table 2-D Models of a Concrete Gravity Dam for Computer Code Validation", Technical Report DSO-98-13, Dam Safety Office, Bureau of Reclamation, Denver, CO.

[3] Harris, D. W., N. Snorteland, T. Dolen, and F. Travers (2000). "Shaking Table 2-D Models of a Concrete Gravity Dam", *Earthquake Engineering and Structural Dynamics*, Vol. 29, pp 769-787.

model of the same Koyna dam. The model cross-section configuration, as defined by GSL, is shown in Figure 1. GSL also defined the scaling relationships that led to the definition of the model material properties. The ERDC Construction Engineering Research Laboratory (CERL) has a large shake table that is capable of the providing the high-frequency motions and large overturning forces needed to test this model. It was anticipated that two identical models would be tested. The first model would be tested using sinusoidal motion to ensure that model response is dominated by the first mode of vibration in the upstream/downstream direction. The second model would be tested with scaled motions that represent the support motions recorded in the 1967 earthquake.

Objectives

The objective of this experimental study was to cast the first 1/20-scale Koyna Dam model and test it using sinusoidal motions near the natural frequency of the model. The response of this model is documented in this report and recommendations are made for testing the second model.

Approach

The model width (cross-stream dimension) was defined based on a linear analysis of the model performed by GSL. GSL also defined the strength and density of the material needed to achieve the scaled material properties. With this information CERL designed and constructed the base beam and model formwork. CERL also worked with GSL materials experts to define the concrete procurement approach. The first Koyna Dam model was cast on 18 October 1999. Formwork was removed on 3 November 1999, instrumentation was installed, and the model was tested to failure on 17 November 1999.

Scope

The first Koyna Dam model was tested to failure with sinusoidal motions only. Although these motions differ greatly from real seismic motions, they should generate a response in the model similar to real seismic motions to the extent that dam behavior is dominated by its first mode of vibration response in the upstream/downstream direction. This sinusoidal test also can be assumed to produce the simplest response that can be readily compared with numerical analysis. The results of the sinusoidal wave test program are to be incorporated into tests of a second model using scaled records from the 1967 earthquake.

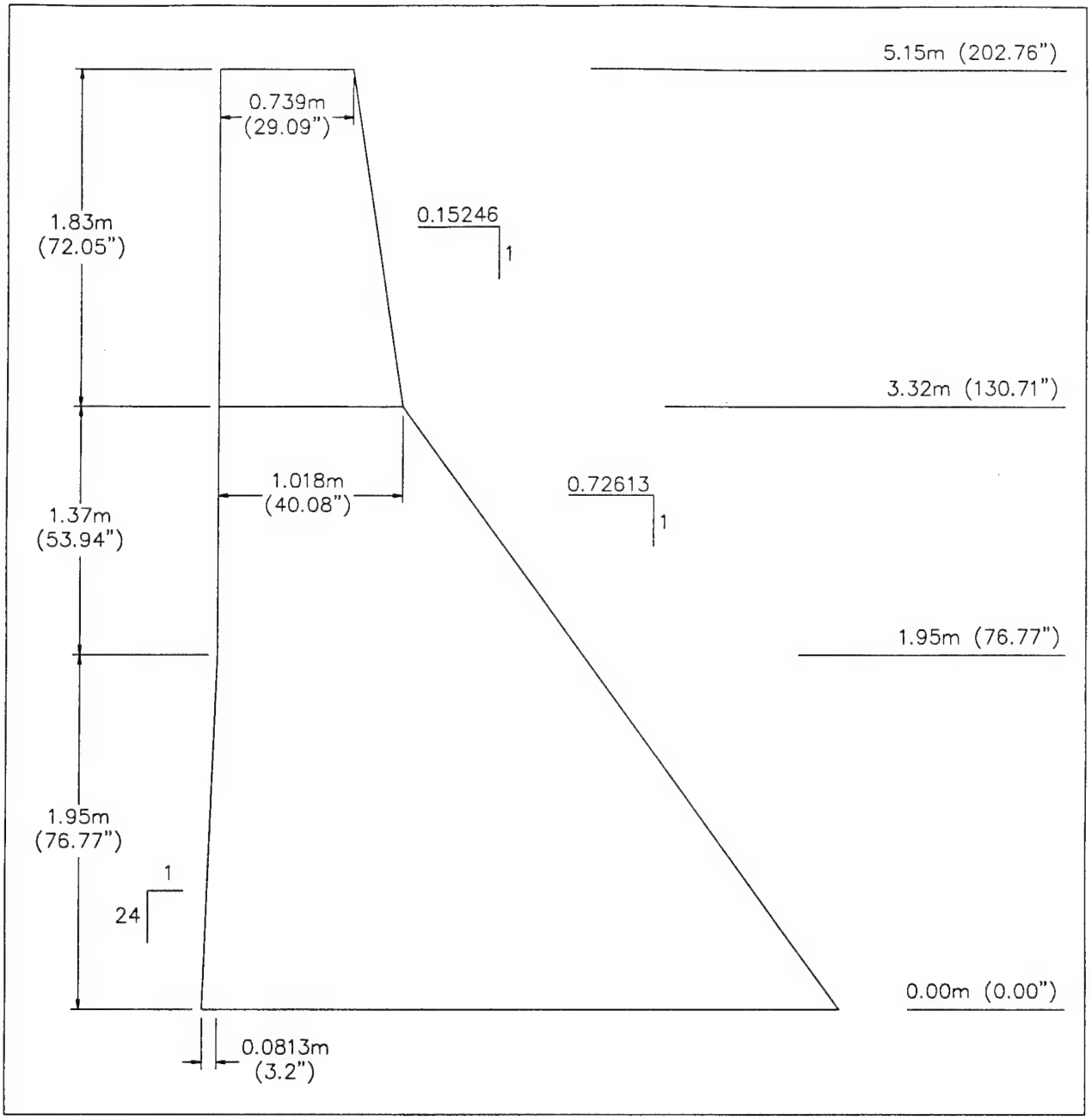

Figure 1. Design dimensions of the Koyna Dam model.

Mode of Technology Transfer

The information provided in this report will be used directly by the GSL and other researchers developing nonlinear numerical analysis procedures for analyzing concrete gravity dams. Portions of the information in this report also may be incorporated into future GSL technical reports, journal articles, or Corps of Engineers criteria documents.

Units of Weight and Measure

U.S. standard units of measure are used throughout this report. A table of conversion factors for the International System (SI) of units is provided below.

SI conversion factors		
1 in.	=	2.54 cm
1 ft	=	0.305 m
1 cu yd	=	0.764 m^3
1 lb mass	=	0.45359 kg
1 lb force	=	4.4482 N
1 pcf	=	16.018 kg/m^3
1 lb-in	=	0.11298 N-m
1 psi	=	6.89 kPa
1 ksi	=	6.8948 MPa

2 Model Configuration, Formwork Construction, and Casting

Model Material Properties

The material properties for the 1/20-scale dam model were defined by GSL researchers using material scaling relationships. The material properties of the actual Koyna dam and 1/20 scale model design values are shown in Table 1. Both the Koyna dam and the 1/20 scale model contain no reinforcing steel.

Table 1. Koyna Dam model material properties.

Material Property	Koyna Dam[4]	1/20-Scale Dam Model Design[5]	Model Avg 28-day Test Cylinder	Model Cores	
				Near Crack	Base
Unconfined Compressive Strength, f'_c	4000 psi 27.6 MPa	200 psi 1.38 MPa	253 psi 1.74 MPa	155 psi 1.07 Mpa	667 psi 4.60 Mpa
Modulus of Elasticity, E	4000 ksi 27.6 GPa	200 ksi 1.38 GPa		200 ksi 1.38 GPa	500 ksi 3.45 GPa
Ultimate Concrete Compressive Strain, ε_c	0.0025	0.0025			0.0060
Density	150 pcf 2403 kg/m^3	150 pcf 2403 kg/m^3	157 pcf 2515 kg/m^3	124.5 pcf 1994 kg/m^3	148.4 pcf 2377 kg/m^3

Determining the Model Width

The width of the model in the cross-stream direction was defined based on linear finite element analyses of a three-dimensional model of the Koyna Dam monolith. Table 2 shows the modes of vibration for the dam model at monolith widths

[4] Hall, J.F. (1988)., "The Dynamic and Earthquake Behavior of Concrete Dams," *Soil Dynamics and Earthquake Engineering*, 7(2).

[5] Provided by GSL researchers.

of 30 in. (0.76 m), 60 in. (1.52 m) and 90 in. (2.29 m), which represent the scaled width of 1, 2, and 3 monoliths, respectively. The tests conducted in this study are valid only for motions in the in-plane or upstream/downstream (i.e., transversal) direction. Actual dams are most vulnerable to motions in this direction, because the adjoining monoliths support each other in the cross-stream direction. Therefore all shake table motions were in the in-plane direction only. However, Table 2 shows that the 30 in. (0.76 m) wide model has an out-of-plane mode of vibration at a much smaller natural frequency (6.29 Hz) than in the in-plane direction. Small variations in symmetry, either in geometry or material properties, could result in exciting out-of-plane response due to in-plane support motions. This slender model may also be quite weak in the out-of-plane direction and could fail due to motions that would normally be prevented in a real dam due to the support of the adjoining monoliths. Therefore, one of the wider models was concluded to be more suitable for the analysis. The wider models both would be much stronger than the 30 in. (0.76 m) model. However, for the 90 in. (2.29 m) wide model, Table 2 shows that the 1st out-of-plane mode has a very similar frequency as the 1st in-plane mode (15.7 Hz versus 15.6 Hz). This unwanted response in the out-of-plane direction could easily be coupled with the desired in-plane motions to produce an unrealistic result. Therefore, the 90 in. (2.29 m) wide model is not a good choice for the desired tests. Figure 2 shows the frequency variation of the 1st out-of-plane and in-plane modes of vibration with respect to model width.

Table 2. Modes of vibration for variable monolith widths.

	Width =	30 in.	60 in.		90 in.
Mode No.	Mode	Freq (Hz)	Freq (Hz)	Mode	Freq (Hz)
1	1st out-of-plane bending	6.29	11.48	1st in-plane bending	15.62
2	1st in-plane bending	15.59	15.60	1st out-of-plane bending	15.74
3		25.19	39.24		35.60
4		34.87	41.35		41.75
5		41.65	41.70		48.75
6		54.61	54.62		54.62
7		58.90	70.19		65.88
8		65.44	80.89		80.91
9		80.85	84.75		94.52
10		96.30	114.58		106.34

The frequency in the out-of-plane direction is primarily a bending mode of vibration, so the frequency should increase proportionally to the width of the model. This is because the frequency is proportional to the square root of the stiffness over the mass; stiffness increases by the cube of the width, while the mass increases proportionally to the width. This relationship explains why the fre-

quency of the 60 in. (1.52 m) wide model (11.5 Hz) is almost twice that of the 30 in. (0.76 m) model (6.3 Hz). However, this 1st out-of-plane mode includes some shear response, particularly for the wider models. Shear response frequency remains constant with increasing width because both the stiffness and mass are proportional to width. Therefore, the frequency in the out-of-plane direction increases somewhat less than proportionally to the increase in width.

In terms of 30 in. (0.76 m) scaled monolith increments, the 60 in. (1.52 m) model width provides the best model width because unlike the 90 in. (2.29 m) model, it should not respond with unwanted out-of-plane motions when excited by in-plane support motions. Therefore, it was decided to use a 60 in. (1.52 m) model width for the Koyna dam failure tests (see Chapter 1, Figure 1). (Data reported in Chapter 4 demonstrate that, in fact, no significant out-of-plane motion did occur in the 60 in. model.

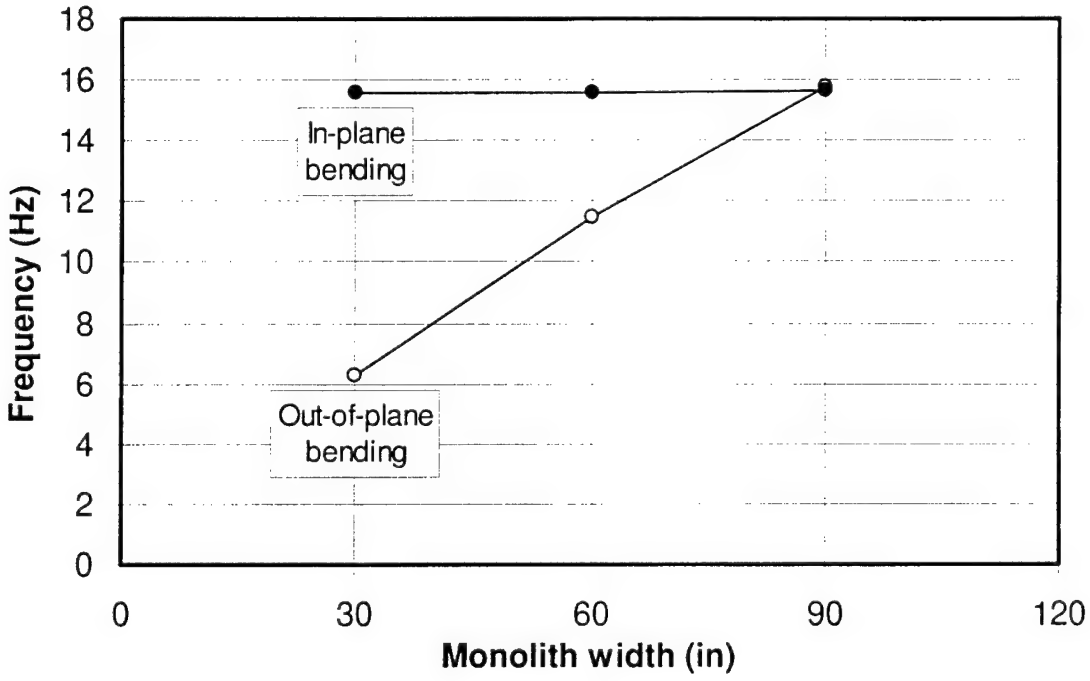

Figure 2. The frequency variation of the 1st out-of-plane and in-plane modes of vibration with respect to model width.

Design of Model Base Beam and Formwork

The dam model was anchored to the shake table by constructing a base beam that contained reinforcing steel which extended 24 in. (0.61 m) above the base beam and into the model. This reinforcing steel prevented any cracking or slip-

page between the base beam and model. Figure 3 shows a cross-section drawing of the base beam and dam model. The dam model dimensions in plan at its base are 138.2 in. (3.51 m) in the upstream/downstream direction by 60 in. (1.52 m) in the cross-stream direction. Appendix A provides details on the design of the base beam. Figure 4 shows the base beam before the longitudinal reinforcing steel was added and before the model formwork was attached.

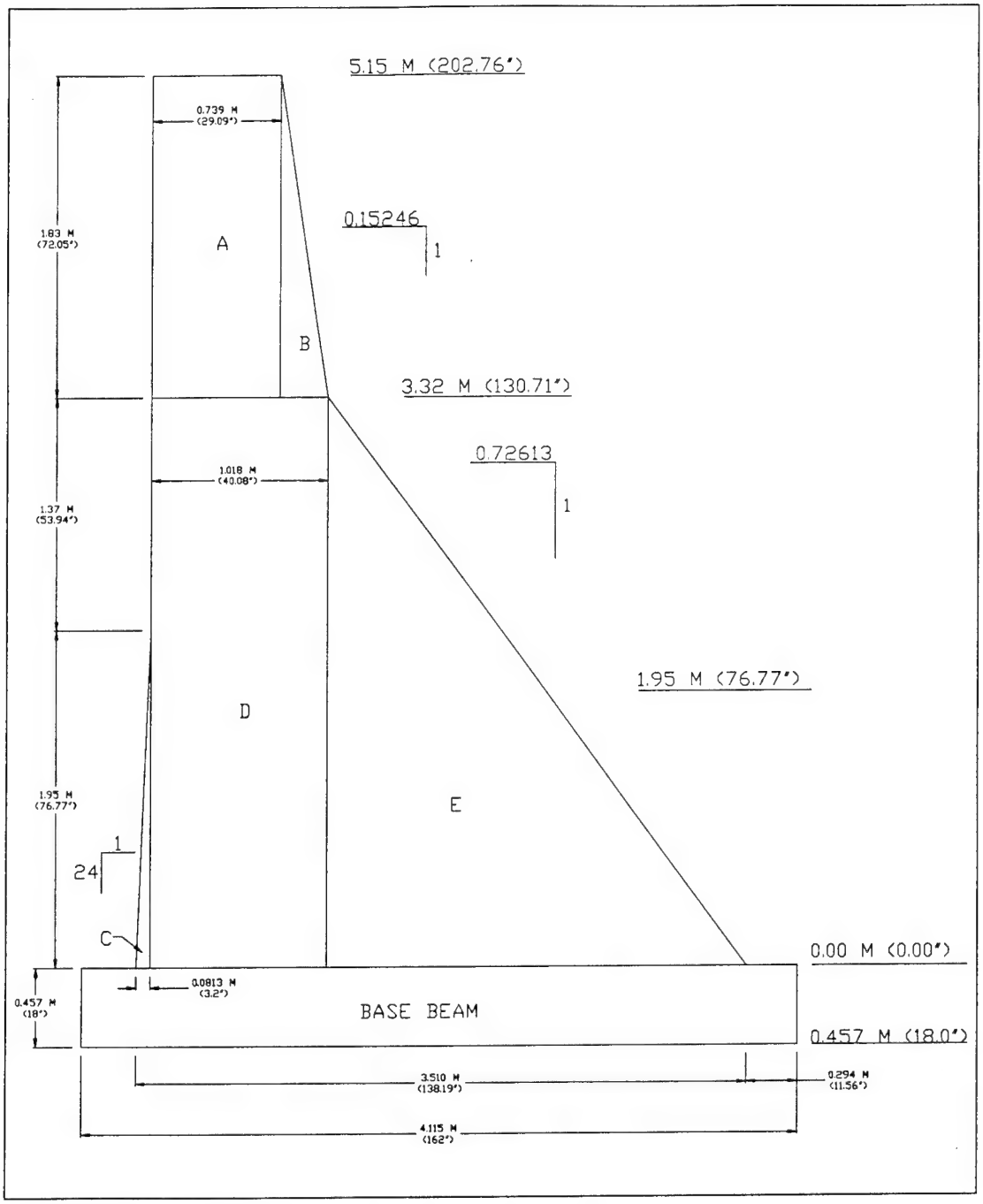

Figure 3. Cross-section of the base beam and dam model.

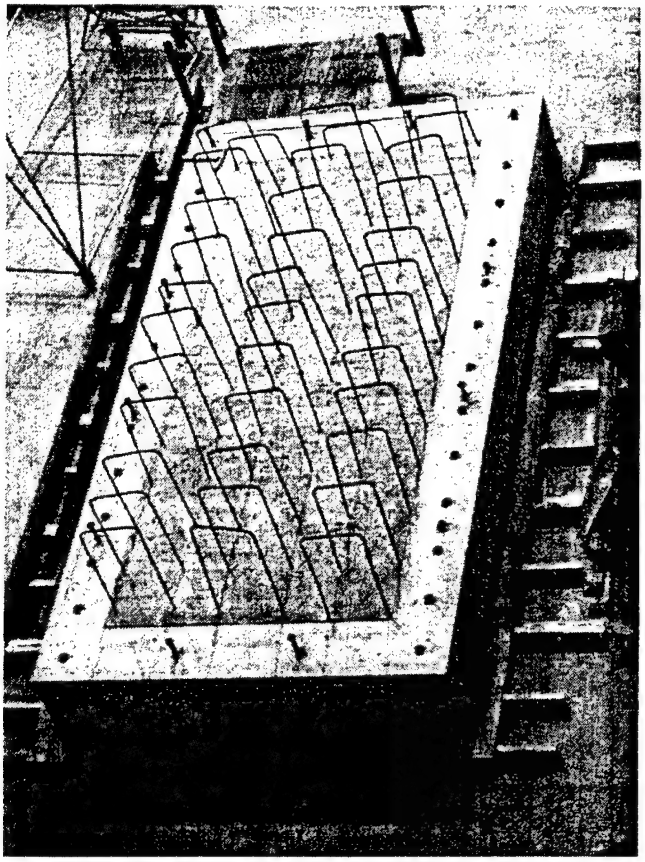

Figure 4. Base beam before attachment of longitudinal reinforcing steel and model formwork.

The formwork was designed to resist the full hydrostatic pressure of the model material. The concrete used in the dam model was very fluid and was not expected to set-up until 24 hours after casting. Also, because of the fluid consistency of the concrete, the formwork needed to be almost watertight. Figure 5 shows the downstream and front face of the dam formwork soon after casting began. Note the pump line at the left side of the photograph. Figure 6 shows the back face of the dam formwork. The top of the formwork was 12 in. (0.305 m) above the top of the model so the material could be cast several inches above the desired elevation, allowing for the significant predicted settlement after casting. Specifically, a 2 percent reduction in concrete volume due to settlement was predicted, which meant the elevation at the top of the forms would drop almost 10 in. (0.25 m), leaving 10 in. (0.25 m) of water at the top. Appendix A provides more details on formwork design and detailing. The formwork was almost entirely wood, but incorporated steel angle irons to resist the uplift forces from the sloped downstream face. Vertical steel angles on the front and back faces transferred loads from the downstream walers to horizontal angles at the base of the model. Horizontal angles went around the perimeter of the formwork and anchored it to the base beam during casting.

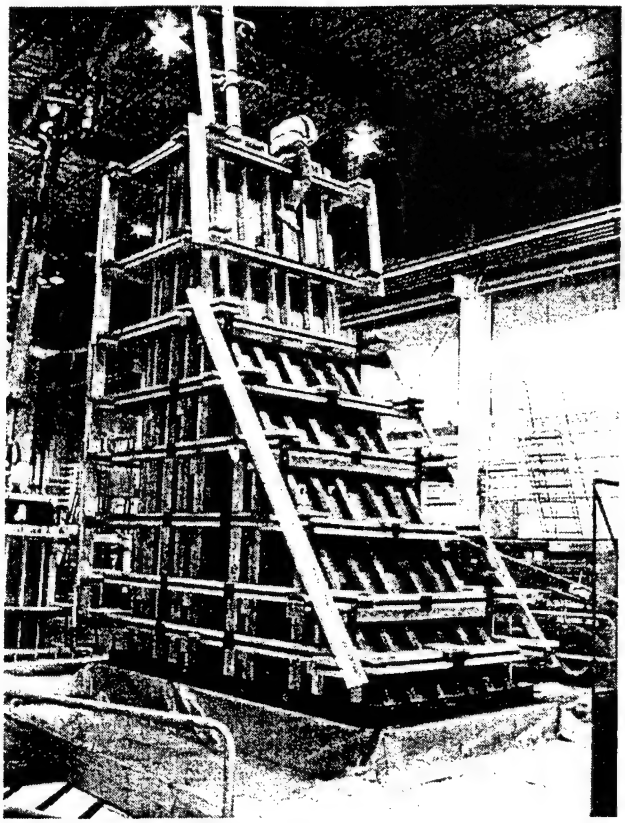

Figure 5. Downstream and front face of dam formwork.

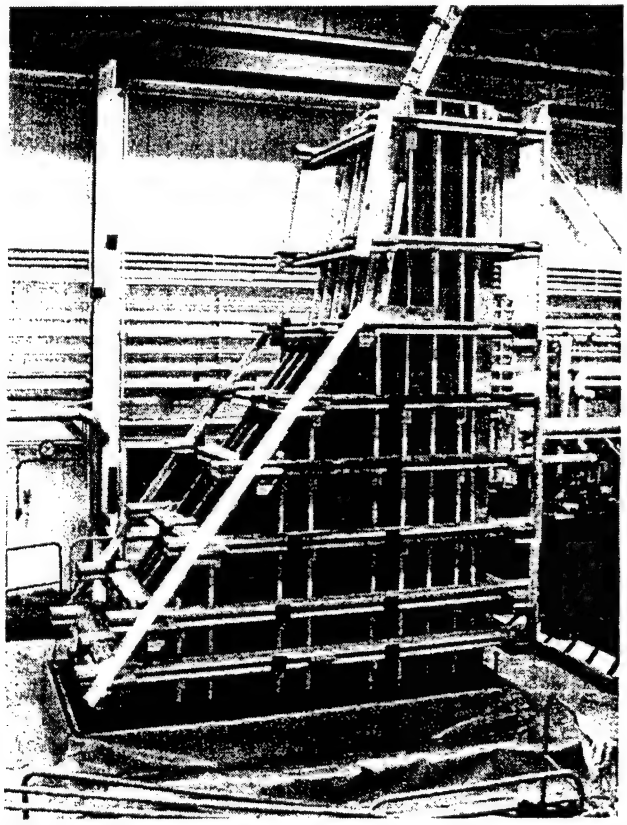

Figure 6. Back face of dam formwork.

Bolt inserts were cast into the model by attaching them to the inside face of the formwork. These inserts were installed for safety reasons during the test, and demolition purposes after the test. Electrical mechanical tubing (EMT) was installed in the upstream/downstream direction for demolition purposes. Both the inserts and EMT tubing were installed far enough away from the predicted failure surface so as not to interfere with the behavior of the model during seismic testing. Appendix A provides detailed information on the configuration and location of all hardware cast into the dam model.

Shake Table Protection Frame

The Koyna dam model was cast on CERL's shake table, the Triaxial Earthquake and Shock Simulator (TESS). Because the mix was predicted to be extremely fluid, minor form leakage was expected in spite of all precautions to make the formwork watertight. To avoid damaging TESS, a "moat" was constructed around the perimeter of the model base beam.

During seismic testing, the model was expected to crack across the entire cross-section, beginning at the change in slope on the downstream face. Appendix A explains how the overhead crane was attached to the section above the expected crack to stabilize it and prevent it from falling onto the shake table or actuators. However, a remote possibility remained that this entire 14,000 lb (6350 kg) portion of the model could break free from the insert connections and fall in the upstream direction 13 ft (4.0 m) down to the TESS actuators below. To minimize any damage arising from such an unlikely event, a TESS protection frame was constructed. Figure 7 shows the Koyna dam model during modal testing using a 50 lb (222 N) shaker at its top, with the TESS protection frame around its base. This protection frame was designed to also serve as a "moat" during casting. However, the protection frame construction could not be completed in time for casting, so a simple moat was temporarily constructed for casting. It consisted of 2 x 12s (nominal lumber measurements, inches) on edge about 4 ft (1.2 m) from the base beam and plywood on the TESS surface. The entire surface, from the top of the base beam to the edge of the moat, was covered with plastic sheets which can be seen at the bottom of Figure 5. Appendix A provides details on the design of the TESS protection frame.

Casting the Koyna Dam Model

To achieve the material properties shown in Table 1, materials researchers at GSL developed the mix design shown in Table B1 (Appendix B). The total vol-

ume of material required for a 60 in. (1.52 m) version of the model shown in Figure 1 is 18 cu yd (13.8 m^3). However, a considerably larger quantity — 28 cu yd (21.4 m^3) —was batched in order to provide for the large predicted settlement and cast a 4 cu yd (3.1 m^3) test block, test cylinders, and beams. Appendix B details how the unique materials were obtained and batched. Test cylinders were cast during batching of the model, and these were tested at 7, 14, and 28 days. Cylinder properties at 28 days are reported in Table 1 on page 15. Appendix B also provides details on the casting process, performance of formwork, and the achieved properties of the model material.

The material settled considerably during casting, as expected, and it appeared that the material at the base of the model may have been denser and stronger than near the top. To quantify these apparent differences, core samples were taken from near the model failure surface and near the base of the model. Material properties determined from testing these core samples are reported in Table 1 on page 15.

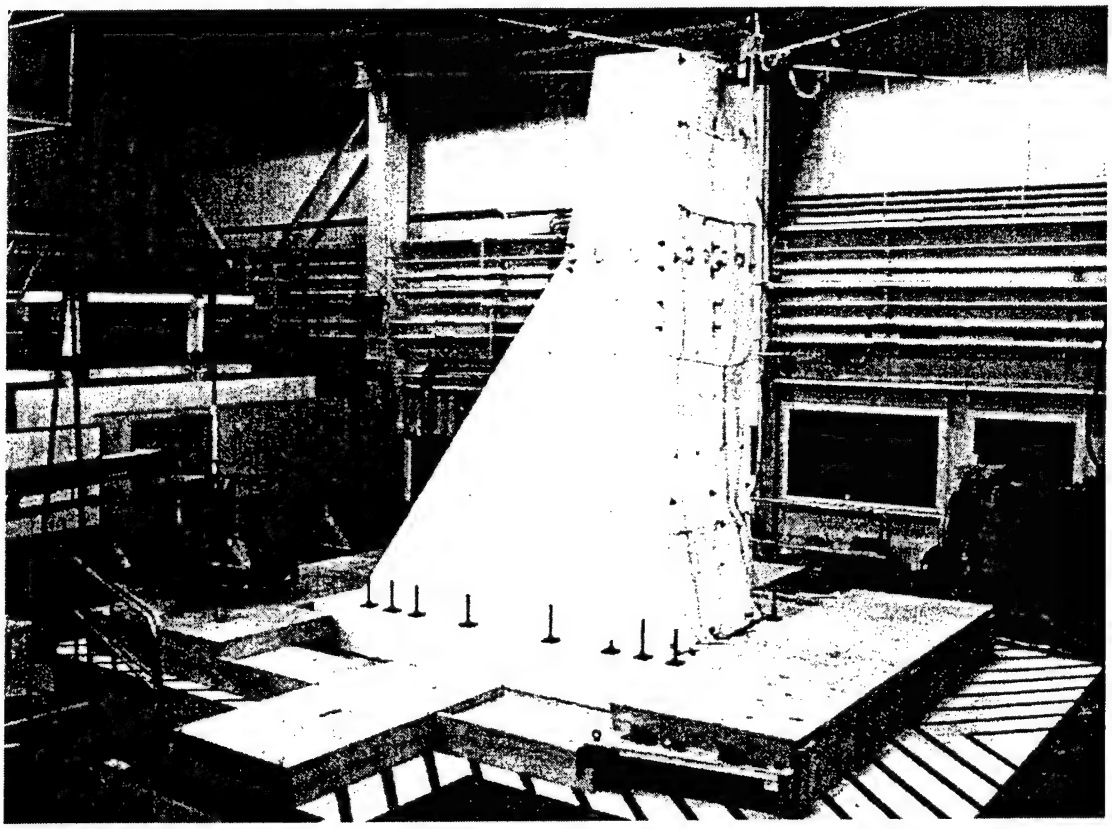

Figure 7. Koyna dam model during modal testing using a 50 lb (222 N) shaker at its top, showing the TESS protection frame around its base.

Model Curing, Formwork Removal, and Surface Preparation

The materials experts who developed the dam mix said that the model surface must not be allowed to dry at all, or large cracks would form. Therefore, special precautions were taken to ensure that the surface remained moist until a curing compound could be applied. Appendix B provides details of model curing, formwork removal, and surface preparation.

3 Test Plan and Instrumentation

Koyna Dam Model Test Plan

A test plan was developed and reviewed by representatives of GSL prior to testing. The purposes of the test plan were to evaluate the experimental procedure used to test the first Koyna Dam model and to assure a common understanding of the objectives and progression of all experiments. The test plan defined the test schedule, configuration and instrumentation, and detailed steps planned to complete all shake table testing. The test configuration and instrumentation is summarized in the next section, and the test dates are reported in Chapter 4. The detailed test plan followed in this program is presented in Appendix C.

Koyna Dam Model Instrumentation

GSL researchers specified instrumentation types and locations. These were selected specifically to ensure that recorded data could be compared directly with numerical model results. Instrumentation included accelerometers, strain gages, and linear variable differential transducers (LVDTs) all installed on the model surface. Strain gages and LVDTs were installed near the expected crack location. The strain gages were intended to measure the linear strains before cracking began, and the LVDTs were placed in a such a way as to measure the relative displacement between sensor anchors after cracking. Additional accelerometers were installed on the model base beam and others were located inside the TESS shake table. Table 3 identifies the sensor number, location, direction of measurement, full-scale range and resolution of each accelerometer installed on the model. Table 4 provides the sensor number, location, direction of measurement, full-scale range, and resolution of each strain gage. Table 5 provides sensor number, location, direction of measurement, full-scale range, and resolution of each LVDT.

Figure 8 shows the location of each accelerometer, strain gage, and LVDT mounted on the upstream face of the model. The actual average elevation of the top of the model was 198 in. (5.03 m), as seen in Figure 8, which is 4.8 in. (0.12 m) below the design elevation shown in Figure 1. This difference is due to the excessive settlement of the design mix and the decision to not cast to the top of

the formwork because of the significant leakage. (See Appendix B for a discussion of these casting issues). Figure 8 also shows the accelerometers mounted to the base beam (A1x, A6x, A6y, A6z, and A11x). All accelerometer sensor numbers begin with A (e.g., A1x), all strain gage sensor numbers begin with S (e.g., S1z), and all LVDT sensor numbers begin with D (e.g., D1z). All accelerometers with the same number (e.g., A6x, A6y and A6z) have the same location. The letter at the end of the sensor number (i.e., x, y or z) indicates the direction of measurement as shown in Tables 3, 4, and 5. Sensor number ATx provides the average acceleration in the x direction, as measured by sensors inside the TESS. The accelerometers attached to the base beam represent the input motions driving the model and these should be in agreement with the table motions (ATx). Figure 8 shows that three columns of accelerometers were installed on the upstream face to check for any undesired torsional response. For example, if A5x, A10x, and A15x measure essentially the same motion, there is not a torsional response. The accelerometers located just above the base beam (A2x, A7x, A7y, A7z, and A12x) were installed there to check for slippage of the model along the surface of the base beam. Each accelerometer was mounted to a block that was in turn screwed or adhered to the plates cast into model,[6] as indicated Figures A7, A8, and A9 (Appendix A). For each LVDT, two plates were cast into the model at the locations indicated in Figures A7, A8, and A9. One side of each LVDT was attached to the two LVDT plates. The centers of the plates were spaced 8 in. (203 mm) apart so the sensors would measure the relative displacement between the two locations, as shown in Figure 8.

Figure 9 shows the location of each strain gage and LVDT mounted on the front face of the model. The front and back faces did not have accelerometers. As with the upstream face, the strain gages and LVDTs were located near the expected failure surface, with the predicted crack either propagating diagonally down from the change in slope on the downstream face, or straight across from the change in slope.

[6] Plates were cast into the model for all accelerometers and LVDTs except for the A5x, A10x, A10y, A10z, A15x, and A20x accelerometers at the top of the model. These plates were attached to the formwork, but were not cast into the model because the final elevation of the model was below the original elevation of the plates. Therefore, after casting, holes were drilled at new locations (shown in Figures 8 – 11) and filled with a two-part, 5-minute epoxy. Next, round-head machine screws were attached to the plates, and the screws were inserted into the epoxy-filled holes so the plates fully contacted the model surface. Because the downstream face was sloped, that surface was shaved to provide a vertical surface against which the plate supporting the A20x accelerometer was installed.

Table 3. Koyna Dam model accelerometers.

Sensor Number	Face of Model	Sensor Coordinates X (in.)	Y (in.)	Z (in.)	Sensor Direction	Full Scale (g)	Resolution (g)
ATx	TESS	59.75	36	-36	Longitudinal (X)	4.0	0.0020
A1x	Upstream	-12.25	57	-2	Longitudinal (X)	5.0	0.0024
A2x	Upstream	0	57	3	Longitudinal (X)	4.9	0.0024
A3x	Upstream	0	57	50.79	Longitudinal (X)	4.8	0.0024
A4x	Upstream	0	57	129.53	Longitudinal (X)	4.9	0.0024
A5x	Upstream	0	57	195	Longitudinal (X)	5.0	0.0024
A6x	Upstream	-12.25	30	-2	Longitudinal (X)	4.9	0.0024
A6y	Upstream	-12.25	30	-2	Lateral (Y)	4.9	0.0024
A6z	Upstream	-12.25	30	-2	Vertical (Z)	4.9	0.0024
A7x	Upstream	0	30	3	Longitudinal (X)	5.0	0.0024
A7y	Upstream	0	30	3	Lateral (Y)	5.0	0.0025
A7z	Upstream	0	30	3	Vertical (Z)	4.9	0.0024
A8x	Upstream	0	30	50.79	Longitudinal (X)	4.9	0.0024
A9x*	Upstream	0	30	129.53	Longitudinal (X)	4.8	0.0024
A9y	Upstream	0	30	129.53	Lateral (Y)	4.9	0.0024
A10x	Upstream	0	30	196	Longitudinal (X)	5.0	0.0025
A10y	Upstream	0	30	196	Lateral (Y)	4.9	0.0024
A10z	Upstream	0	30	196	Vertical (Z)	4.9	0.0024
A11x	Upstream	-12.25	3	-2	Longitudinal (X)	4.9	0.0024
A12x	Upstream	0	3	3	Longitudinal (X)	4.9	0.0024
A13x	Upstream	0	3	50.79	Longitudinal (X)	4.9	0.0024
A14x	Upstream	0	3	129.53	Longitudinal (X)	4.9	0.0024
A15x	Upstream	0	3	195	Longitudinal (X)	4.8	0.0024
A16x	Downstream	149.75	30	-2	Longitudinal (X)	4.9	0.0024
A17x	Downstream	135.89	30	3	Longitudinal (X)	4.8	0.0024
A17z	Downstream	135.89	30	3	Vertical (Z)	5.0	0.0024
A18x	Downstream	99.19	30	50.79	Longitudinal (X)	5.0	0.0024
A19x	Downstream	40.94	30	129.53	Longitudinal (X)	5.0	0.0024
A20x	Downstream	30.25	30	196	Longitudinal (X)	5.0	0.0024

* This data channel was not recorded properly.

Figure 10 shows the strain gage and LVDT instrumentation on the back face. This instrumentation is laid out as a mirror image of the front face.

Figure 11 shows the locations of all sensors on the downstream face. This face contains one column of five accelerometers. All the strain gages and LVDTs were located near the change in slope on this faces, where the crack was expected to begin. Figure 11 shows that the A19x accelerometer block was centered 1.2 in. (30 mm) below the change in slope and the strain gages were centered 1 in. (25 mm) above the change in slope. The LVDTs were centered on the change in slope, spanning across this location and oriented as shown in Figure A15 (Appendix A).

Table 4. Koyna Dam model strain gages.

Sensor Number	Face of Model	Sensor Coordinates X (in.)	Y (in.)	Z (in.)	Sensor Direction	Full Scale (micro in/in.)	Resolution (micro in/in.)
S1z	Upstream	0	48	130.71	Vertical (Z)	421	0.21
S2z*	Upstream	0	36	130.71	Vertical (Z)	421	0.21
S3z	Upstream	0	24	130.71	Vertical (Z)	421	0.21
S4z	Upstream	0	12	130.71	Vertical (Z)	421	0.21
S5z	Front	3	0	111.02	Vertical (Z)	421	0.21
S6z	Front	20.04	0	117.66	Vertical (Z)	421	0.21
S7z	Front	13.36	0	130.71	Vertical (Z)	421	0.21
S8z	Front	26.72	0	130.71	Vertical (Z)	421	0.21
S9z	Front	37.08	0	130.71	Vertical (Z)	421	0.21
S10z	Back	3	60	111.02	Vertical (Z)	421	0.21
S11z	Back	20.04	60	117.66	Vertical (Z)	421	0.21
S12z	Back	13.36	60	130.71	Vertical (Z)	421	0.21
S13z	Back	26.72	60	130.71	Vertical (Z)	421	0.21
S14z	Back	37.08	60	130.71	Vertical (Z)	421	0.21
S15z	Downstream	39.93	12	131.71	Vert/Long (ZX)	421	0.21
S16z	Downstream	39.93	24	131.71	Vert/Long (ZX)	421	0.21
S17z	Downstream	39.93	36	131.71	Vert/Long (ZX)	421	0.21
S18z	Downstream	39.93	48	131.71	Vert/Long (ZX)	421	0.21

* This data channel was not recorded properly.

Table 5. Koyna Dam model LVDTs.

Sensor Number	Face of Model	Sensor Coordinates X (in.)	Y (in.)	Z (in.)	Sensor Direction	Full Scale (in.)	Resolution (in.)
D1z	Upstream	0	30	111.02	Vertical (Z)	0.20	0.00010
D2z	Upstream	0	32	130.71	Vertical (Z)	0.20	0.00010
D3z	Front	3	0	111.02	Vertical (Z)	0.20	0.00010
D4z	Front	3	0	130.71	Vertical (Z)	0.20	0.00010
D5z	Back	3	60	111.02	Vertical (Z)	0.20	0.00010
D6z	Back	3	60	130.71	Vertical (Z)	0.20	0.00010
D7z	Front	38.08	0	130.71	Vertical (Z)	0.20	0.00010
D8z	Back	38.08	60	130.71	Vertical (Z)	0.20	0.00010
D9z	Downstream	40.88	16	130.71	Vert/Long (ZX)	0.20	0.00010
D10z	Downstream	40.08	44	130.71	Vert/Long (ZX)	0.20	0.00010

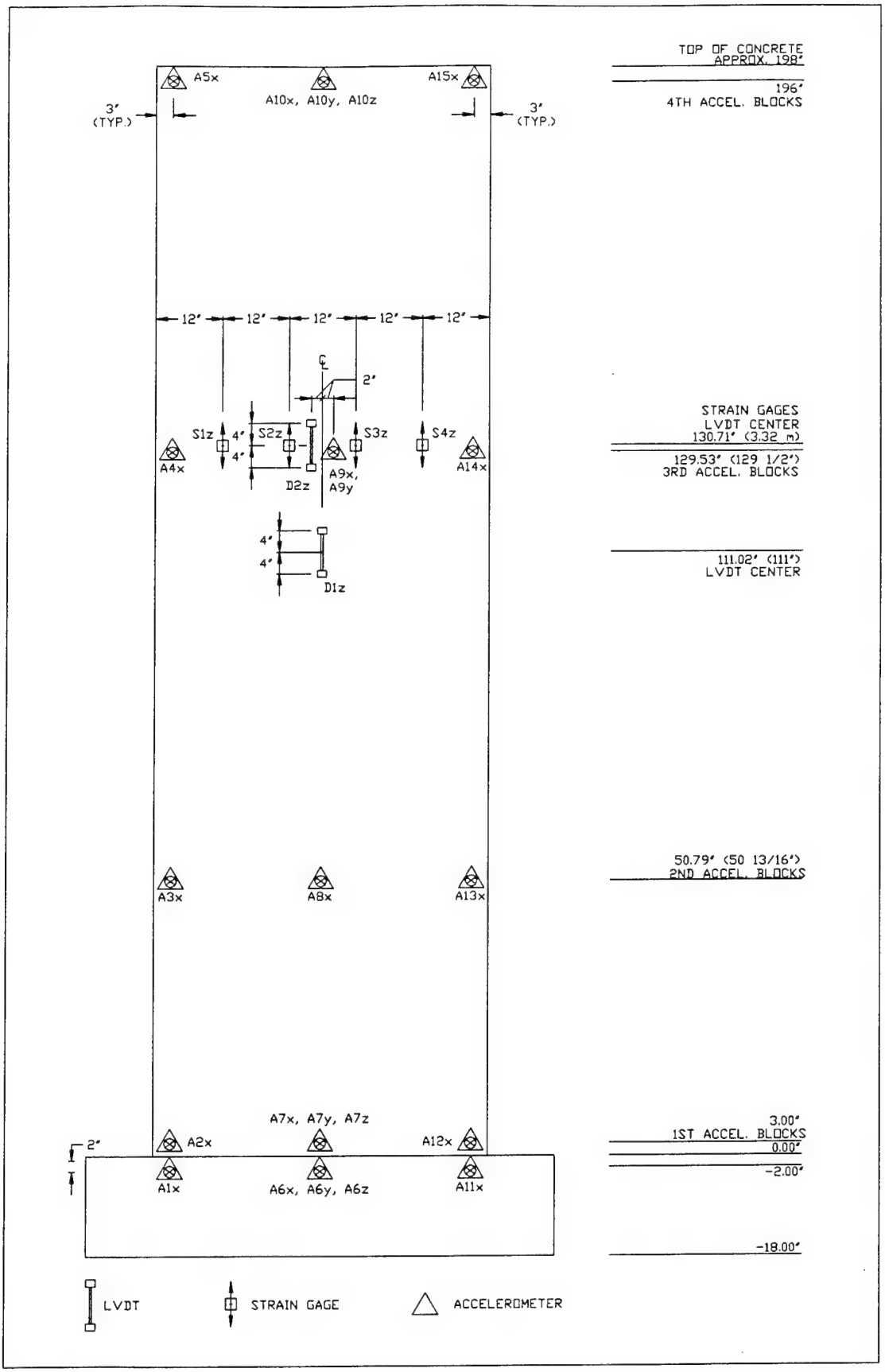

Figure 8. Location of accelerometers, strain gages, and LVDTs on upstream face of the model.

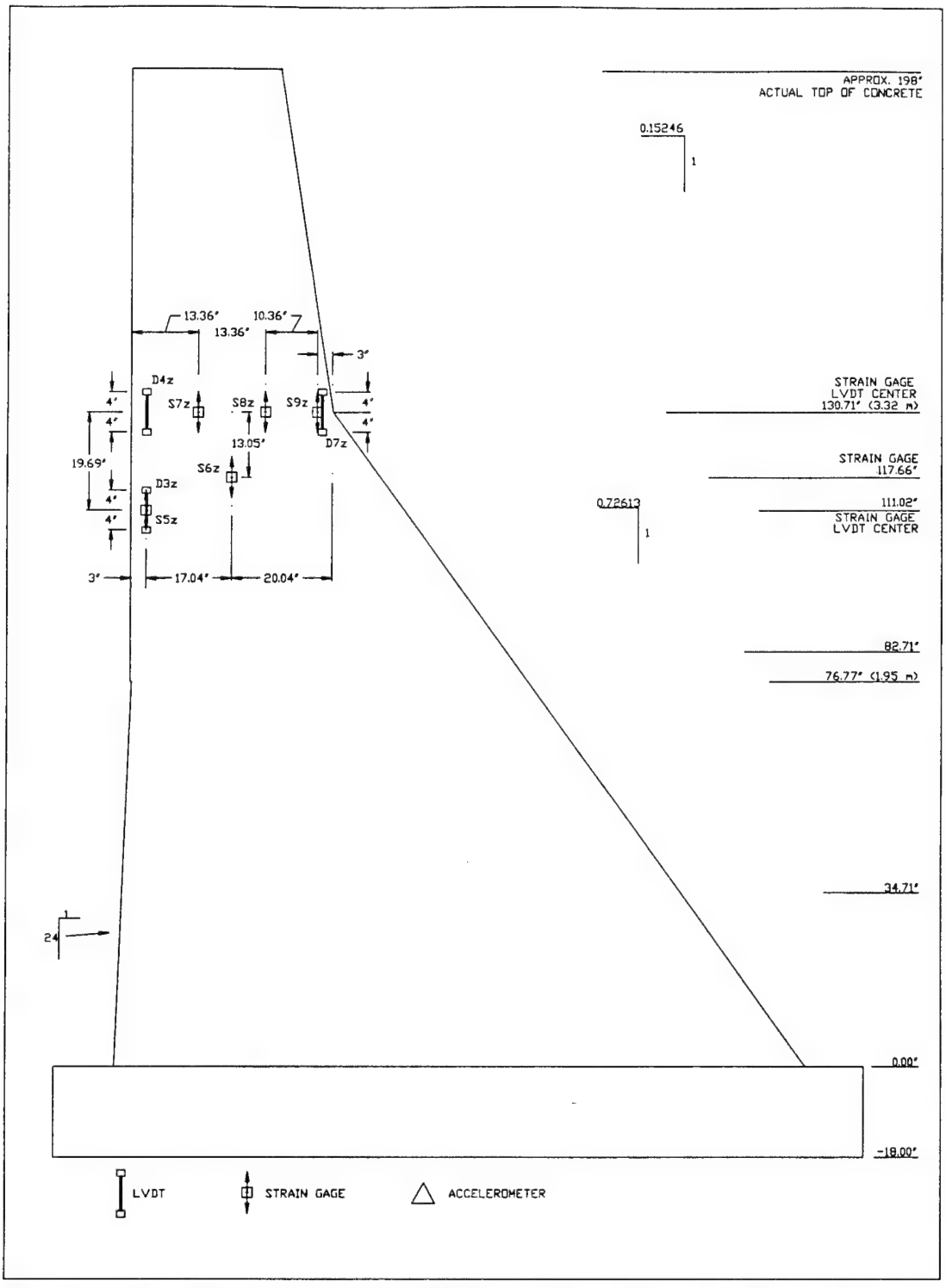

Figure 9. Location of each strain gage and LVDT mounted on the front face of the model.

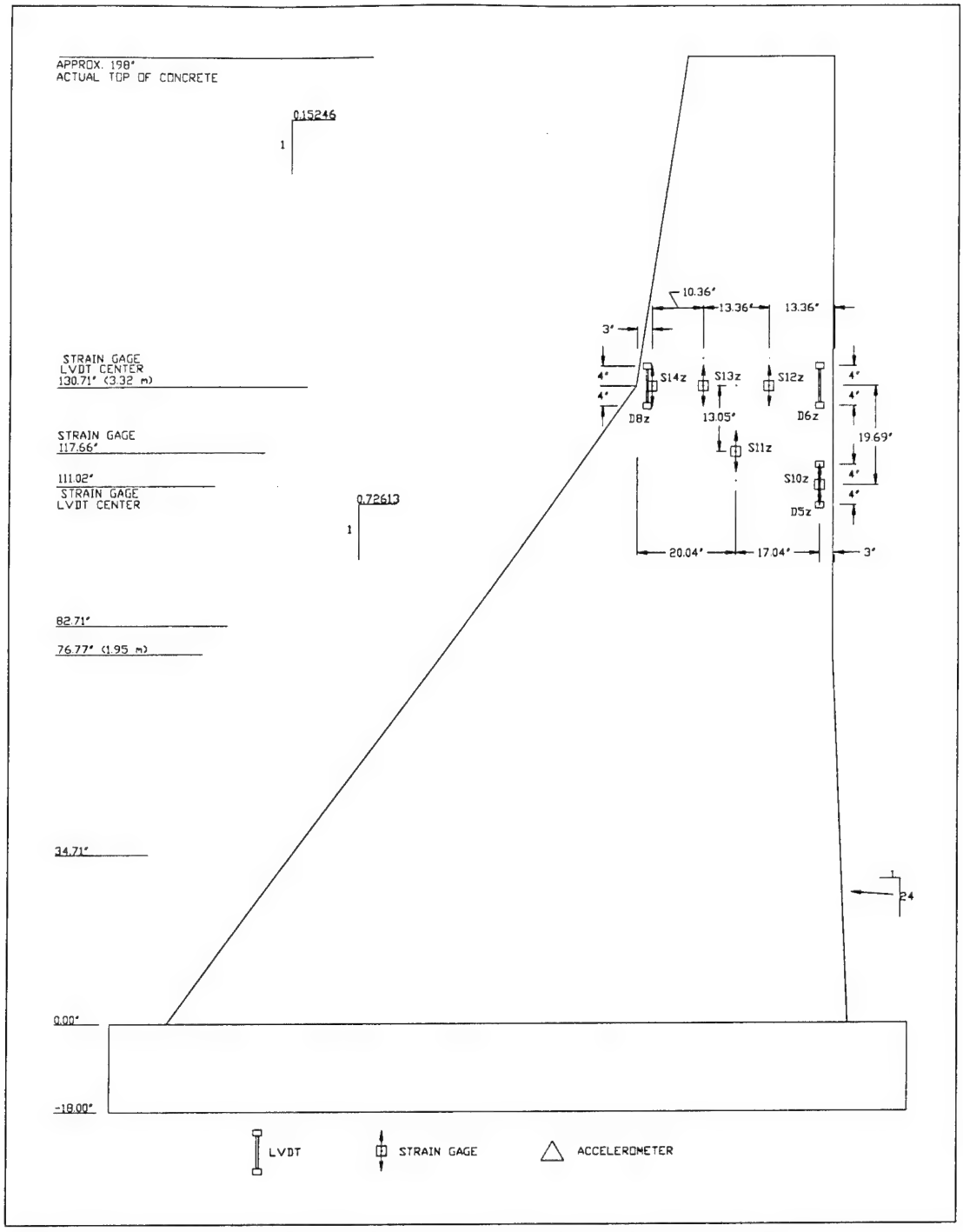

Figure 10. Strain gage and LVDT instrumentation on the back face of the model.

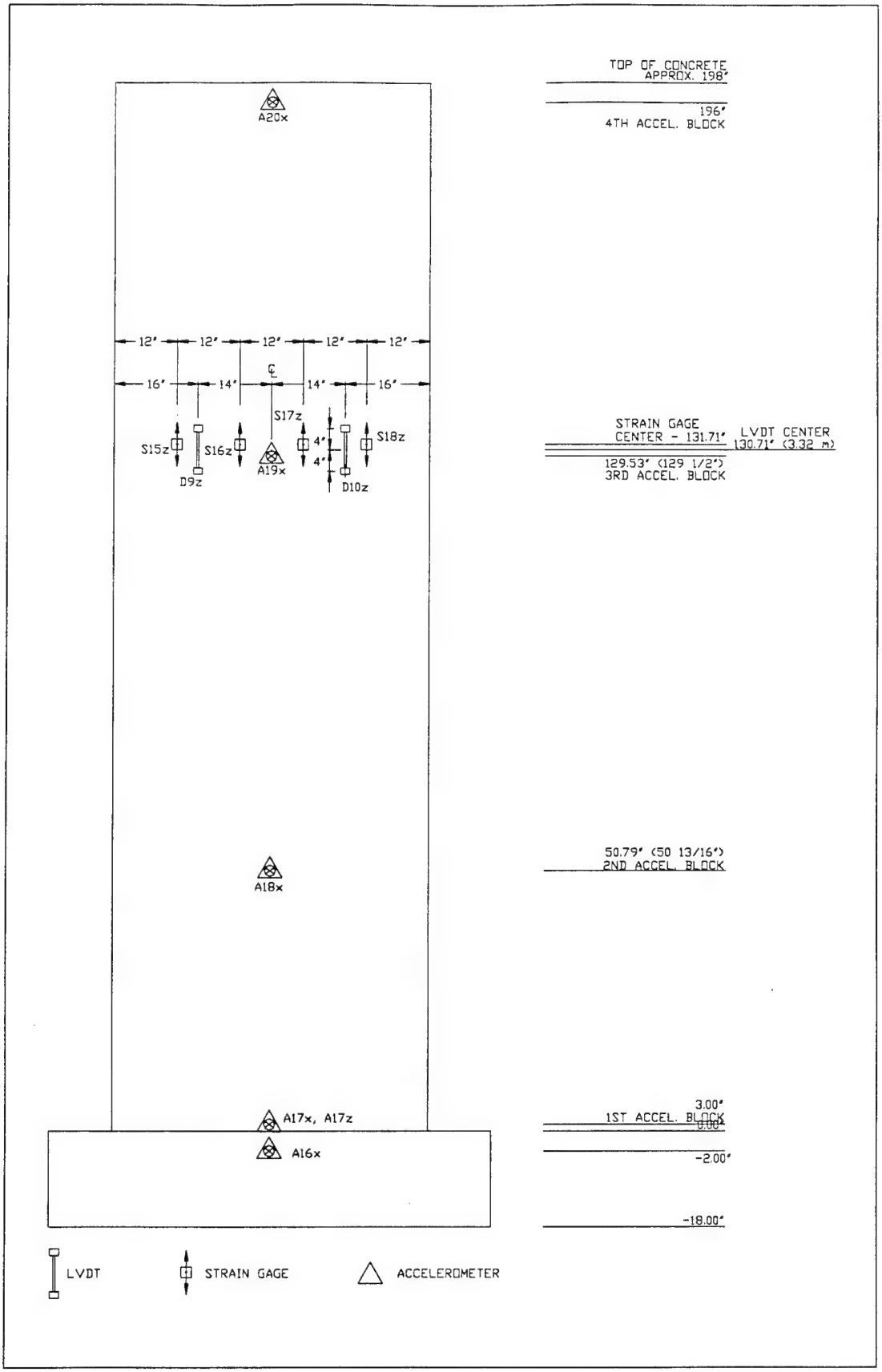

Figure 11. Locations of all sensors on the downstream face of the model.

4 Koyna Dam Model Behavior

Test Block Insert Tests

Bolts inserts were cast into the model by attaching them to the inside face of the formwork, as described in Appendix A. These were installed as a safety precaution (also for demolition purposes) to stabilize the large section of the model above the expected failure surface. The capacity of the inserts would be limited by the strength of the weak model material, so a test block was cast to determine how the bolt inserts would perform. The test block weighed 16,000 lb (7250 kg) and was heavier than the model section above the expected crack. The same bolt inserts as used in the model were cast into the test block. On 12 November an attempt was made to lift the test block using an overhead crane attached to the inserts in the same configuration as it would be attached to the top of the model during the shake table testing. The test block material failed, with diagonal cracks forming around the inserts. These cracks formed only in the immediate area of the inserts and did not propagate up through the material above. This local failure allowed the inserts to pry out, bending as they were pulled up. This prying action applied vertical forces, which caused a horizontal crack across the test block at an elevation a few inches above the center of the inserts. It appeared that the inserts were carrying over half the weight of the test block when the material began to fail directly around the inserts. After this initial failure the lifting capacity of the inserts rapidly dropped. The block test indicated that the inserts at the top of the model would likewise have inadequate capacity to lift the section of the model above the failure surface. However, the overhead crane attached at these inserts would still provide significant lateral support to prevent the top of the model from toppling or sliding along the fracture surface.

Modal Testing

Before conducting any shake table tests, modal tests were conducted using a 50 lb (222 N) electrostatic shaker. (Figure 7 (Chapter 2) shows this shaker attached to the upstream face of the dam model.) The shaker stinger was attached to a force transducer that was in turn attached to the plate used for the A10x, A10y and A10z accelerometers at the location shown at the top center of Figure 8. The shaker was supported vertically by the overhead crane, and was restrained from

rotation by nylon ropes. GSL conducted modal tests using this shaker and recorded the model response using a scanning laser vibrometer system. The vibrometer was located 507 in. (12.875 m) directly in front of the upstream face with the laser head positioned at an elevation halfway between the base and the top of the model upstream surface. The vibrometer was used to measure the displacement profile and modal parameters at various levels of excitation. The shaker produced random motions to excite the model, and the response was measured on a grid pattern on the upstream face of the model. From these tests the fundamental frequency in the X-direction (i.e., the upstream/downstream or in-plane direction) was measured at 13.2 Hz and the damping was 5.5 percent of critical (see Table 6). These tests were conducted on 15 November 1999.

Table 6. Koyna Dam model measured modal parameters.

Parameter Measured	Test Used to Obtain the Parameter		
	Scanning Laser Vibrometer	SWP3	Sine2
1st in-plane bending mode frequency	13.4 Hz	12.7 Hz	13.2 Hz
1st mode damping (percent Critical)	3.2 percent	8.0 percent	7.7 percent
2nd in-plane bending mode frequency	34.3 Hz	37.0 Hz	

Preparation for Shake Table Testing

The bolts used to anchor the base beam to the TESS surface were unintentionally overtightened (over 1,000,000 lb [4450 kN]), and this cracked the base beam in bending in its short direction. The bottom of the base beam was not completely flat, leaving slight gaps between the beam and the table surface. As the beam was drawn down to the TESS surface, it bent in flexure enough to cause a vertical crack in the top surface of the base beam near the downstream face. The crack propagated up into the dam model, within the bottom 30 in (0.8 m). The crack would soften the model in the Y-direction (out-of-plane) to such an extent that modal tests in this direction would no longer be valid. Also, the crack made the model vulnerable to motions in the Y- direction. Therefore, all tests were conducted in the X-direction only (in-plane).

The crack had little impact on the shake table testing because it only prevented modal tests in the Y-direction. The crack appeared to have no influence in the X-direction modal characteristics or model vulnerability. The crack damage at this location did not increase during sine-sweep, time history, or sinusoidal testing.

Instrumentation problems caused minor delays in the test schedule. All TESS shake table tests were conducted on 17 November 1999 (30 days after casting rather than the desired 28 days). All shake table tests were recorded at a sampling rate of 250 Hz (0.004 second time step).

Sine-Sweep Tests

Usually random tests are conducted on models mounted on the TESS to characterize the model in terms of mode shapes, frequencies, and damping. However, due to the fairly high damping it was decided to use sine-sweep tests to more precisely excite the modes of vibration and in the process measure the modal parameters. Sine-sweep tests were conducted at slow sweep rates of 6 or 12 octaves per minute, as defined in Appendix C. The test designated as SWP3 was conducted a rate of 6 octaves per minute in an attempt to achieve a sharper resonance response. Each test began at a frequency of 4 Hz and swept up to 64 Hz (4 octaves) at a rate of either 5 or 10 seconds per octave. At a sweep rate of 6 octaves per minute, or 10 seconds per octave, the total test duration for SWP3 was 40 seconds. The other tests used a sweep rate of 12 octaves per minute, or 5 seconds per octave, resulting in a total test durations of 20 seconds (see Table 7). These tests began at low levels and were gradually increased until the model was sufficiently excited to record modal parameters with good data resolution. All sine-sweep tests were performed in the X-direction only, because of the vertical crack that developed near the base of the model as previously noted. Table 7 summarizes the parameters used to define all sine-sweep tests. SWP3, which was conducted at the slower sweep rate, provided the cleanest signals so it was used to calculate the model frequencies.

Table 7. Sine-Sweep test parameters.

Test Name	Beginning Frequency (Hz)	Ending Frequency (Hz)	Sweep Rate (octaves/min)	Test Duration (sec)	TESS Amplitude (g)
SWP1	4	64	12	20	0.006
SWP2	4	64	12	20	0.012
SWP3	4	64	6	40	0.012
SWP4	4	64	12	20	0.013

Figures 12a and 12b show the average TESS horizontal acceleration (ATx) and at the center top of the model on the upstream face (A10x) for the SWP3 test. The ATx acceleration record agrees very well with the record at the base of the model, taken at the center of the upstream face (A7x). The total test duration was 40 seconds, but Figure 12a zooms in on the record between 15 and 17 sec-

onds, which corresponds to a frequency range of 11.3 to 13.0 Hz. This range corresponds to the frequency range that excited the 1st bending mode of vibration in the X-direction. Figure 12b zooms in on the record between 30 and 32.2 seconds, which corresponds to a frequency range of 32.0 to 37.3 Hz, which excited the 2nd mode of vibration in the X-direction. Both Figures 12a and 12b reveal significant amplification or resonant response as seen by comparing the amplitude of motion at the top of the model (A10x) relative to the base motions (ATx). A transfer function between A10x and ATx was generated and this is plotted in Figure 13. From the transfer function peak magnitudes, the frequencies for the 1st and 2nd modes of vibration in the X-direction were measured as 12.7 and 37.0 Hz, respectively. (These measured natural frequencies are shown in Table 6.) Damping for the 1st mode (8.0 percent of critical, as shown in Table 6) was computed by the half-power method.

Earthquake Time History Tests

Figures C2 and C3 (see Appendix C) show the original 1967 earthquake transversal motions for the base of the Koyna dam and the scaled record. As explained in Appendix C, the first Koyna dam model was tested at very low levels with the record shown in Figure C3 to determine if support motions in the X-direction would excite an unwanted response in the Y-direction. Such a response would be due either to a Y-direction lateral response or to torsion, but neither of these responses would be permitted in the real dam due to the restraint provided by the adjoining dam monoliths in the cross-stream direction (Y-direction). The final time history test used a support motion that was 7 percent of the amplitude shown in the Figure C3 scaled record. Figure 14 shows the support motion at the base of the model (A7x), which agrees well with the record shown in Figure C3. Figure 15 shows the same base motion and the response at the top of the model (A5x, A10x, A10y, and A15x) for the region of highest response (0.7 to 1.0 seconds). The A10y amplitude of response is very small relative to that of A10x (maximum of 11 percent), indicating that there was little out-of-plane response (Y-direction) to the in-plane (X-direction) support motions. The A5x, A10x, and A15x all have very similar amplitude and are in phase with each other, indicating very little torsional response. These results demonstrate that a future 60 in. (1.52 m) wide model, representing two monoliths, can be tested with the full-scale 1967 earthquake records (Figure C3) without concern about any unrealistic out-of-plane response that could confuse the test results.

The support motion at the base of the model (A7x) shown in Figure 14 should be 7 percent of the motions scaled from the 1967 earthquake motions shown in Figure C3. However, the achieved motion shown in Figure 14 has a somewhat

greater concentration of energy near the frequency of the 2nd mode of the dam model (see Figure 13 and Table 6). Figure 16 shows that the response spectra at 5 percent damping for both 7 percent of the scaled motion from the 1967 earthquake (Figure C3) and motions achieved in the earthquake time history test (Figure 14). This figure shows that the peak amplitude of the response spectra for the achieved motions is at 35.5 Hz, and is somewhat greater than the scaled earthquake record between 30 and 39 Hertz. The difference in spectra in this range is not severe but it does suggest the model, resonating at its 2nd mode, amplified the motion of the TESS near this same frequency.

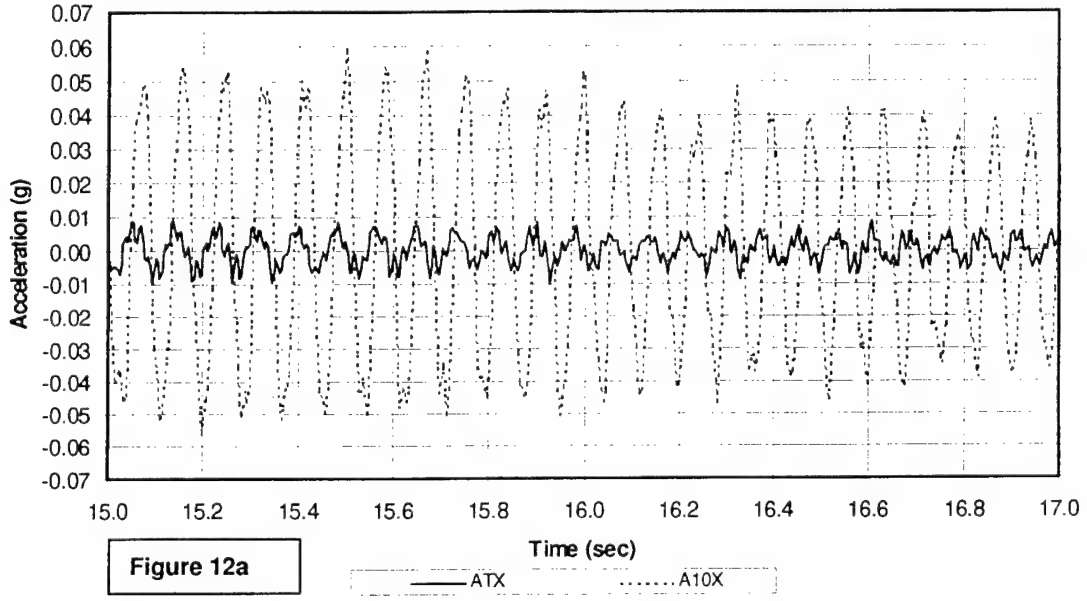

Figure 12a

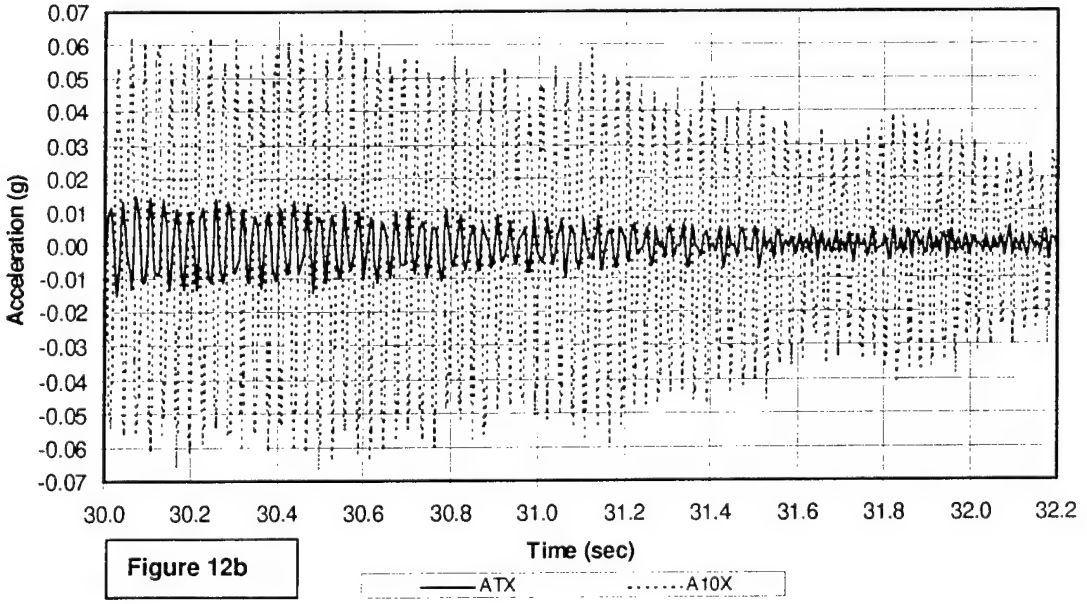

Figure 12b

Figure 12. Plots of average TESS acceleration (ATx) and acceleration at top of model (A10x) from the SWP3 test for (a) 15 to 17 sec (11.3 to 13 Hz) and (b) 30 to 32.2 sec (32 to 37.3 Hz).

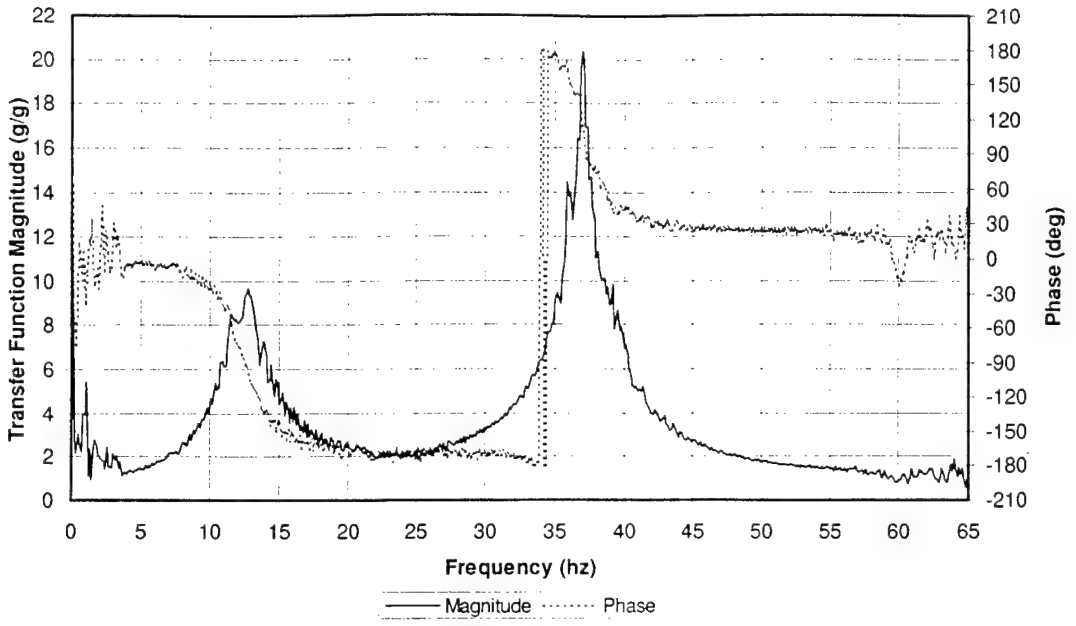

Figure 13. Transfer function magnitude and phase between A10x and ATx from the SWP3 test showing 1st and 2nd resonant peaks.

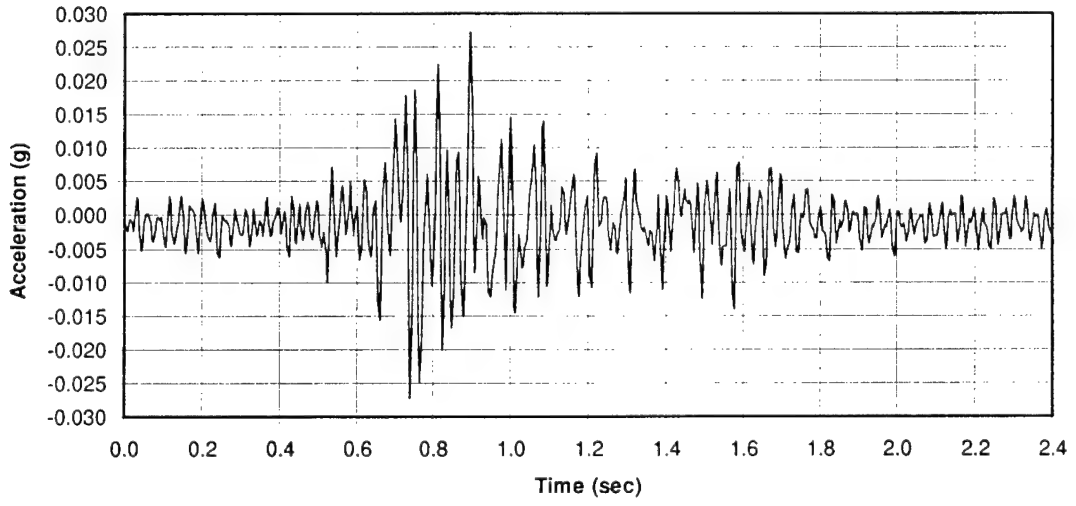

Figure 14. Model base motion (A7x) at 7 percent of scaled 1967 earthquake record.

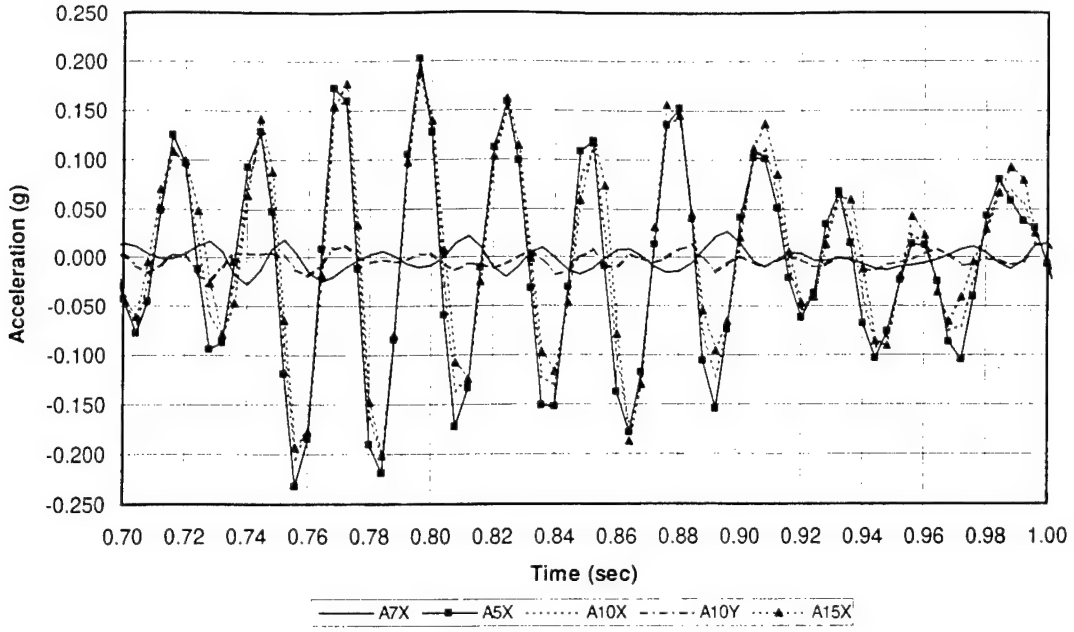

Figure 15. Base motion and the response indicating little out-of-plane or torsional response.

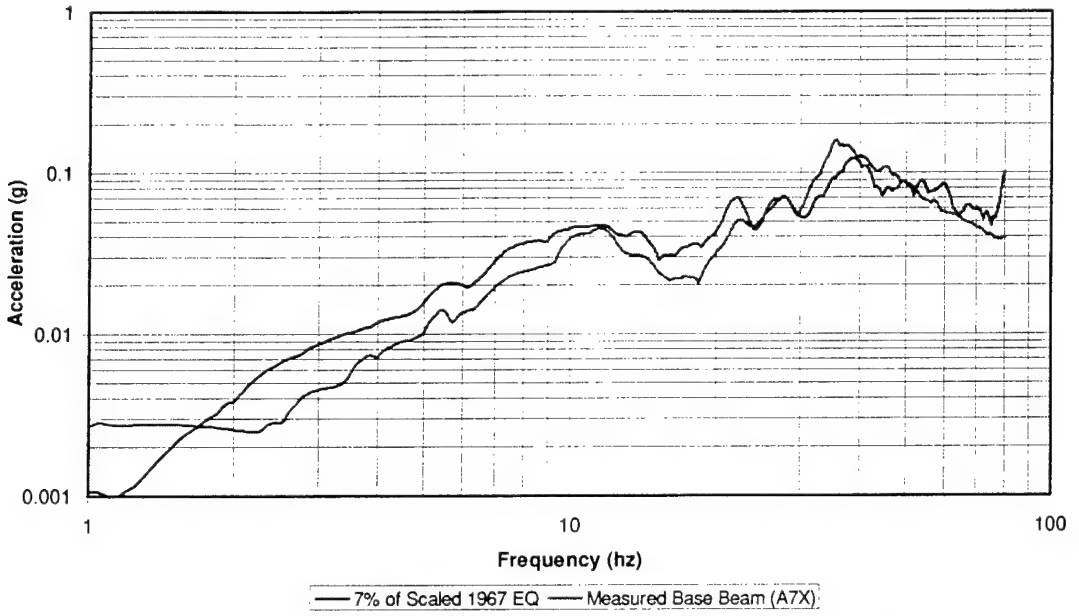

Figure 16. Response spectra at 5 percent damping for both 7 percent of scaled 1967 earthquake motion and achieved shake table motion shown in Figure 14.

The original motions of the 1967 earthquake appear to have a concentration of energy at the dam's 2nd mode. This can be seen by the response spectrum of the scaled 1967 earthquake record shown in Figure C4, where the greatest response is between 34 and 41 Hz, which coincides with the measured 37 Hz frequency of the model 2nd mode. Because the scaling of the earthquake record corresponds to the scale of the model, the actual Koyna dam likely has a 2nd mode at a fre-

quency that would agree with a concentration of energy in the 1967 recorded motion, i.e., 37 Hz / $\sqrt{(20)}$ = 8.3 Hz. Therefore, it appears that the original recorded motions from the 1967 earthquake may not represent entirely free-field motions, but includes motions that could have been amplified by the 2nd mode response of the taller monoliths near the center of the dam. The possible interaction between the tallest monoliths and foundation, and its effects on the recorded motions, is beyond the scope of this study. Significantly, the instrument used to record the 1967 earthquake was located in a gallery at mid-height of a short monolith, near an abutment. This is considered the official record representing ground motion at the site because the short monolith behaved essentially as a rigid structure.[7]

Sinusoidal Koyna Dam Model Tests — Linear Response

Testing Procedure

This first Koyna dam model was tested to failure with sinusoidal motions near the 1st in-plane natural frequency of the model. Modal testing conducted by GSL measured this value at 13.2 Hz, and the sine-sweep tests provided a value of 12.7 Hz. All sinusoidal tests were conducted with a frequency of 14 Hz. If damage had begun, this would have reduced the model's stiffness, which would likewise reduce the model's frequency. The support motion frequency was offset slightly from the model frequency so as not to overexcite the model. Figure C1 shows the response of single degree-of-freedom (SDOF) oscillators, excited by harmonic (sinusoidal) support motion, which have 2, 5, and 10 percent critical damping. It is preferable for sinusoidal support motions to be above the model frequency rather than below. If support motions were below the natural frequency, the natural frequency would move to the support motions as damage increased, which could further amplify model response just as serious damage occurred. This could lead to a rapid and uncontrolled increase in damage. For safety reasons, therefore, it was better to test with support motions above the natural frequency, and 14 Hz was specified for these reasons. Figure C1 shows that an SDOF oscillator at 13.2 Hz with 5 percent damping, excited with 14 Hz support motion, would respond at 6.15 times the sinusoidal support motion. These sinusoidal tests began at very low levels (0.005 g for Sine1, as shown in

[7] Chopra, A.K., and P. Chakrabarti, "The Koyna Earthquake and the Damage to Koyna Dam," *Bulletin of the Seismological Society of America*, Vol. 63, No. 2, pp. 381 – 397, 1973.

Table 8), and response measurements were reviewed. Each of the sinusoidal support motions ramped up linearly to the full TESS amplitude levels in 1 second, maintained this level for 5 seconds, then ramped down to zero in 1 second. Test levels were gradually increased as shown in Table 8 to determine the linear response of the dam. The input motions for the Sine2 test were modified to stop at the end of the constant amplitude sinusoid motion (i.e., no ramp-down), thereby ending input excitation. This permitted measurement of the free decay of the 1st mode using logarithmic decrement. Table 6 shows that 1st mode damping was calculated at 7.7 percent of critical.

The response of the Koyna model remained essentially linear up through test Sine5 (0.12 g support motion). Only the Sine5 results are reported here because the Sine1 through Sine4 tests created a linear response almost identical to the Sine5 results, but at lower amplitude. The Sine5 test differed slightly from Sine4 in that the Sine5 support motions were closer to an ideal 0.12 g, 14 Hz sinusoid. This improvement was based on additional random testing used to create a new computer compensation model that corrects for the shake table interaction with the model.

Measured Acceleration and Relative Displacements for Linear Tests

Figure 17 shows the sinusoidal motion at the base of the dam model (A7x) for Sine5, illustrating the 1-second ramp-up, 5 seconds at a constant peak amplitude, and 1 second of ramp-down. These measured motions agree well with Table 8, showing the 0.12 g amplitude of the sinusoidal motion and frequency of 14 Hz (0.07 sec/cycle).

Table 8. Sinusoidal Koyna dam model tests.

Test Name	Motion Frequency (Hz)	TESS Amplitude (g)	Full Amplitude Duration (sec)	Total Test Duration (sec)
Sine1	14	0.005	5	7
Sine2	14	0.02	5	7
Sine3	14	0.08	5	7
Sine4	14	0.12	5	7
Sine5	14	0.12	5	7
Sine6	14	0.16	5	7

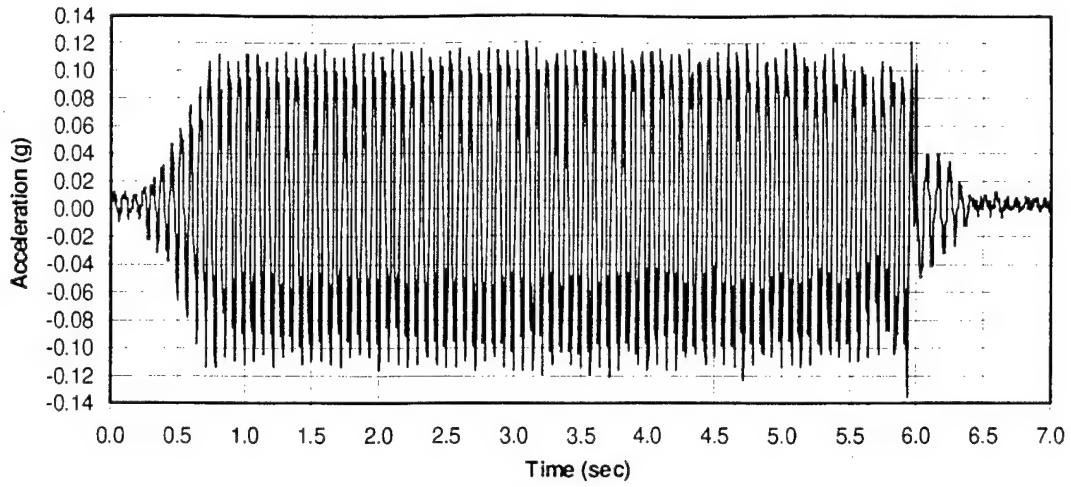

Figure 17. Support motion for Sine5 showing ramp-up, constant amplitude, and ramp-down.

Figure 18 shows the measured acceleration from this test at the base beam (A6x) and elevations of 3 in. (A7x), 50.8 in. (A8x), 129.5 in. (A4x/A14x), and the top of the model at 196 in. (A10x). The elevations and other locations of these sensors are given in Table 3. All of these acceleration measurements were taken from the center of the upstream face except for A4x/A14x, which is the average of the values from A4x and A14x. This average was used in place of A9x because data were not recorded properly at A9x. A9x was located directly between A4x and A14x, both of which were at the same elevation as A9x. Also, A4x and A14x provided almost identical data because there was no torsional response. The sinusoidal data are shown for only the region of 3.7 to 3.9 seconds, which comprises less than 3 cycles. This region has slightly greater accelerations than the rest of the record. However, because the acceleration response overall varies little with time, this small portion of the record is representative of the entire record, and is therefore suitable to illustrate by itself for purposes of clarity. Figure 18 shows that the model base acceleration (A7x) differs only slightly from the base beam acceleration (A6x). The model response accelerations (A8x, A4x, and A10x) are out of phase with the input acceleration (A6x and A7x), due to the response of the model and some overturning response at the base.

Figures 19a, 19b, and 19c show the measured (absolute) accelerations A7x, A8x, A4x/A14x, and A10x over the entire test duration. The figures show that the response accelerations remain fairly constant, indicating linear model response and essentially no damage. Table 9 provides the peak-measured accelerations along the center of the upstream face (A7x, A8x, A4x/A14x, and A10x). For each peak value shown in Table 9, the sensor number, measurement elevation (vertical location), and time of measurement are given. The dam model quickly reached a steady-state response, as seen in Figure 19a through 19c. The average of the peak steady-state response from each cycle best reflects the response of

the model, and an estimate of this value is given in Table 9. This table provides a summary of the peak linear response for key sensors measured during the Sine5 test.

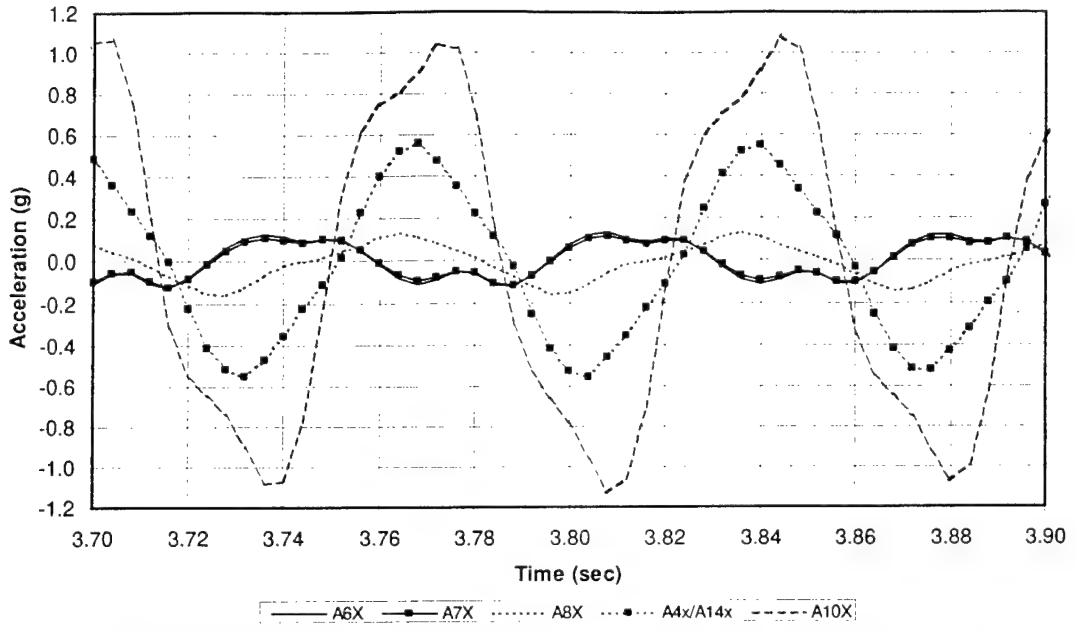

Figure 18. Measured acceleration at the base beam, model base, and elevations of 50.8 in., 129.5 in., and 195 in. between 3.7 and 3.9 sec.

Table 9. Peak measured linear response from Sine5 test.

Measurement	Elevation	Peak Response Time (sec)	Peak Value	Steady State Value
Base Beam Acceleration, A6x	Z = -2 in.	3.092	0.139 g	0.122 g
Model Base Acceleration, A7x	Z = 3 in.	5.928	-0.136 g	0.112 g
Upstream Face Acceleration, A8x	Z = 50.8 in.	5.988	0.214 g	0.136 g
Upstream Face Acceleration, A4x/A14x	Z = 129.5 in.	3.696	0.568 g	0.523 g
Upstream Face Acceleration, A10x	Z = 195 in.	3.808	-1.131 g	1.042 g
Upstream Face Displacement, $DA8x_{Rel}$	Z = 50.8 in.	1.052	-0.0013"	0.0003"
Upstream Face Displacement, $DA4x/DA14x_{Rel}$	Z = 129.5 in.	3.84	-0.0076"	0.0055"
Upstream Face Displacement, $DA10x_{Rel}$	Z = 195 in.	4.164	0.0211"	0.0180"
Upstream Face Strain, S3z	Z = 131.7 in.	3.82	92 micro in/in	82 micro in/in
Downstream Face Strain, S15z	Z = 131.7 in.	3.82	-115 micro in/in	106 micro in/in
Upstream Face LVDT, D1z	Z = 111 in.	3.916	0.0006"	0.0005"
Upstream Face LVDT, D2z	Z = 130.7 in.	4.024	-0.0009"	0.0008"
Downstream Face LVDT, D9z	Z = 130.71	3.704	-0.0017"	0.0013"

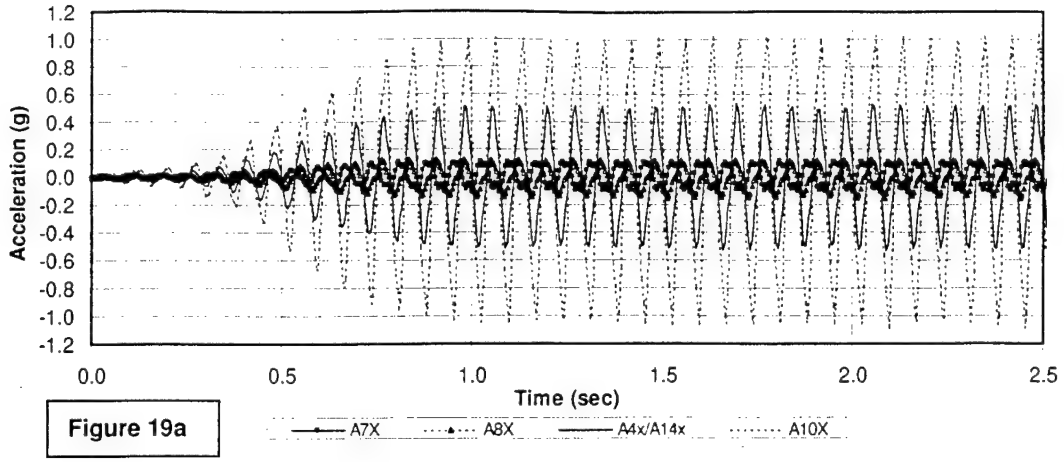

Figure 19a

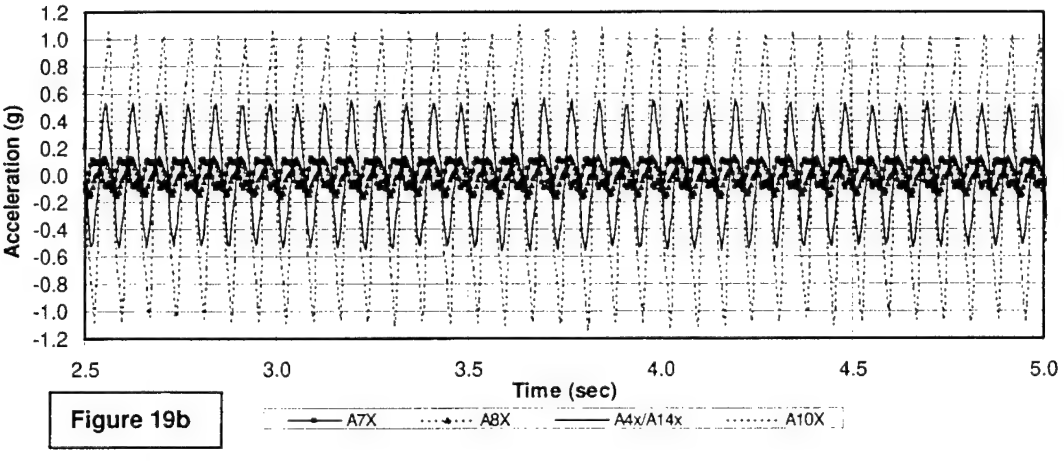

Figure 19b

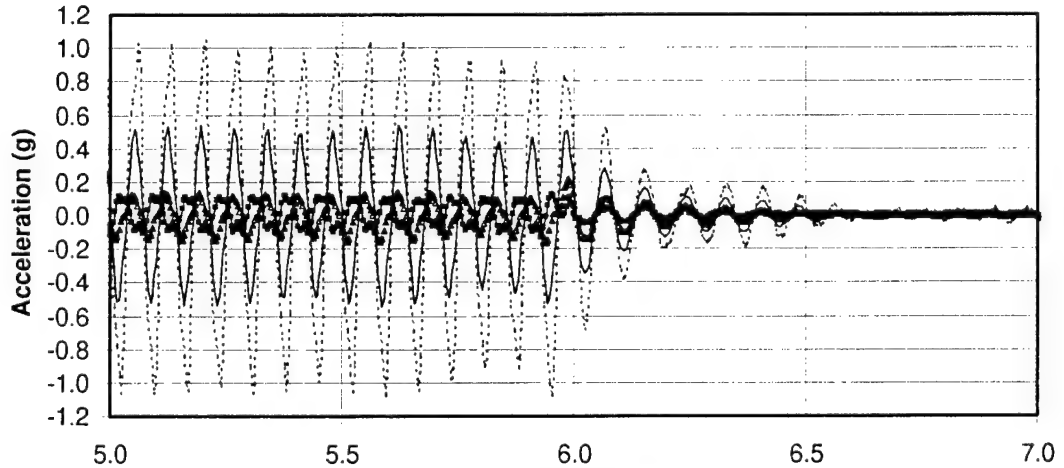

Figure 19c

Figure 19. Measured (absolute) accelerations along the upstream face over entire test duration.

Appendix B described the casting of the dam model on the TESS shake table. Significant form leakage occurred, which led to the damage of four accelerometers (two horizontal and two vertical) inside the TESS. The damage to the vertical accelerometers may have led to a problem with significant overturning accelerations. Figure 20 shows the vertical accelerations at the upstream (A7z) and downstream (A17z) base of the model. These accelerations are out-of-phase with each other, demonstrating the overturning motion of the TESS. Figure 20 also shows the base in-plane acceleration (A7x), which shows that the overturning vertical acceleration at the base was actually larger than the horizontal motion at the base. However, these absolute accelerations still represent the accelerations affecting the model, and all accelerations are reported in this way. The response acceleration values can still effectively be compared with analytical models, but the large overturning motions must be taken into account as these represent a significant portion of the motions that excited the model.

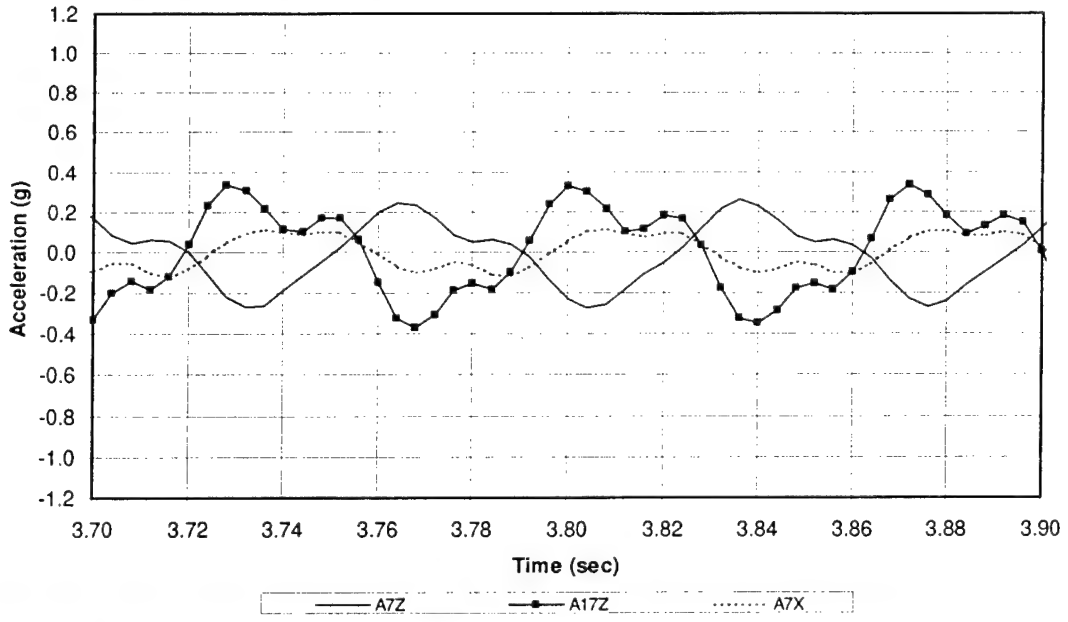

Figure 20. Overturning accelerations relative to in-plane horizontal accelerations.

However, relative rather than absolute displacements are reported. Absolute displacements are first calculated by integrating the absolute accelerations twice. The absolute accelerations were first high-pass filtered,[8] then double inte-

[8] The data filtering was performed in Matlab using an Equiripple high-pass filter, 110 order, with 5 Hz cutoff frequency, 2 dB passband ripple, 2 Hz stop band frequency and –40 dB stop band attenuation.

grated,[9] and the resulting displacement records were corrected for drift using a 6th order curve fit.[10] Figure 21 shows the absolute displacements along the upstream face of the dam. These displacements use the symbols DA7x, DA8x, DA4x/DA14x (average of DA4x and DA14x), and DA10x, which have been obtained by integrating the A7x, A8x, A4x, A14x, and A10x accelerations, respectively. As expected, the response displacements (DA8x, DA4x/DA14x and DA10x) are out-of-phase with the base displacement (DA7x) due to the response of the model. Vertical accelerations at the base of the model on the upstream and downstream faces (A7z and A17z) were integrated also in the same manner, and resulting absolute displacements (DA7z and DA17z) were plotted in Figure 21 for comparison with the horizontal data. Figure 21 shows that the vertical displacements (DA7z and DA17z) were also out-of-phase with each other. An overturning base rotation (θ_B) time history was calculated by the difference between the displacements divided by the horizontal distance between them, which is expressed as follows:

$$\theta_B = \frac{DA17z - DA7z}{X_{A17z} - X_{A7z}} = \frac{DA17z - DA7z}{135.9in.} \qquad \text{[Eq 1]}$$

X_{A7z} and X_{A17z} in Equation 1 are the positions of the A7z and A17z sensors in the X-direction.

Relative X-direction displacements along the upstream face are calculated. These values are given relative to the model base displacement and relative to the base rotation, so the values represent the true deformation in the model. The relative displacements along the upstream face, $DAnx_{Rel}$, were calculated as follows:

$$DAnx_{Rel} = DAnx - DA7x + (Z_{Anx} - Z_{A7x})\theta_B \qquad \text{[Eq 2]}$$

where,

n = the number in accelerometer names A8x, A4x/A14x, and A10x,

---

[9] Integration was done using the Numerical Trapezoidal Rule, available in DPLOT. DPLOT is a graphing utility for plotting, viewing, manipulating, and printing two-dimensional plots in Microsoft Windows 3.x and Windows 9X/NT. It was developed and maintained by GSL.

[10] The 6th order curve fit was performed using a least-squares curve fitting procedure available in DPLOT.

Z_{Anx} = the elevation (Z coordinates) for accelerometers A8x, A4x/A14x, and A10x given in Table 3, and

Z_{A7x} = the elevation (Z coordinate) for accelerometer A7x, which equals 3 in. (76 mm) as shown previously in Table 3.

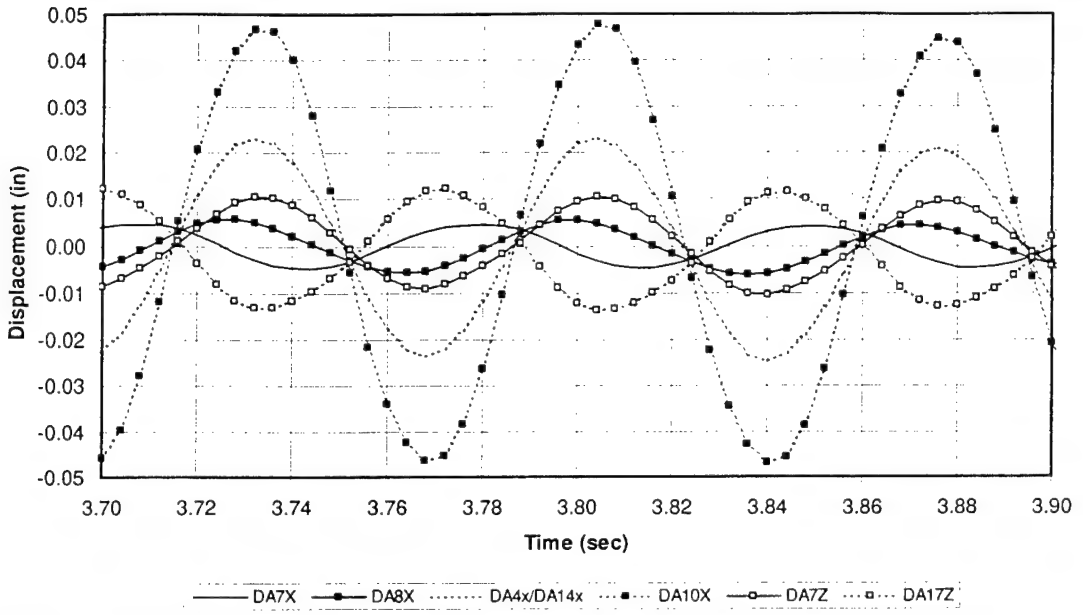

Figure 21. Absolute displacements along the upstream face plus vertical displacement at the base of the upstream and downstream faces.

These relative displacements are plotted in Figure 22 for the 3.7 to 3.9 second region of the Sine5 test. The overturning motion (seen in the DA7z and DA17z data shown in Figure 21) is a major component of the base motion. A large portion of the absolute displacements is due to this rotation. Figure 23 graphically shows the absolute displacements of the dam model profile at 3.84 seconds for each sensor shown in Figure 22. Figures 21 and 22 both indicate that the dam model has reached a peak absolute and relative displacement at this time. The rotation, θ_B, is positive at this time, and it is also shown in Figure 23. All of these displacements are plotted proportionately at 1000 times their true amplitude to graphically emphasize the displaced and rotated shape of the model. Figure 23 also plots the relative displacements, showing the deformed model shape in profile at the same magnified scale. This plot in profile at 3.84 seconds demonstrates that a large portion of the absolute displacements is due to base rotation, showing the relative magnitude of relative and absolute displacement. The magnitudes of both the absolute and relative displacements are included in Figure 23. The absolute accelerations and resulting inertial forces reflect the true loading of the Koyna dam model, and the relative displacements reflect the true deformed shape. But Figure 23 illustrates that it is very important that

comparisons with analytical models account for the significant base rotations that occurred in the physical model test.

Figures 24a, 24b, and 24c show the relative displacements from along the upstream face ($DA8x_{Rel}$, $DA4x/DA14x_{Rel}$, and $DA10x_{Rel}$) over the entire test duration. These plots show a low-frequency modulation of the data due to the filtering and integration scheme. Nevertheless, these data show that the deformations of the model represented by the relative displacements remain fairly constant, indicating linear model response and essentially no damage. Table 9 provides the peak relative displacements along the center of the upstream face ($DA8x_{Rel}$, $DA4x/DA14x_{Rel}$, and $DA10x_{Rel}$). The peak values shown in Table 9 are the averages of the peak-to-peak values for the largest single cycle, thereby canceling the effect of the modulation in data. Table 9 also provides an average of the peak steady-state response of the relative displacements.

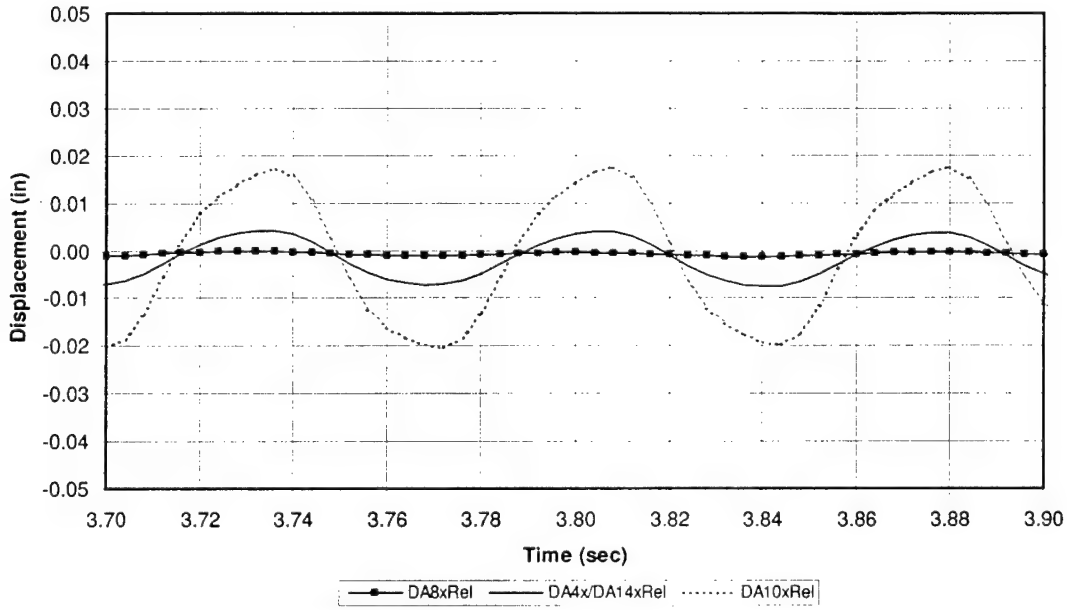

Figure 22. Relative displacements along the model upstream face showing the model deformation for the Sine5 test.

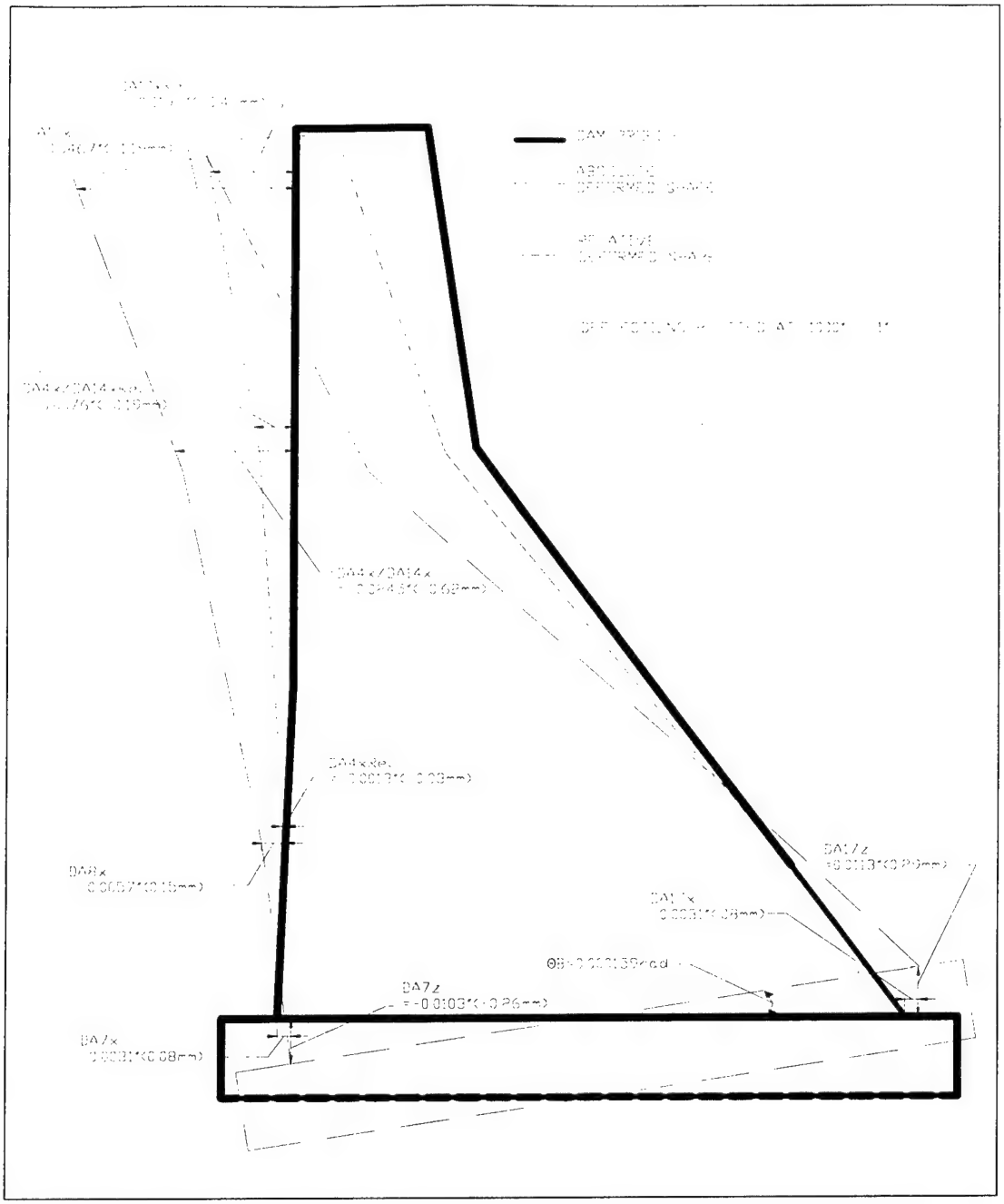

Figure 23. Deformed Koyna dam model at 3.84 seconds.

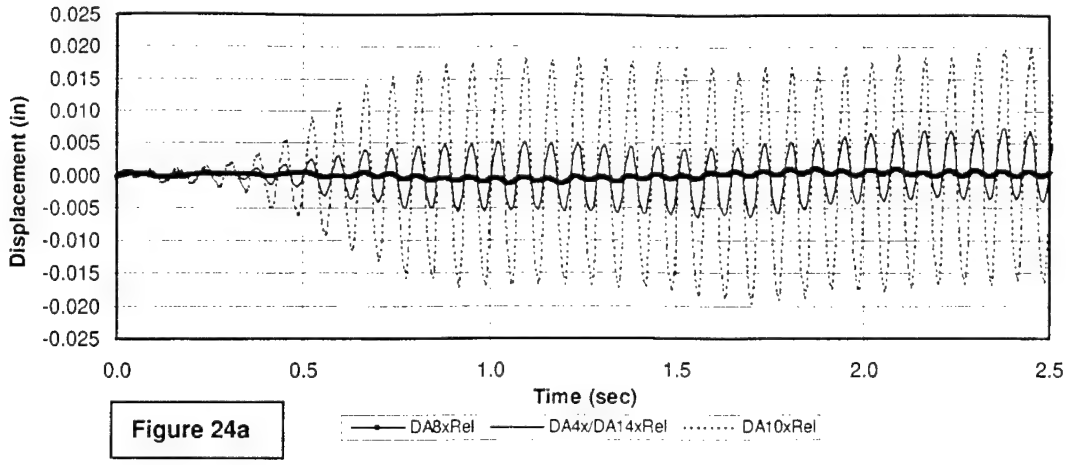

Figure 24a

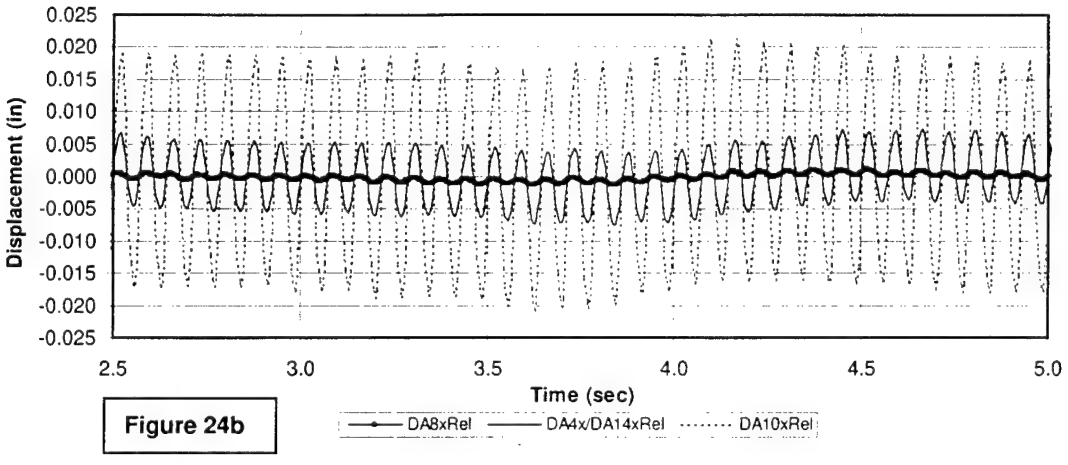

Figure 24b

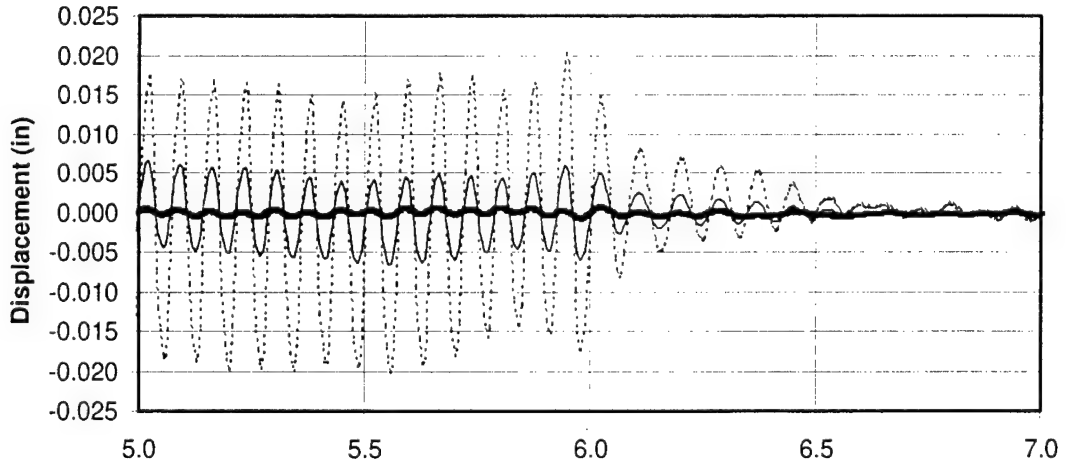

Figure 24c

Figure 24. Relative displacements along the upstream face over the entire test duration.

Measured Strains for Linear Tests

Strains were measured in the region of the expected failure, at the elevation of the change in slope of the downstream face. Table 4 and Figures 8 through 11 show the locations of all strain gages. The strain measurements can be compared with linear behavior of numerical models. The greatest strains were measured at the downstream face near the change in slope, as expected. Figure 25 shows the strain measurements from all four gages on this face (S15z, S16z, S17z, and S18z) for the same time range as the accelerometer and displacement data presented in Figures 18, 20, 21, and 22 (3.7 to 3.9 sec). This region also gives the greatest strain measurement, which for S17z is 130 micro in./in. at 3.82 seconds. Figure 25 shows the variation in strain along the downstream face. One of the exterior gages along this face would be expected to provide the greatest strain due to minor out-of-plane or torsional response, but in this test the greatest strain value came from the S17z interior gage. The smallest strain was recorded at S16z, which was also an interior gage. Strain gage S15z provides the best average of the gages along the downstream face. Figure 26 shows the strain measured at S15z for the entire duration of the Sine5 test. Table 9 provides the time and value of the peak response of strain gage S15z, and also provides the steady state average strain for S15z.

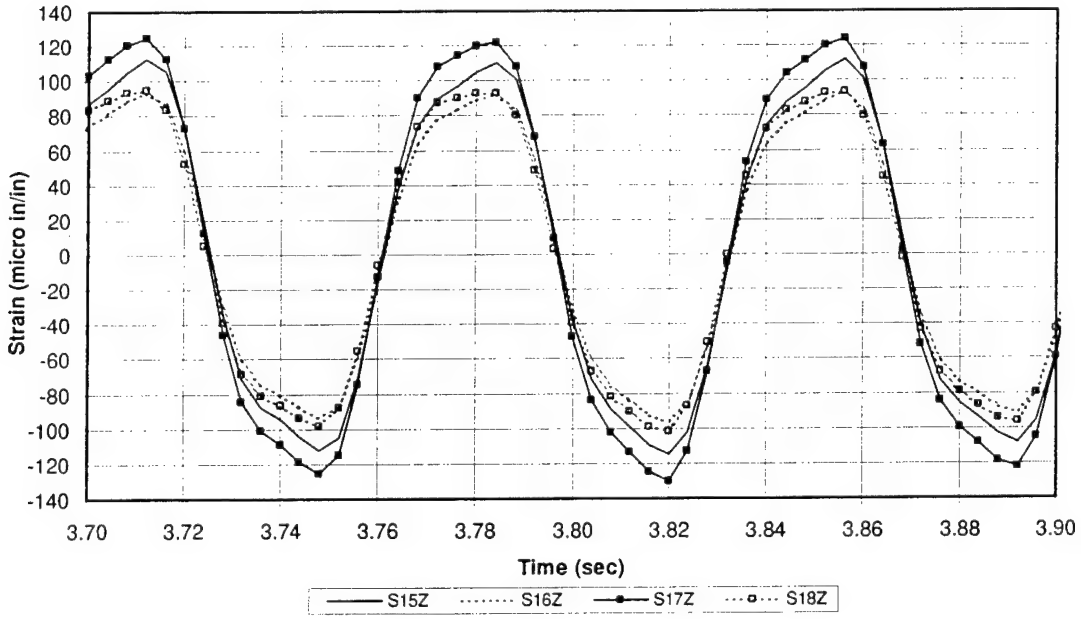

Figure 25. Strain measurements along the downstream face.

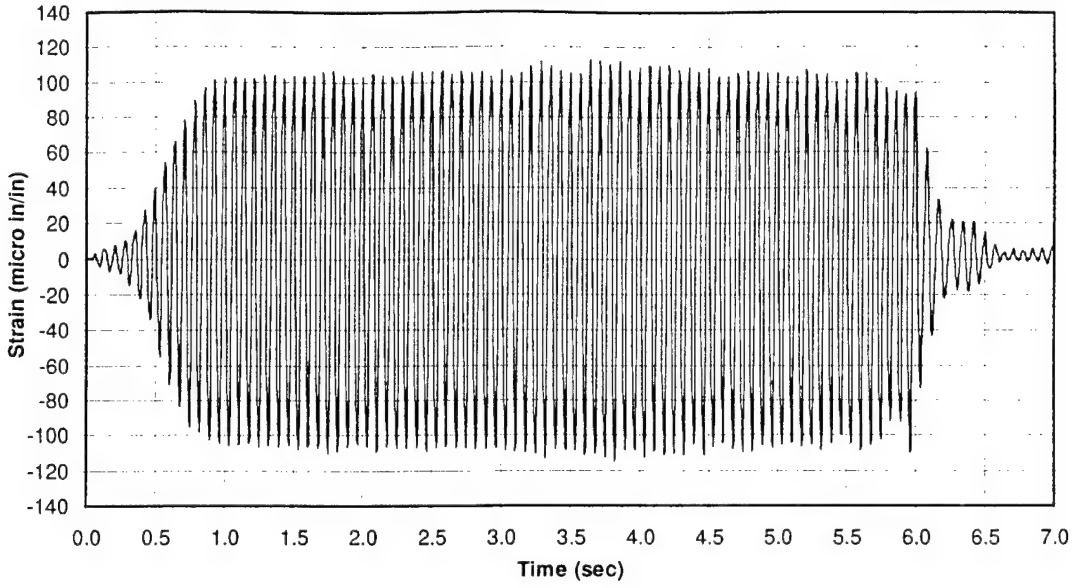

Figure 26. Strain measurements along the downstream face at S15z only for the Sine5 test.

Strain measurements along the upstream face (S1z, S3z, and S4z) are shown in Figure 27 for the 3.7 to 3.9 second time region. Cables for strain gage S2z were interfering with TESS control so the sensor had to be disconnected and therefore provided no data. The 3.7 to 3.9 second time region gives the greatest strain measurement for this face, which for S4z is 96 micro in./in. at 3.82 seconds. Figure 27 shows the variation in strain along the upstream face. The greatest strains on the upstream face were measured at S4z, which is an exterior gage (see Figure 8, Chpater 3). The smallest strain was measured at the other exterior gage along the upstream face at S1z, suggesting a minor torsional response. However, as described earlier, the strains measured on the downstream face indicated no torsion. The variation in strain measurements is more likely due to variations in local strain of the material or calibration of the sensors. Strain gage S3z provides the best average of the gages along the upstream face (see Figure 27). Figure 28 shows the strain measured at S3z for the entire duration of the Sine5 test. Table 9 provides the time and value of the peak response of strain gage S3z, and also provides the steady state average strain for S3z.

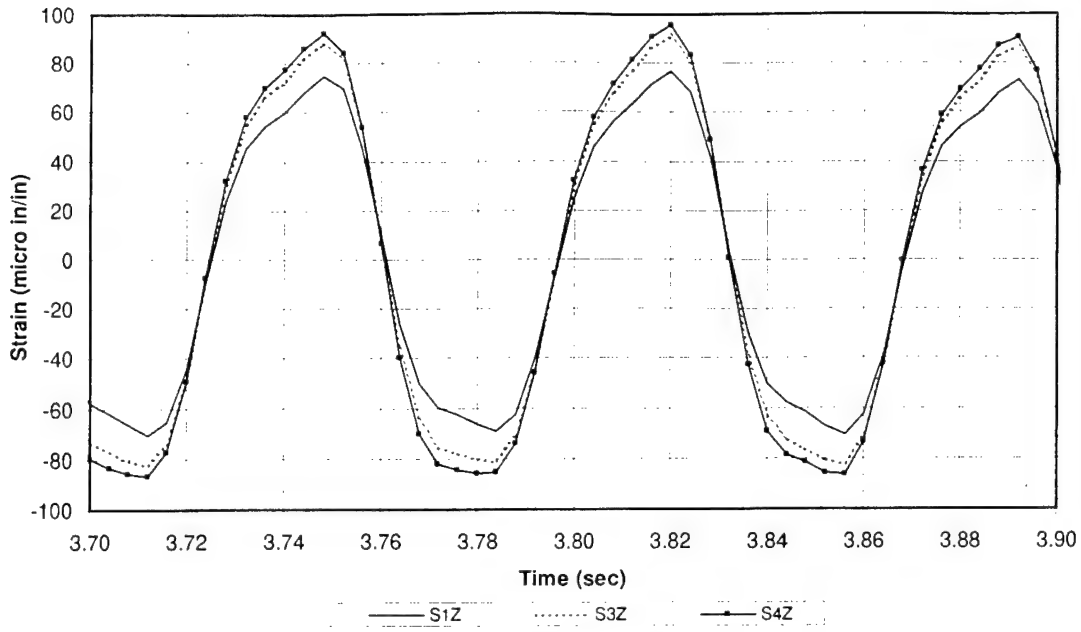

Figure 27. Strain measurement along the upstream face.

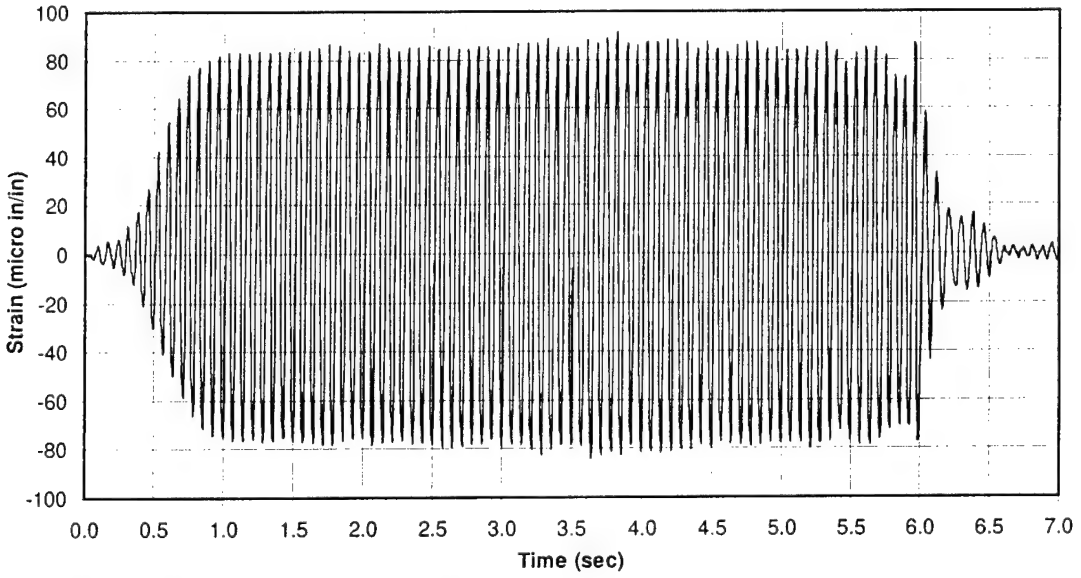

Figure 28. Strain measurement along the upstream face at S3z only for the Sine5 test.

Strains were also measured along the front face at the locations shown in Figure 9 and Table 4 (Chapter 3). These strains (S5z, S6z, S7z, S8z, and S9z) are plotted for the time region from 3.7 to 3.9 seconds in Figure 29. Similarly, strains were measured along the back face at the locations shown in Figure 10 and Table 4 (Chapter 3), and these (S10z, S11z, S12z, S13z and S14z) are plotted from 3.7 to 3.9 seconds in Figure 30. As expected, the strain gage closest to the downstream face on the back face (S14z) gives the largest values for this face (see Figure 30). The S14z measurements are in phase and less than the downstream face strains. However, the strains measured at the same location of the front

face (S9z) is considerably smaller than the one measured on the back face. These gage reading are questionable due to the lack of consistency with the back face and downstream readings. The strain gages closest to the upstream face on both the front face (S5z and S7z) and back face (S10z and S12z) are in phase with the upstream face readings and with each other, and they have lower magnitudes than measurements from the upstream face. With the exception of the S9z measurements, the strains measured on the front and back faces agree well with the upstream and downstream measurements.

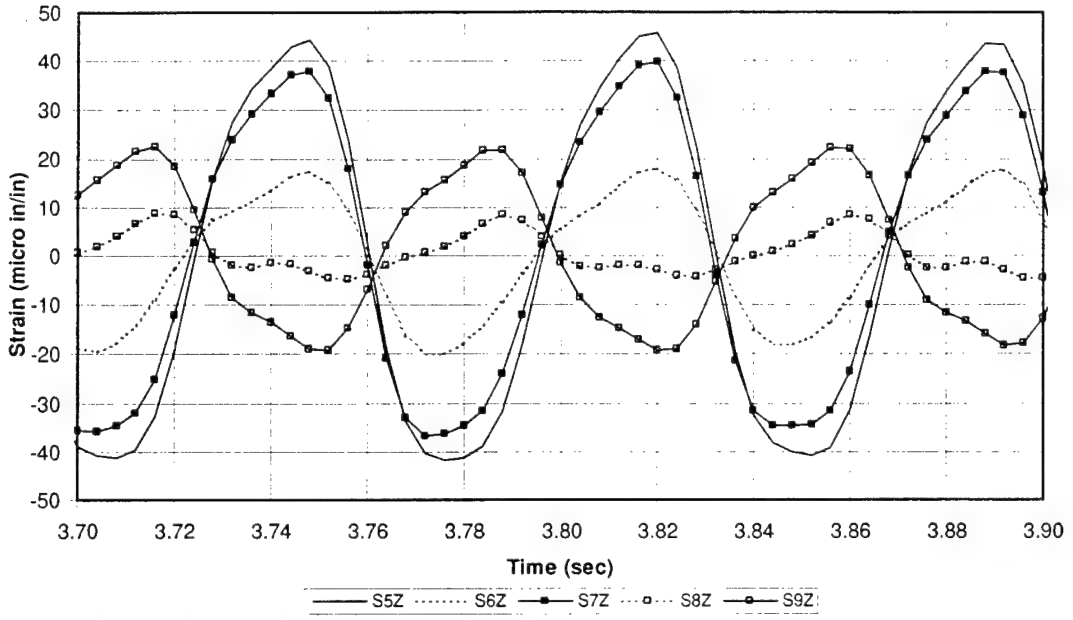

Figure 29. Strain measurements along the front face.

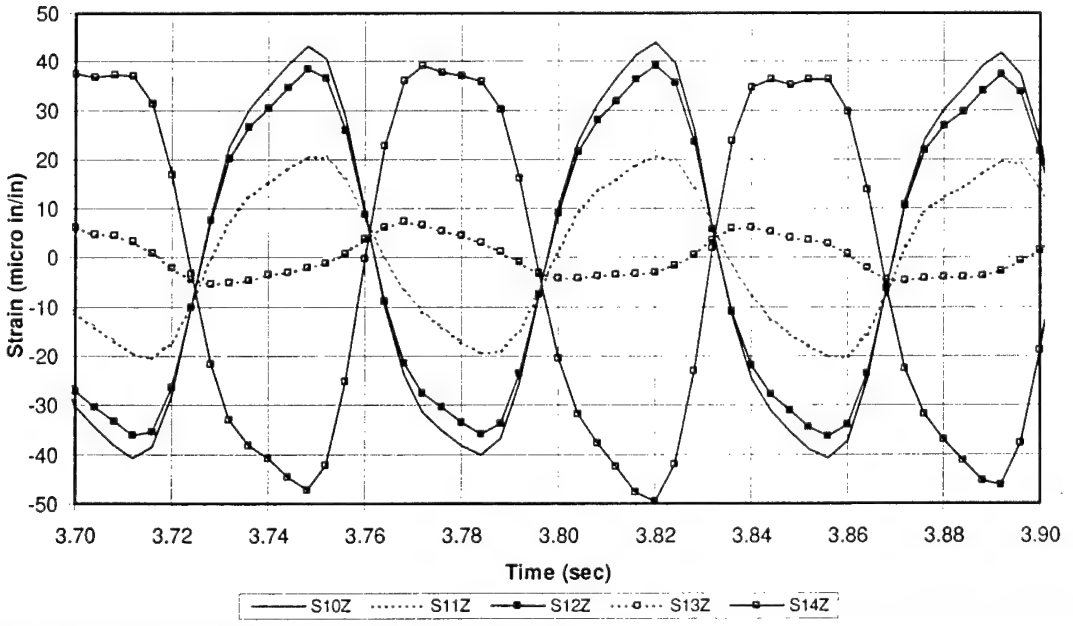

Figure 30. Strain measurements along the back face.

Measured Deformations for Linear Tests

Deformations of the Koyna dam model were measured in the region of the expected failure using linear variable differential transformers (LVDTs). Each of these sensors measured the relative deflection between two points 8 in. (200 mm) apart at the locations shown in Figures 8 through 11, with the midpoint between these points shown in Table 5 (see Chapter 3). The LVDT measurements can be compared with nonlinear behavior (crack initiation and propagation) of numerical models. These measurements are of greater interest relative to the nonlinear response documented during the Sine6 test, but they are reported here for purposes of report organization.

The greatest deformations were measured at the downstream face across the change in slope, as expected. These sensors (D9z and D10z) measured the relative displacements between points 4 in. (25 mm) above and 4 in. (25 mm) below the change in slope. Figure A15 in Appendix A shows the orientation of these sensors. Figure 31 shows these LVDT measurements for sensors D9z and D10z, for 3.7 and 3.9 sec the same time range as the accelerometer, displacement and strain data presented previously. As for the other data, this time region also gives the greatest LVDT measurements, which for D9z is -0.0017 in. (0.042 mm) at 3.704 seconds. Figure 31 shows that the deformations measured at the other LVDT on the downstream face (D10z) are in phase with and only slightly less than D9z. Figure 32 shows the D9z deformations for the entire duration of the Sine5 test. Table 9 provides the time and value of the peak response of the D9z LVDT plus the steady-state average.

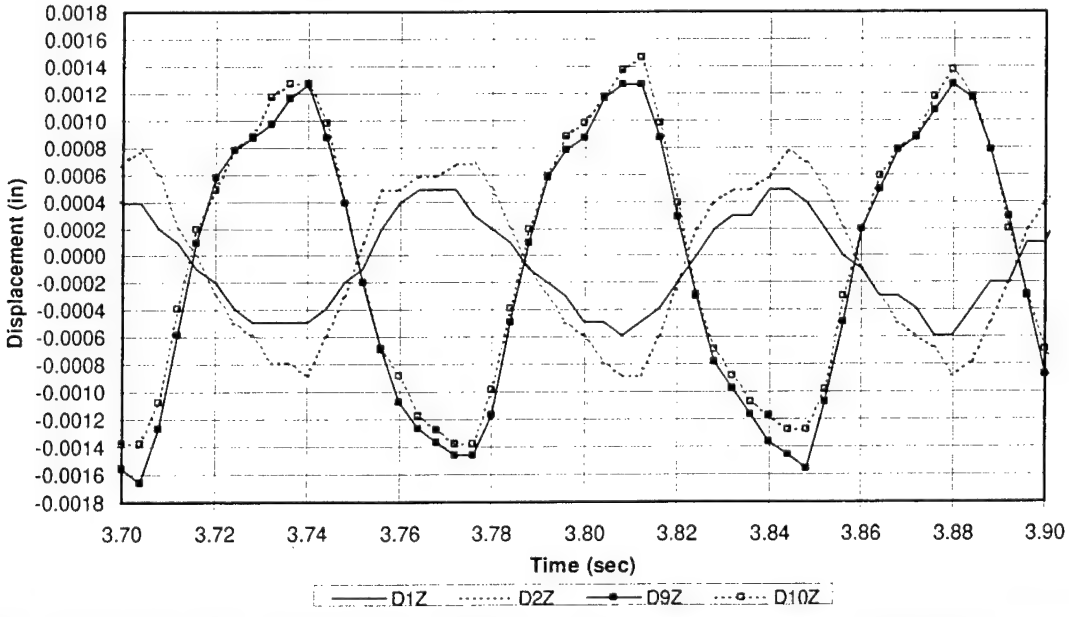

Figure 31. LVDT measurements at the upstream and downstream faces of the Sine5 test.

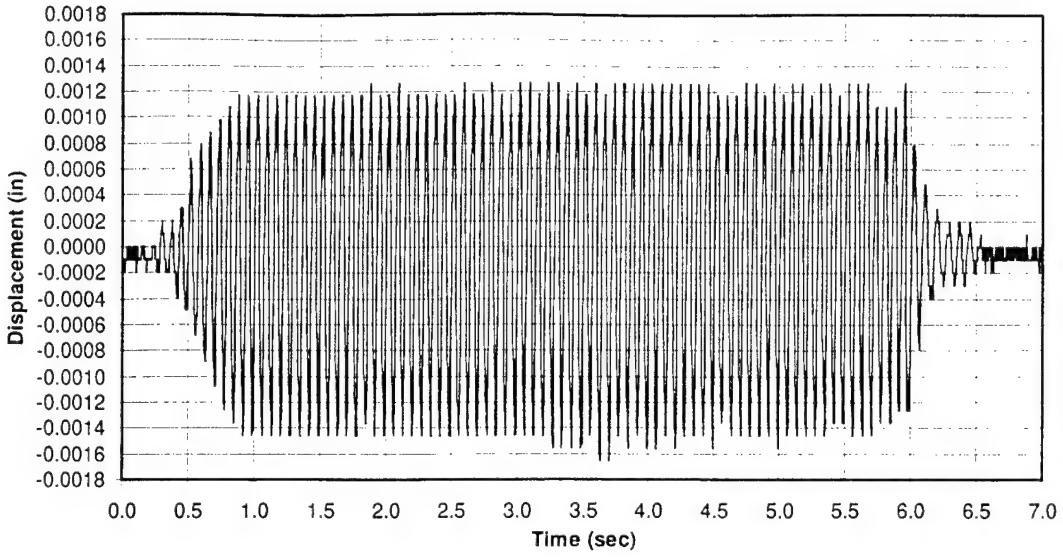

Figure 32. D9z LVDT deformation on the downstream face for the entire Sine5 test.

Deformations were also measured at two elevations on the upstream face, 111.0 in. (2.82 m) for sensor D1z and 130.7 in. (3.32 m) for D2z. These deformations are shown in Figure 31 for the 3.7 to 3.9 second time region. The deformations measured at D2z are always greater than D1z, but less than either LVDT on the downstream face. The D2z deformations are expected to be greater than D1z because more bending response should take place at this higher elevation. The greater bending response occurs because the D2z LVDT is directly across from the change in slope on the downstream face, which creates a narrower dam cross-section at higher elevations. Figures 33 and 34 show the deformations measured at the D1z and D2z LVDTs, respectively, for the entire duration of the Sine5 test. Table 9 provides the time and value of the peak response for both the D1z and D2z LVDTs, plus the steady-state averages.

The resolution of the LVDTs measured deformations shown in Figures 31 through 34 is 0.00010 in. (0.0025 mm) (see Table 5). The beginning and end of the records in Figures 32 through 34 clearly show this relatively coarse resolution, as much of these data are equal to the resolution. The coarse steps in amplitude throughout these records are also equal to the data resolution. The full-scale amplitude for these sensors is equal to over 100 times the maximum-recorded Sine 5 LVDT data. However, the primary purpose of the LVDT sensors was to measure crack development and propagation and a much greater full scale was needed, as seen in the nonlinear test results.

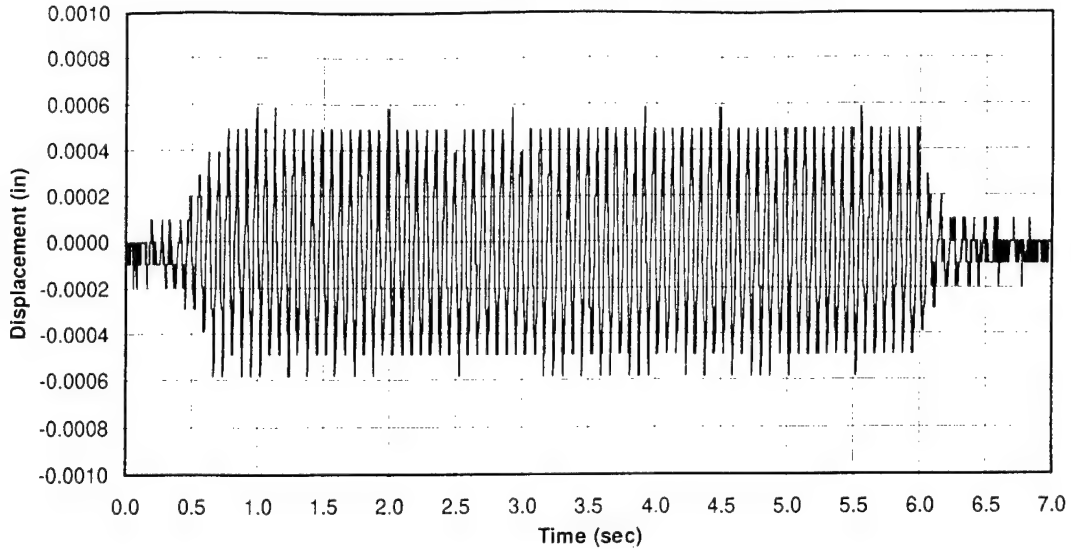

Figure 33. D1z LVDT deformation on the downstream face for the entire Sine5 test.

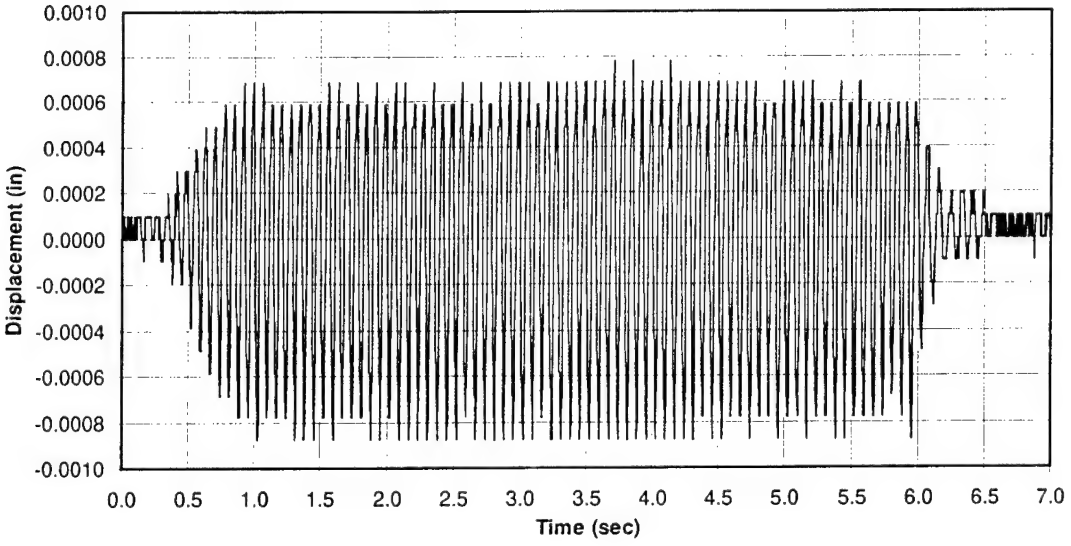

Figure 34. D2z LVDT deformation on the downstream face for the entire Sine5 test.

Deformations were also measured along the front and back faces, but these data are not presented here because they are of little interest in terms of the linear response in the Sine5 test. Almost all of the LVDT measured deformations on the front and back faces are less than those on the downstream or front faces. The only exception is the D4z, which measured slightly greater deformations than D2z.

Sinusoidal Koyna Dam Model Tests – Nonlinear Response

The data plots for the Sine5 test demonstrated linear response. Therefore, sinusoidal tests continued at increased amplitude at the same 14 Hz. The Sine6 test caused the first nonlinear response, which resulted in a crack propagating across the entire cross-section of the dam model, beginning at the change in slope on the downstream face. Figure 35 shows an overall front face view of the dam model after failure in the Sine6 test. Figure 36 shows an overall view of the back face. Figure 37 shows a close-up of the crack on the back face and Figure 38 further zooms in on this crack. Note the change in slope of the downstream face on the left side of Figure 37. This figure shows that the crack propagated diagonally down at an angle approximately perpendicular to the average slope of the downstream face above and below the change in slope. Figure 39 shows the measured coordinates of the primary crack location on the back face. Figure 39 shows that the primary crack seen on the back face in Figure 38 has a horizontal leg near the upstream face; this portion of the crack is perpendicular to the upstream face and measures 13 in. (330 mm) long. Figure 39 also shows secondary cracks (without dimensions) and spalling of the material.

Figure 40 shows a similar crack on the front face, with the horizontal portion of the crack on the left (i.e., upstream) side of the photograph. The horizontal portion of the crack in Figure 40 has been highlighted with a marker to make it more visible. Figure 41 shows that the horizontal portion of the crack on this face is 8.3 in. (210 mm) long. Figure 42 shows that the primary crack on the downstream face was very straight at the change in slope. Figure 43 shows the measured location of the primary crack, along with secondary cracks and spalling. Figures 44 and 45 show a similar drawing and photograph for the upstream face. The crack has been highlighted by a marker to make it more visible. Note the horizontal portion of the crack on the back face that can be seen intersecting the upstream face crack on the left side of Figure 45. These figures, plus observations of the crack surface after demolition, indicate that the crack surface was a fairly straight diagonal crack as described above with a horizontal portion near the upstream face.

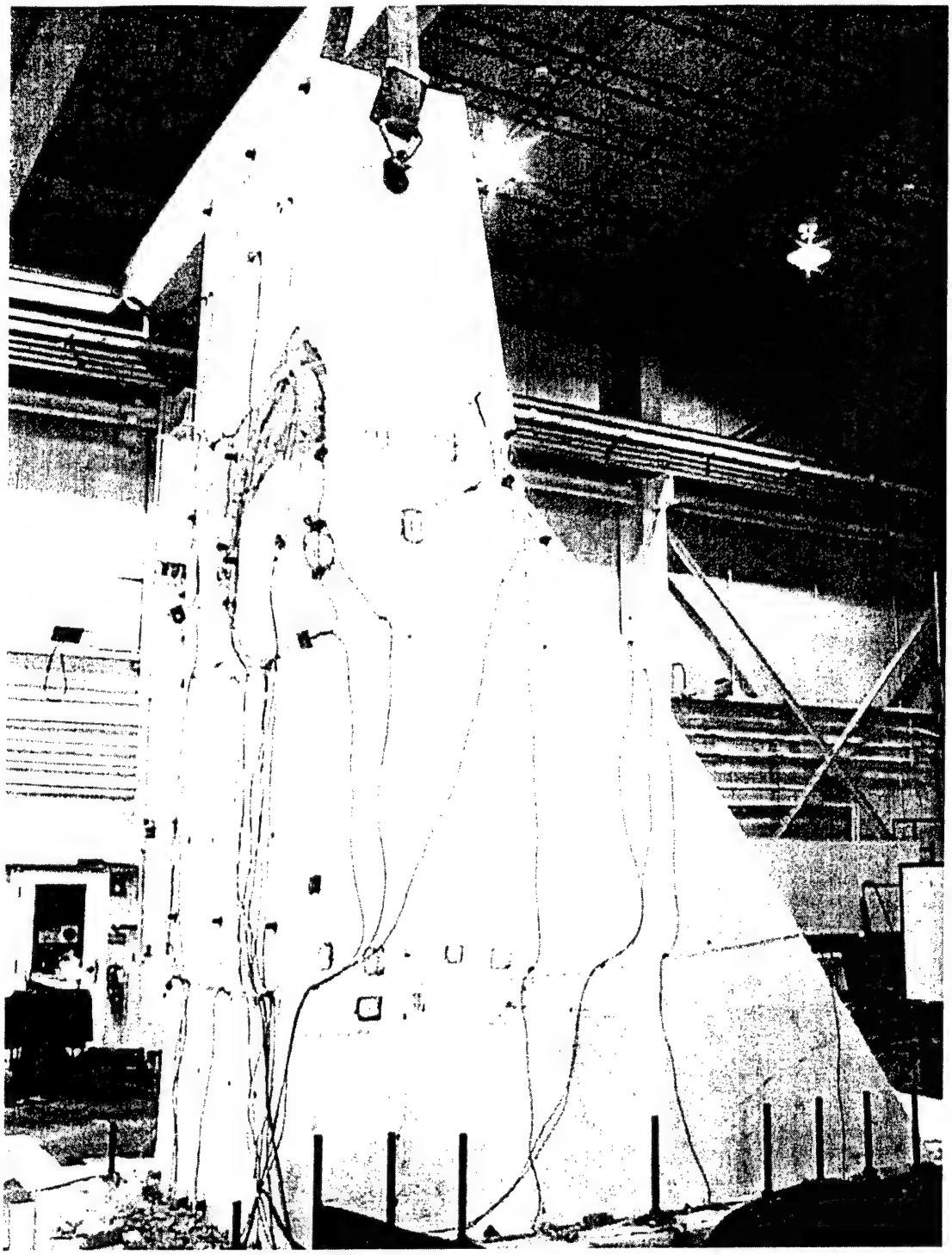

Figure 35. Overall front face view of the dam model after failure in the Sine6 test.

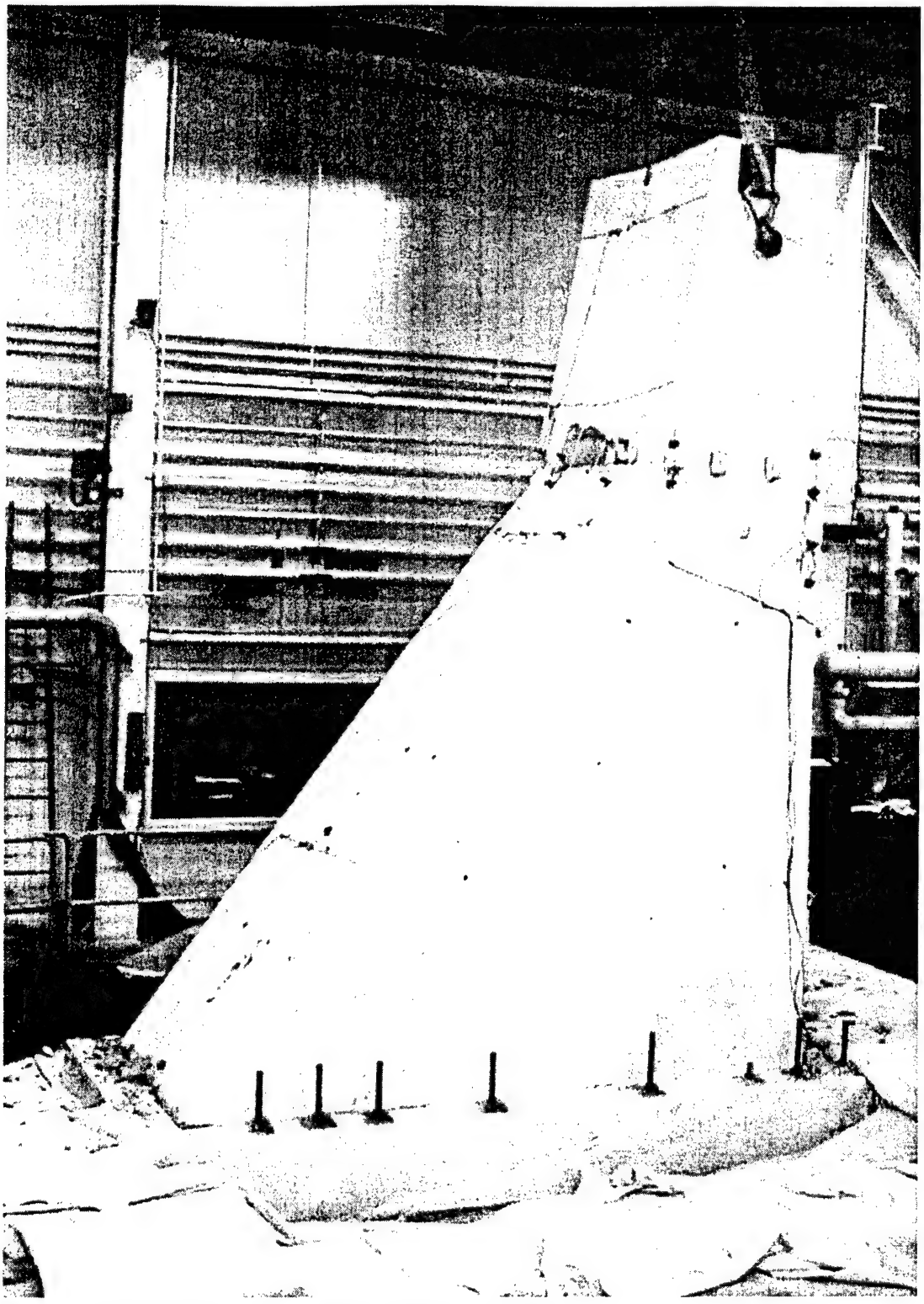

Figure 36. Overall view of the back face of the dam model.

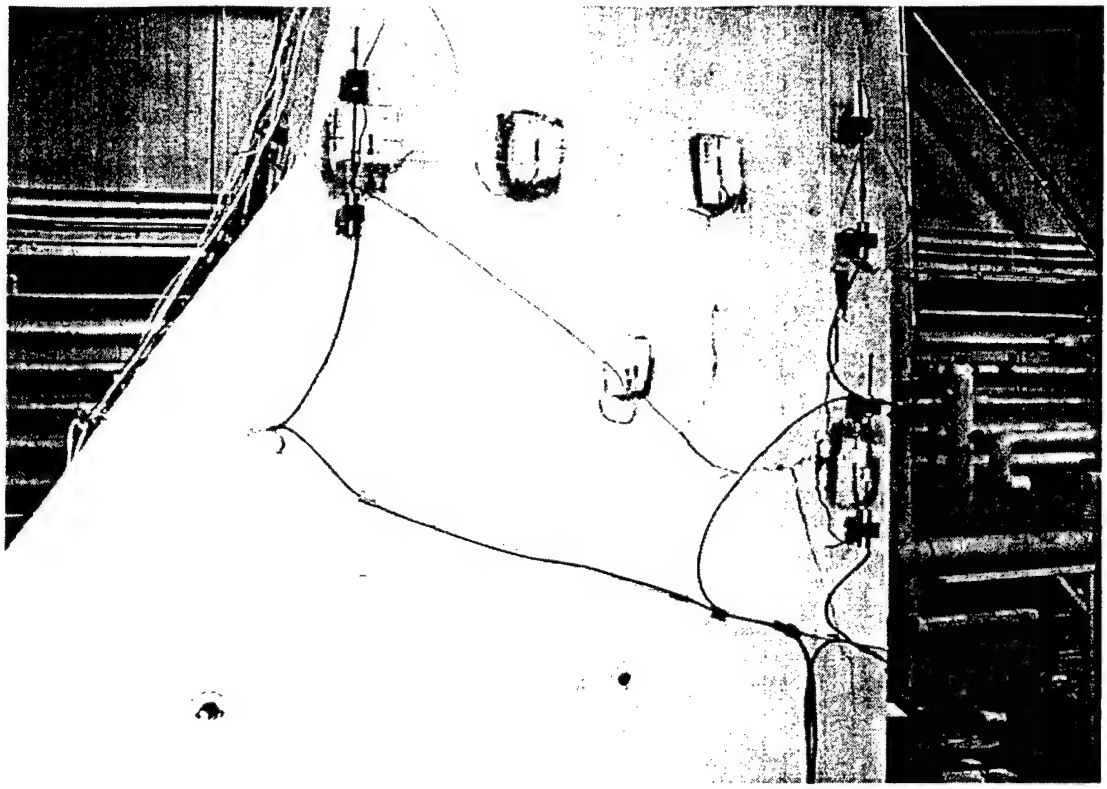

Figure 37. A close-up of the crack on the back face of the dam model.

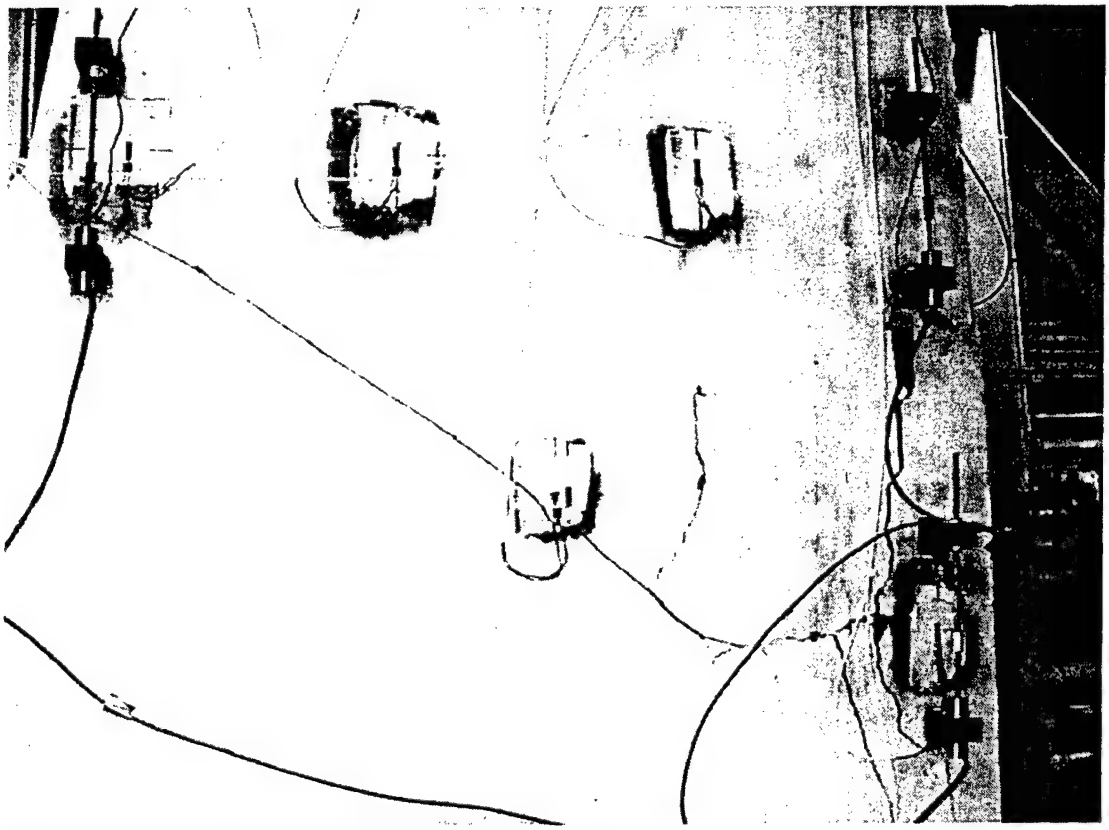

Figure 38. A closer view of the crack on the back face.

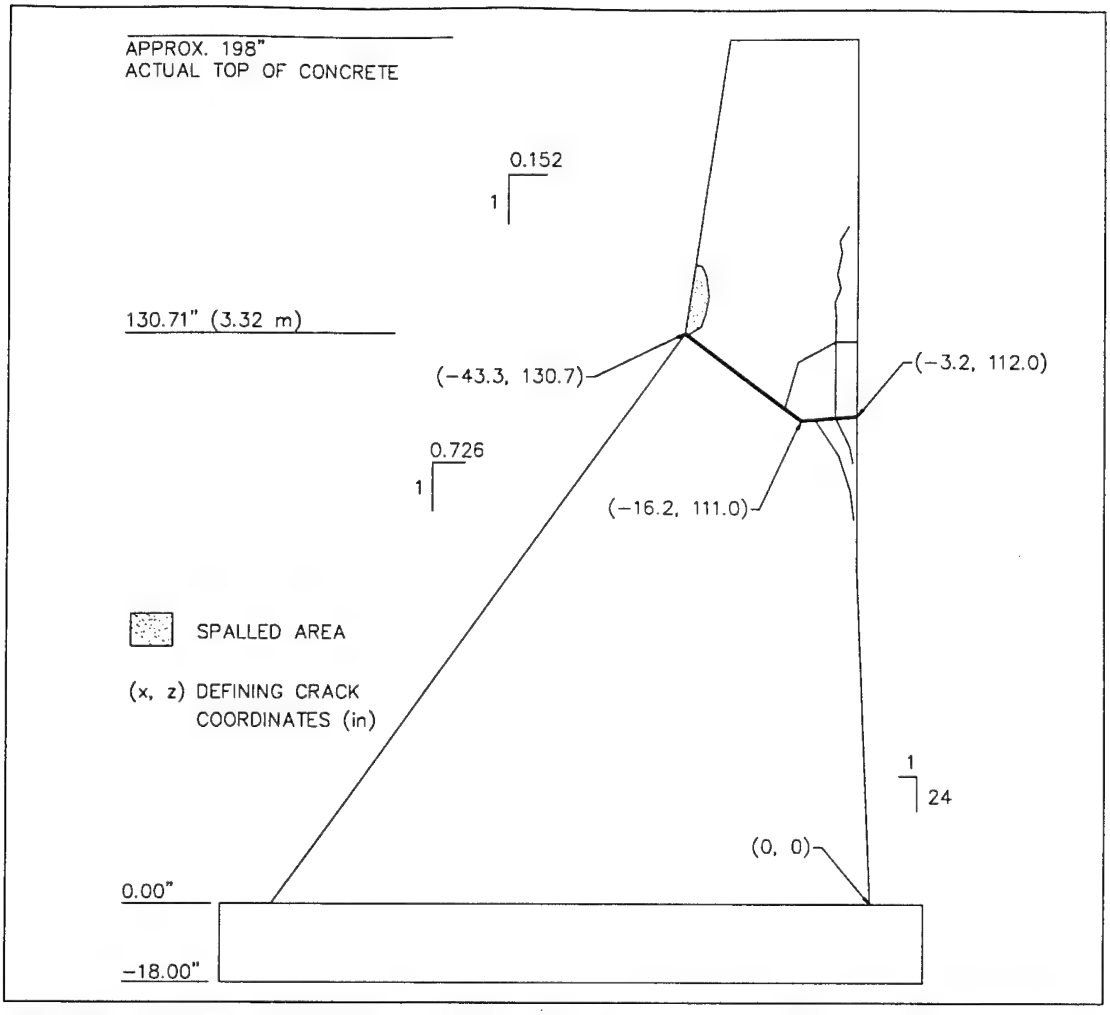

Figure 39. Measured coordinates of primary crack on the back face (with secondary cracks).

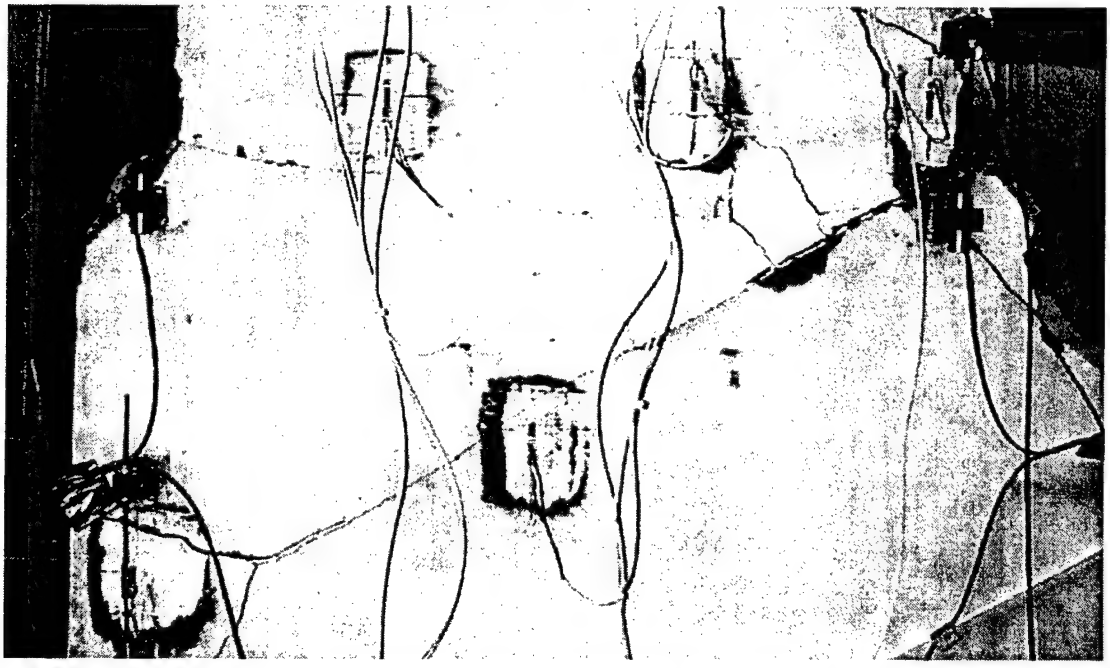

Figure 40. Crack on front face, with horizontal portion on upstream face (left).

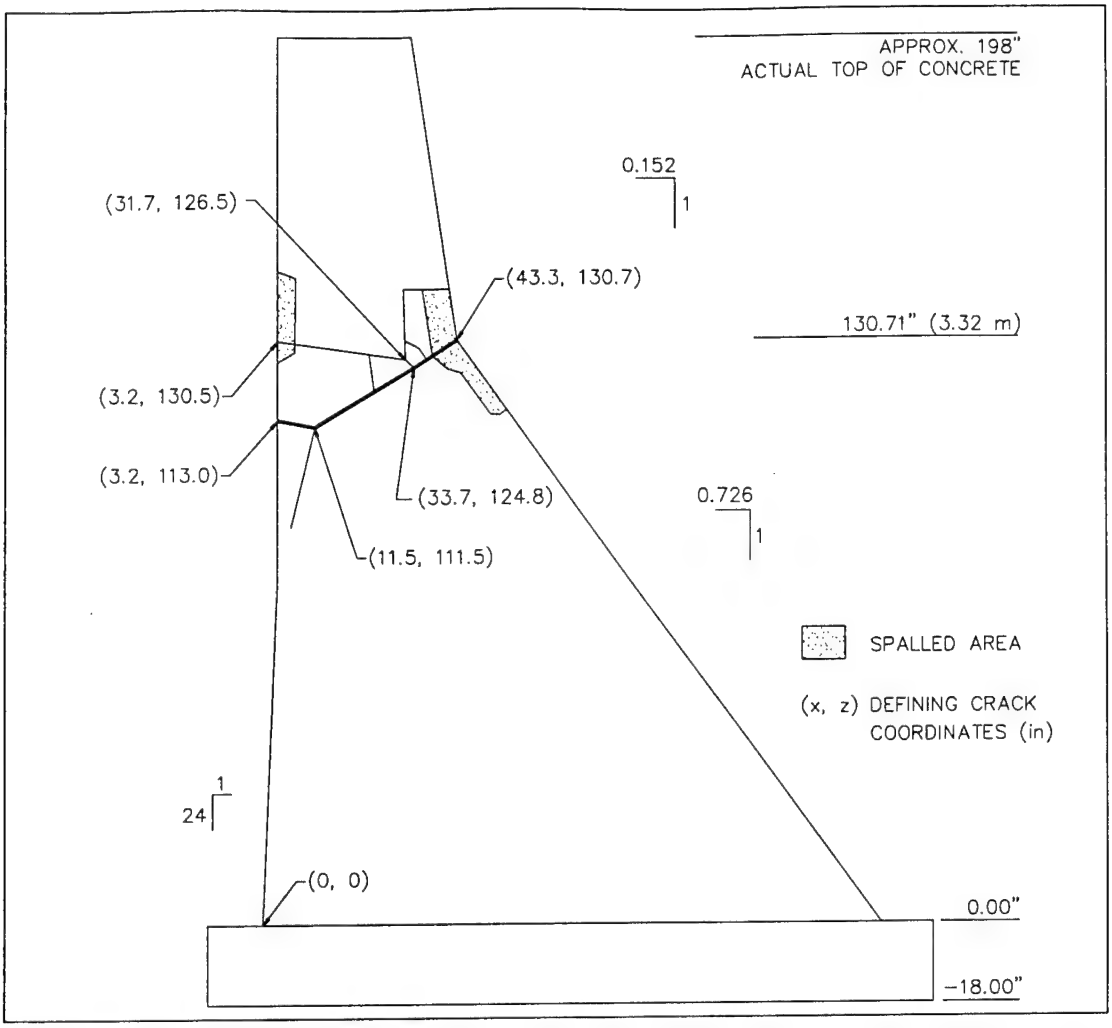

Figure 41. The horizontal portion of crack on front face, measuring 8.3 in. (210 mm) long.

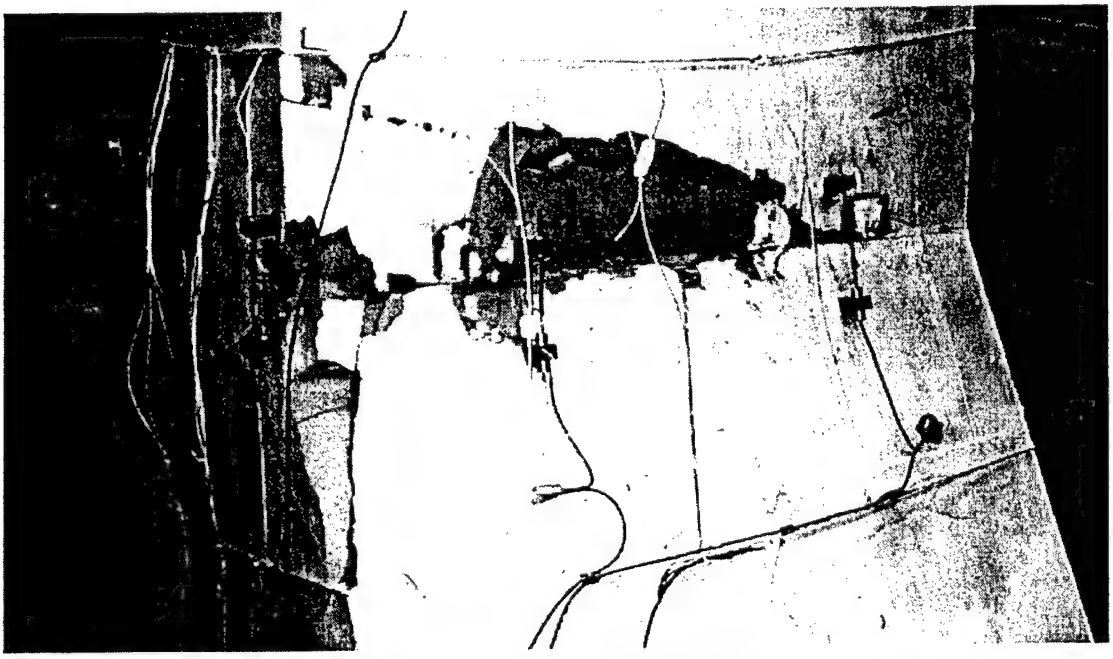

Figure 42. Virtually straight primary crack at change in slope on downstream face.

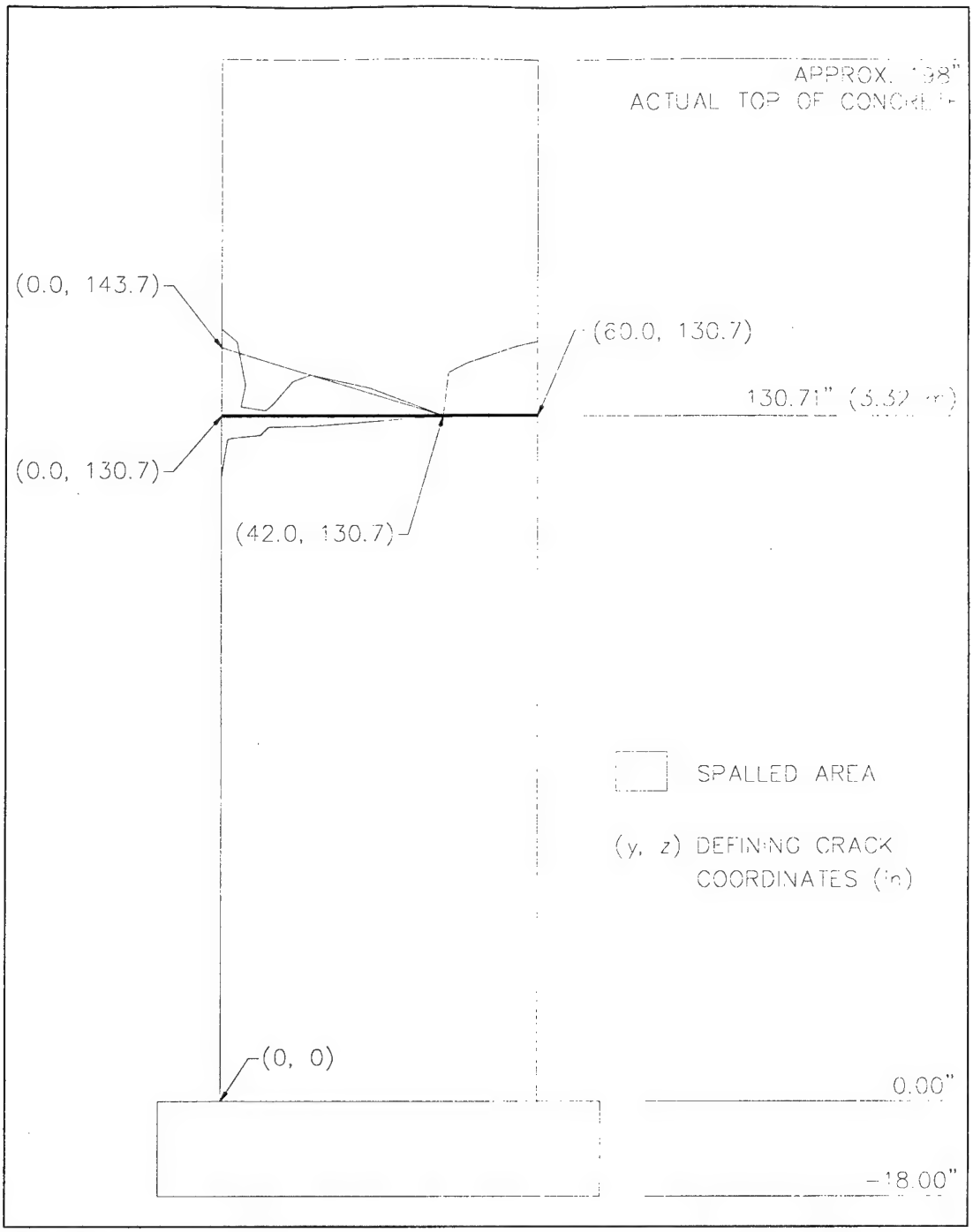

Figure 43. Drawing of the downstream face showing cracks, spalling, and primary crack coordinates.

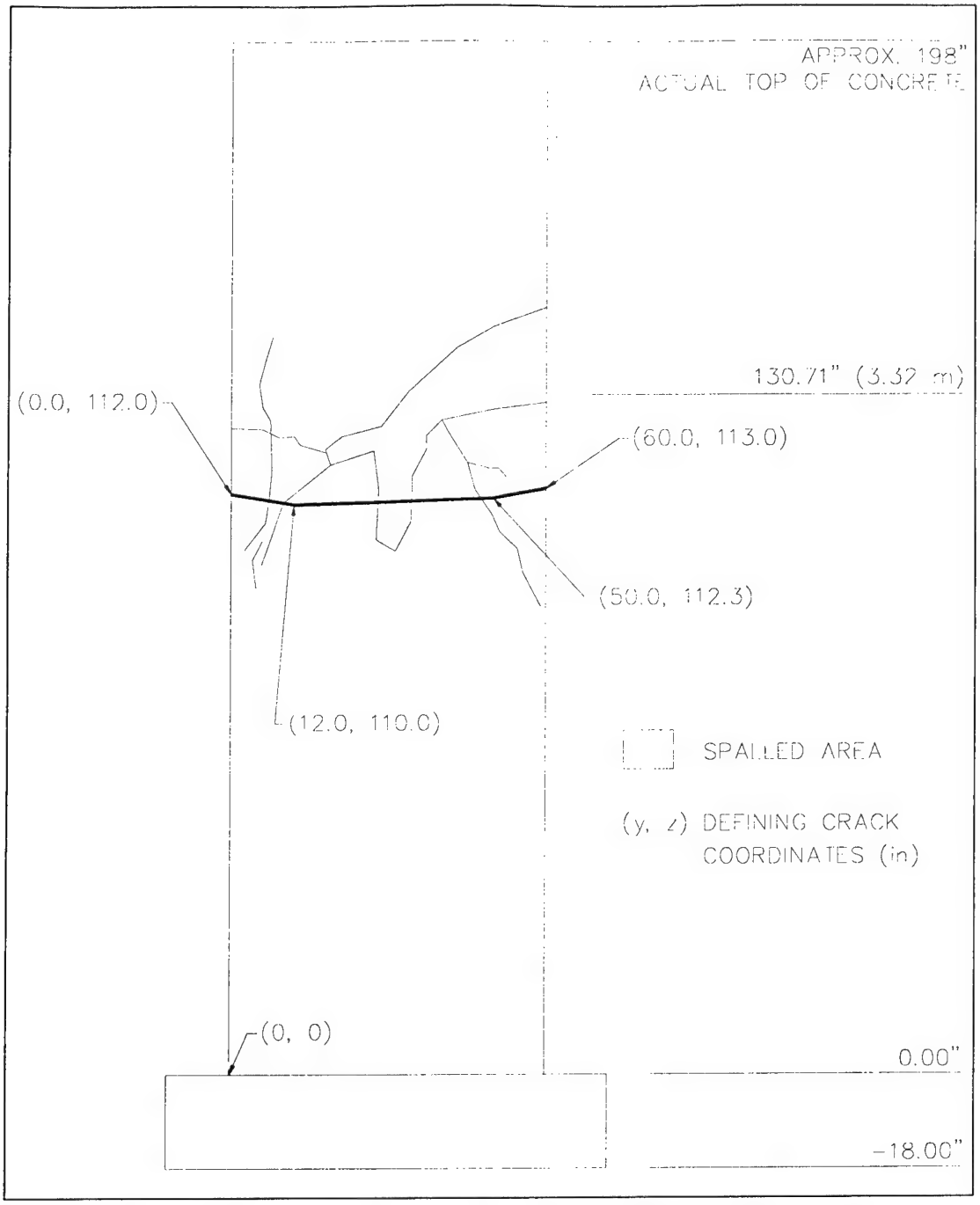

Figure 44. Drawing of the upstream face showing cracks, spalling, and primary crack coordinates.

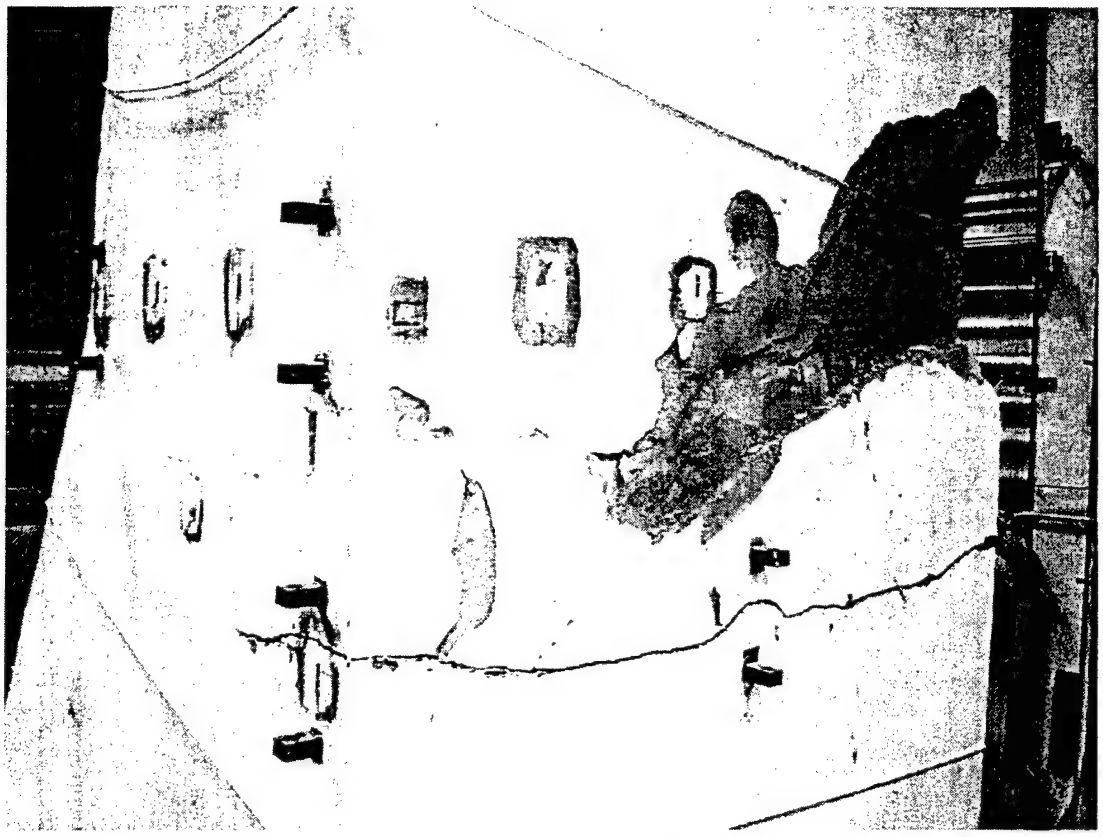

Figure 45. Close-up of the crack on the upstream face of the model.

Measured Acceleration and Relative Displacements for Nonlinear Tests

The support motions for the Sine6 test were identical to Sine5, but at an increased amplitude of 0.16 g. Figure 46 shows the sinusoidal motion at the base of the dam model (A7x) for Sine6. The first 1.4 seconds of this record agrees well with Table 8, showing the 0.16 g amplitude of the sinusoidal motion and a frequency of 14 Hz (0.07 sec/cycle). Figure 47 shows the measured (absolute) accelerations A6x, A7x, A8x, A4x, and A10x for 0.7 through 1.5 seconds. This figure shows that the upstream accelerations reached a steady-state response at 0.8 seconds and maintained those levels until crack initiation near 1.4 seconds, indicating linear model response and no damage until that time. Table 10 provides the peak measured accelerations along the upstream face (A6x, A7x, A8x, A4x, and A10x) before the initiation of the failure. For each peak value shown in Table 10, the sensor number, measurement location, and time of measurement are given. The dam model quickly reached a steady state response, before cracking, as seen in Figure 47. The average of the peak steady-state response from each cycle best reflects the response of the model, and an estimate of this value is given in Table 10. This table provides a summary of the peak linear response for each sensor measured during the Sine6 test before cracking.

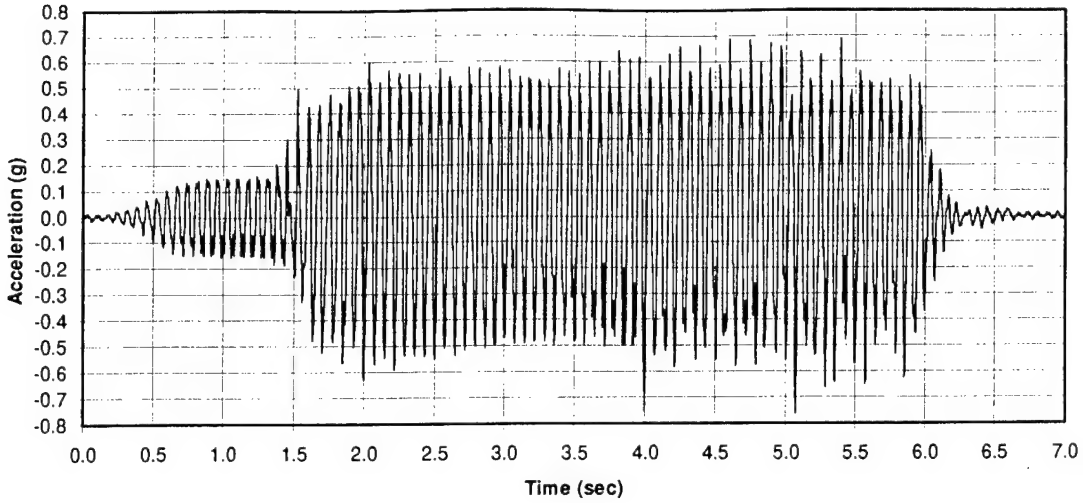

Figure 46. Support motion (A7x) for the Sine6 test.

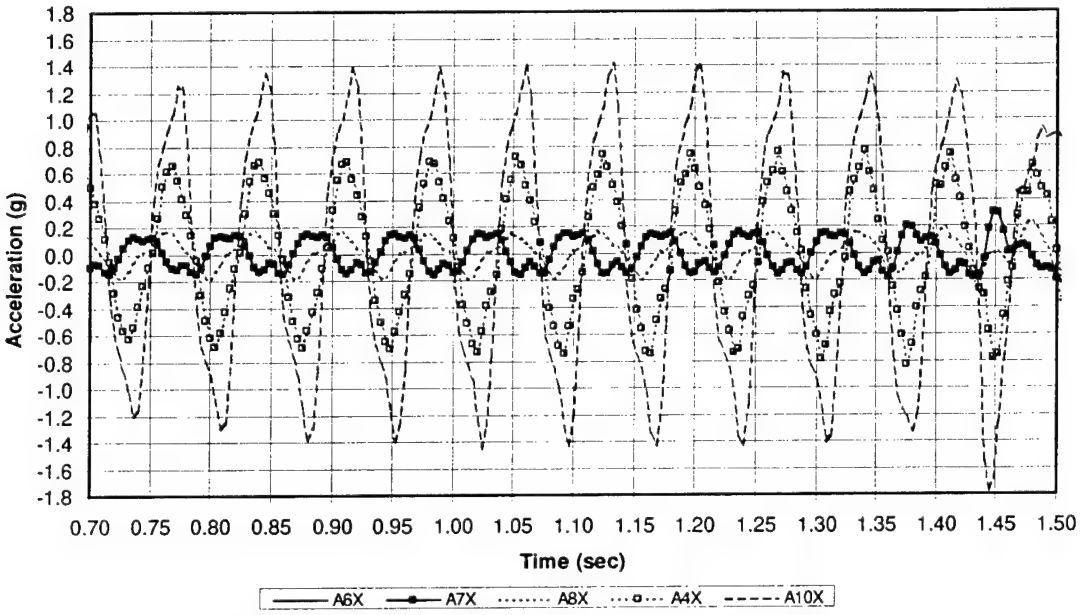

Figure 47. Sine6 measured accelerations at the base beam, model base, and elevations of 50.8 in., 129.5 in., and 195 in. for 0.7 through 1.5 seconds.

Table 10. Peak measured linear response from Sine6 test prior to cracking.

Measurement	Location	Peak Response Time (sec)	Peak Value	Steady State Value
Base Beam Acceleration, A6x	Z = -2 in.	1.376	0.223 g	0.171 g
Model Base Acceleration, A7x	Z = 3 in.	1.376	0.201 g	0.152 g
Upstream Face Acceleration, A8x	Z = 50.8 in.	1.156	-0.200 g	0.174 g
Upstream Face Acceleration, A4x	Z = 129.5 in.	1.376	0.828 g	0.74 g
Upstream Face Acceleration, A10x	Z = 195 in.	1.024	-1.455 g	1.39 g
Upstream Face Displacement, $DA8x_{Rel}$	Z = 50.8 in.	0.728	-0.0005"	0.0004"
Upstream Face Displacement, $DA4x_{Rel}$	Z = 129.5 in.	0.840	-0.0096"	0.0082"
Upstream Face Displacement, $DA10x_{Rel}$	Z = 195 in.	1.236	0.0255"	0.0237"
Upstream Face Strain, S3z	Z = 131.7 in.	1.356	-115 micro in/in	109 micro in/in
Downstream Face Strain, S15z	Z = 131.7 in.	1.036	-144 micro in/in	137 micro in/in
Upstream Face LVDT, D1z	Z = 111 in.	1.272	0.0008"	0.0006"
Upstream Face LVDT, D2z	Z = 130.7 in.	1.240	-0.0013"	0.0010"
Downstream Face LVDT, D9z	Z = 130.71	1.132	-0.0021"	0.0019"

At 1.27 seconds the model begins to fail, and the support motions are significantly amplified after 1.4 seconds due to shake table interaction with the model when it failed. As will be shown in later data plots, the crack propagated completely through the model soon after 1.4 seconds. Measured data immediately after 1.4 seconds are important to document failure progression. However model response at any given time after failure (e.g., 2 seconds) is not important because the damaged model behavior and loading is much different; after failure, the remaining model has completely detached from the portion above the change in slope, and this remaining portion is heavily loaded by impact with the loose portion above the crack. Therefore, data are plotted only to approximately 2 seconds.

Figure 48 shows the measured acceleration from this test at the base beam (A6x) and elevations (Z-coordinate in Table 3) of 3 in. (A7x), 50.8 in. (A8x), 129.5 in. (A4x), and the top of the model at 196 in. (A10x). The locations of these sensors are given in Table 3. All of these acceleration measurements were taken from the center of the upstream face except for A4x. A4x measurements agreed very well with A14x and A19x before significant cracking at 1.4 seconds, but after 1.4 seconds the measurements differed significantly. Therefore, the data at A4x are reported alone; averaging the values with A14x would significantly reduce the plotted values after 1.4 seconds because the A4x and A14x measurements are out of phase with each other after this time. A4x was plotted rather than A14x be-

cause the data from A14x were completely lost at 3.5 seconds when the model surface spalled at this gage location.

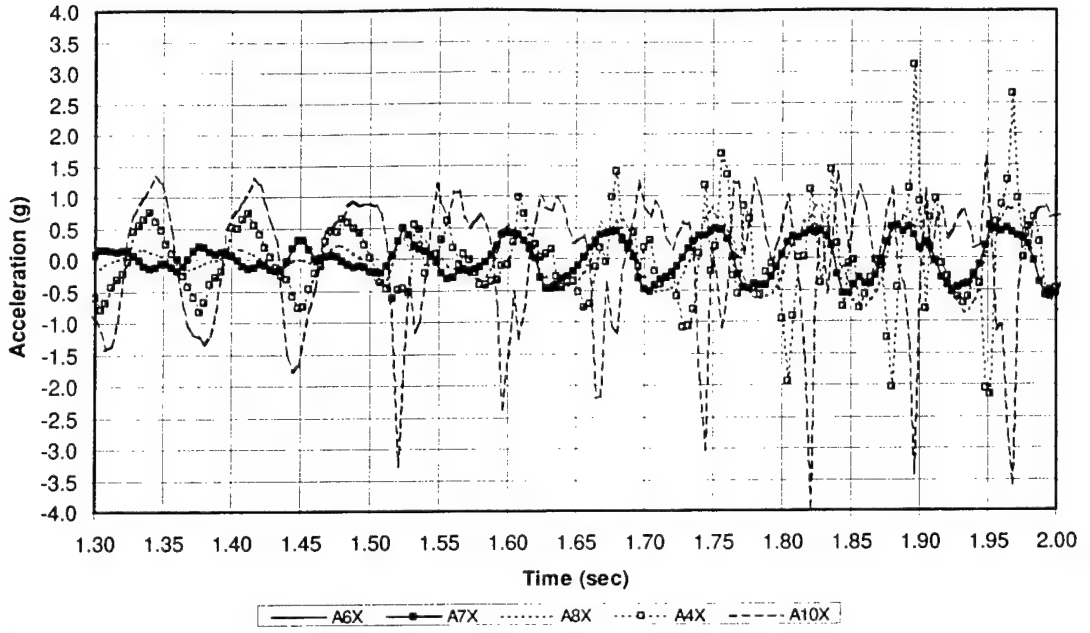

Figure 48. Sine6 measured accelerations at the base beam, model base, and elevations of 50.8 in., 129.5 in., and 195 in. for 1.3 through 2.0 seconds.

The Sine6 sinusoidal data shown in Figures 47 and 48 cover three regions: 0.8 to 1.35 seconds in Figure 47, showing linear steady-state response before crack initiation; 1.35 to 1.9 seconds in Figure 48, showing crack propagation; and after 1.9 seconds when the failed model reached a steady-state behavior (also in Figure 46). After 1.9 seconds the response of the model remained fairly constant except were the surface of the model spalled and the sensor was lost due to later secondary cracks. Figure 48 shows that the model base acceleration (A7x) differs only slightly from the base beam acceleration (A6x) even after model failure. The model response accelerations (A8x, A4x, and A10x) are out of phase with the input acceleration (A6x and A7x) due to the response of the model and some overturning response at the base. The response of the model after 1.4 seconds shows significant amplification and high-frequency spikes due to impact as the fractured portion of the model rocks back and forth.

The Sine6 test also had significant overturning accelerations, as seen by the vertical accelerations at the upstream (A7z) and downstream (A17z) base of the model, shown in Figure 49. These accelerations are out-of-phase with each other, demonstrating the overturning motion of the TESS. As with the linear results in the Sine5 test, the absolute accelerations and relative displacements are reported. Relative displacements were calculated following the same procedure defined for the Sine5 linear test results. These relative displacements

along the upstream face ($DA8x_{Rel}$, $DA4x_{Rel}$, and $DA10x_{Rel}$) are plotted in Figure 50 for the 1.3 to 2.0 second region of the Sine6 test. This plot shows that the deformations of the model represented by the relative displacements remain constant until 1.43 seconds. Table 10 provides the peak relative displacements along the center of the upstream face ($DA8x_{Rel}$, $DA4x_{Rel}$, and $DA10x_{Rel}$), before crack development. Table 10 also provides an average steady-state response of the relative displacements.

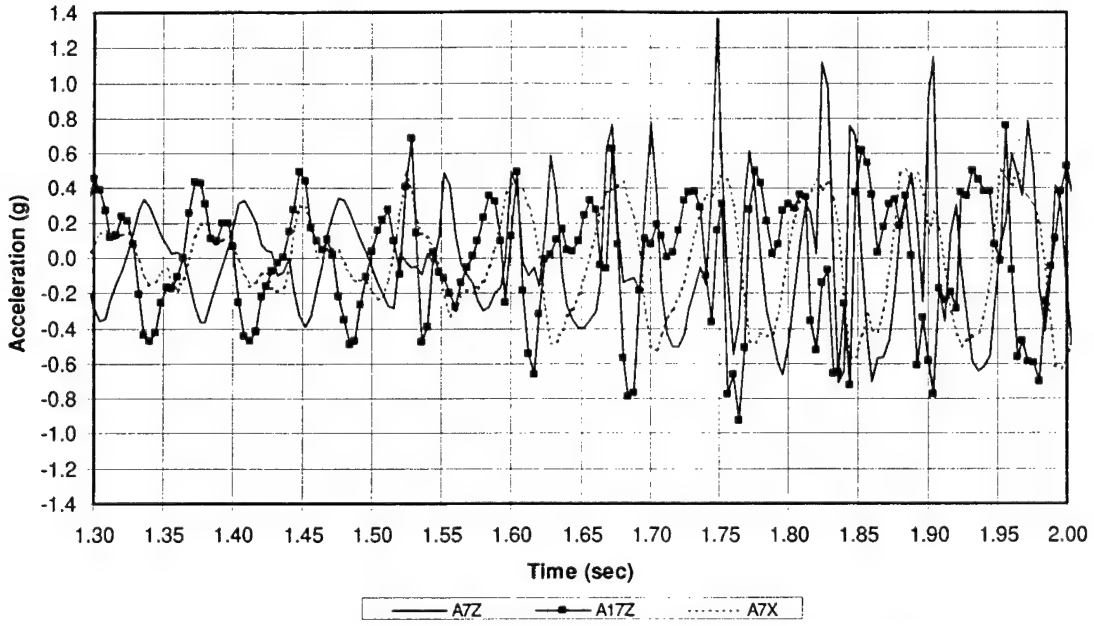

Figure 49. Sine6 overturning accelerations relative to in-plane horizontal accelerations.

Figure 50 shows that the relative displacement at the top of the model ($DA10x_{Rel}$) begins to increase at 1.43 sec. The relative displacement at the top reaches a peak positive value of 0.0318 in. (0.81 mm) at 1.448 sec, followed by a peak negative value of –0.0342 in. (-0.87 mm) at 1.500 sec. The relative displacements prior to cracking (before 1.43 sec) at each level on the upstream face ($DA8x_{Rel}$, $DA4x_{Rel}$, and $DA10x_{Rel}$) are due to model bending. Then, after cracking, the increase in relative deflection is primarily due to crack opening and rotation of the model above the crack. The influence of model rotation above the crack is much greater for $DA10x_{Rel}$ because the sensor is 84 in. (2.13 m) above the crack on the upstream face, while the sensor for $DA4x_{Rel}$ is only 20 in. (0.51 m) above this crack. While the pounding effect of the crack opening and closing does increase accelerations, these high-frequency spike accelerations have little influence on displacements. Figure 50 shows that the $DA4x_{Rel}$ displacements increase slightly at 1.500 sec. The relative displacements at both $DA4x_{Rel}$ and $DA10x_{Rel}$ increase further in later cycles, as shown in Figure 50. As expected, relative displacements never increase at $DA8x_{Rel}$ because the A8x sensor was below the crack.

Measured Strains for Nonlinear Tests

Table 4 and Figures 8 through 11 (Chapter 3) show the location of all strain gages. The greatest strains were again measured at the downstream face near the change in slope. Strains occurring before initiation of the crack can be compared with the linear behavior of numerical models. As was seen in the Sine5 linear test, strain gage S15z provides the best average of the gages along the downstream face. Figure 51 shows the strain measured at S15z through 2.0 seconds of the Sine6 test. Strain gage S3z provides the best average of the gages along the upstream face, and Figure 52 shows these measurements through 2.0 seconds. Table 10 provides the time and value of the peak response of strain gages S3z and S15z prior to cracking. Table 10 also provides the steady-state average strains for S3z and S15z prior to cracking.

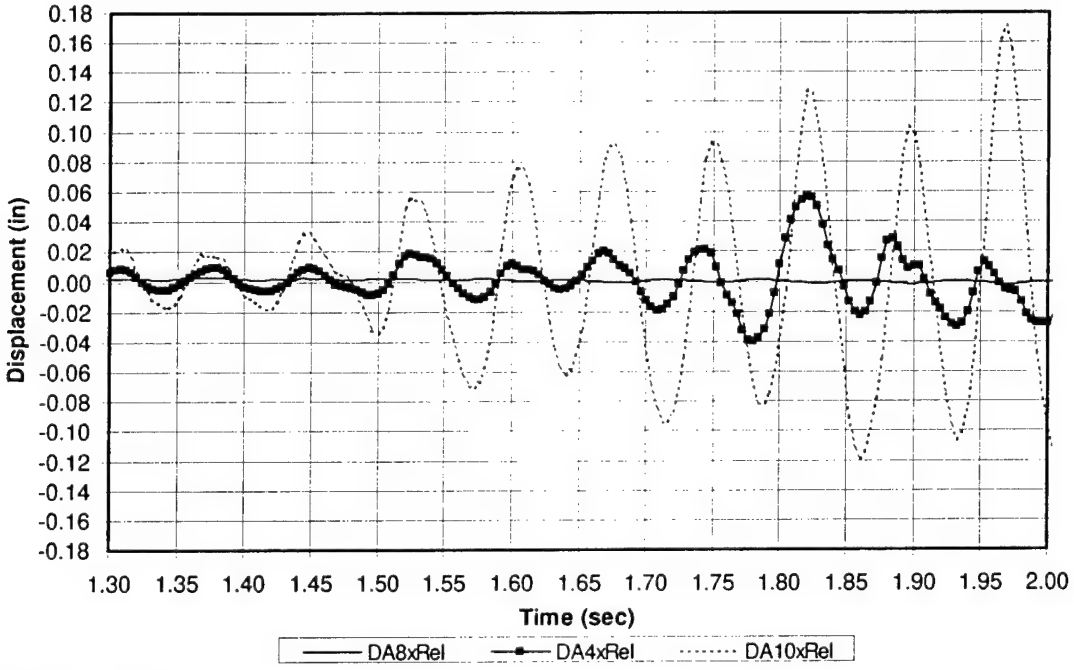

Figure 50. Relative displacements along upstream face showing dam distortions for Sine6 test.

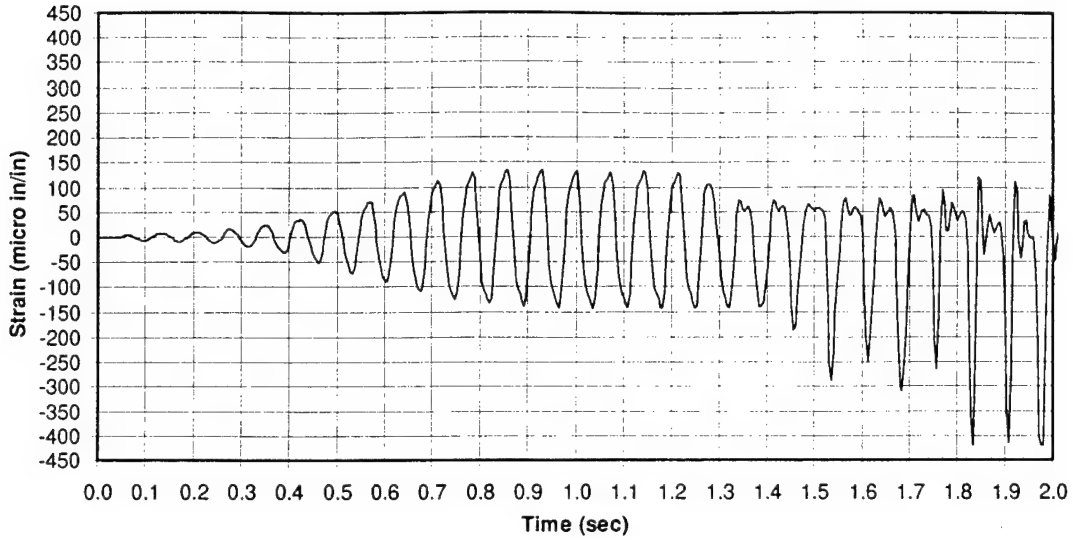

Figure 51. Sine6 strain measurements at S15z along the downstream face.

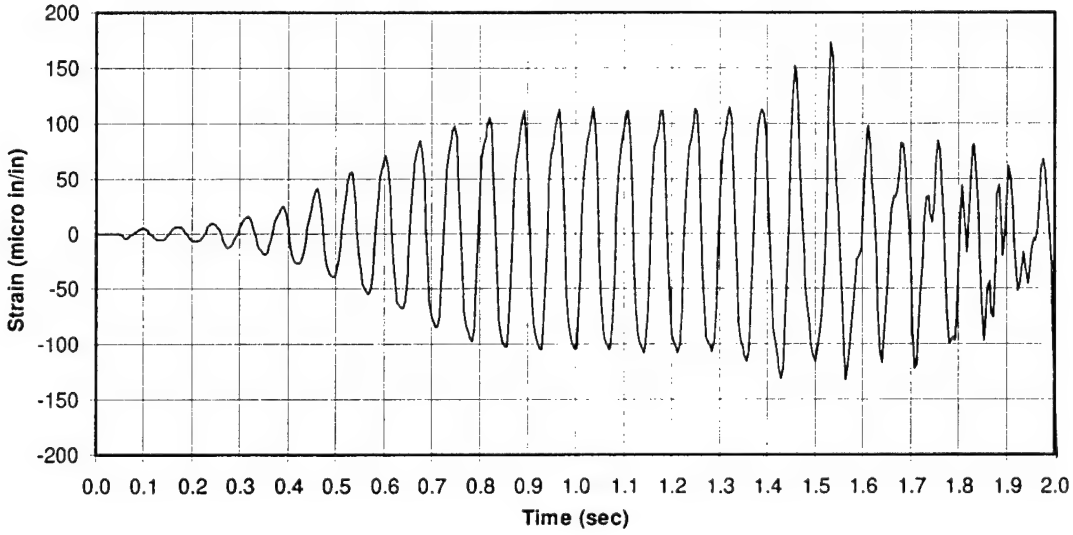

Figure 52. Sine6 strain measurements along the upstream face at S3z only.

Figure 53 shows these strain measurements for all four gages on the downstream face (S15z, S16z, S17z, and S18z), for 1.2 through 2.0 seconds. The strains cycle uniformly until about 1.27 seconds when as shown in Figure 53, both the S15z and S16z (S16z is more visible) strains begin to decrease and flatten on the positive (tension) side of the oscillation. The primary crack forms at the change in slope on the downstream face, which is just 1 in. (25 mm) below the center of the strain gages on this face. The decrease in amplitude of tensile strain and flattening in these gages indicate that the material has weakened and the crack has begun to form. Figure 53 shows that both the S15z and S16z strain on the tensile side of the oscillation has decreased significantly at 1.33 seconds and even further at 1.41 seconds. However, Figure 53 shows that the

S17z and S18z strain gages do not show a decrease until 1.41 seconds, indicating that the crack on the downstream side took three cycles (1.27 sec to 1.41 sec) to propagate across the downstream edge of the crack surface. This suggests the crack began near the front face of the downstream face, which is closest to the S15z strain gage. Figure 53 shows that tensile strains further reduce in later cycles. This figure also shows that the compressive strains begin to increase soon after the tensile strains have reduced and flattened. This indicates that some impact loading took place as the crack began to open and close, creating compression spikes at the strain gages. At 1.83 seconds, Figure 53 shows the amplitudes of impact-induced compression spikes have increased significantly. Figure 53 shows that the compression spikes in later cycles maintain this same amplitude, suggesting that the portion of the model above the crack rocks freely back and forth with each cycle after 1.83 seconds. However, the S15z strain gage reached its full-scale amplitude of 420.1 micro in./in. (see Table 4 for strain gage full scale) at 1.832 seconds, and S15z, S16z, and S17z all reached their full-scale amplitude at 1.976 seconds. Therefore, the true impact-related compression stains might have had spikes of greater amplitude than shown in these plots because the plotted data are limited to the full-scale level. Later cycles begin to indicate smaller tension spikes after 1.84 seconds. These appear to be reflections of strain from the much higher compression spikes after impact.

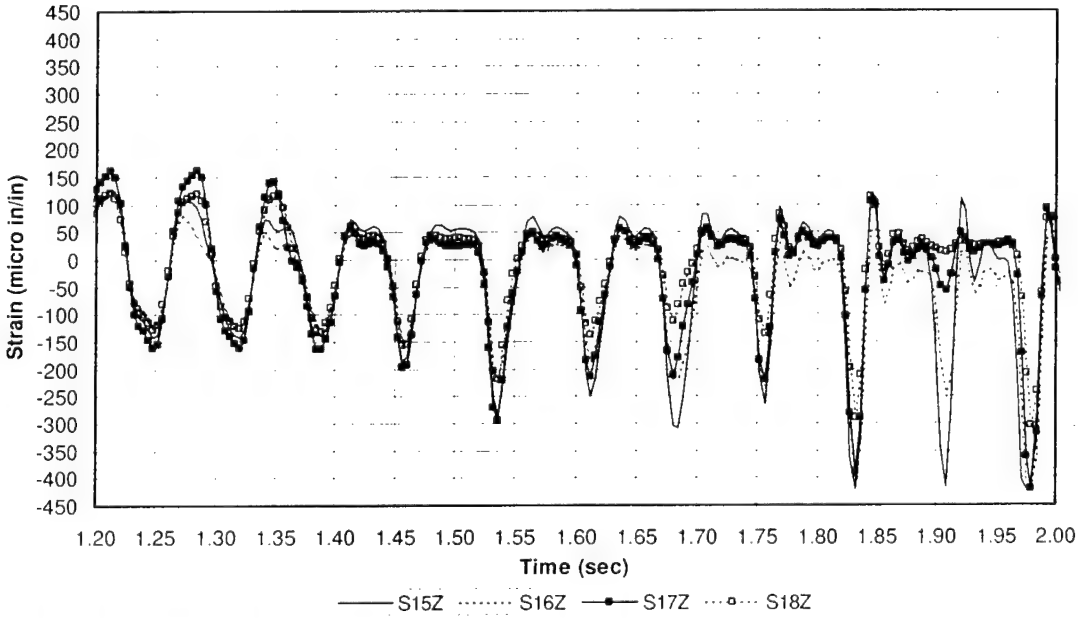

Figure 53. Sine 6 strain measurements along the downstream face.

Strain measurements along the upstream face (S1z, S3z, and S4z) are shown in Figure 54 for the 1.3 to 2.1 second time region. The amplitude of these measurements begins to increase at 1.45 seconds with a tension spike (positive in

Figure 54). Because the dam model is responding in bending, the upstream face strain gages are in tension when the downstream gages are in compression. Therefore, the downstream compression spike at 1.45 seconds (see Figure 53) that resulted from the crack forming on downstream face causes a related tension spike on the upstream face. The amplitude of the next downstream compression spike grows in the next cycle, at 1.53 seconds, due to greater impact loading, and the amplitude of the related tension spike shown in Figure 54 also grows at 1.53 seconds. Figure 54 also indicates that at 1.56 seconds the compression (negative in Figure 54) side of the oscillation loses its previously rounded shape, creating a compression spike. This indicates that the crack has propagated all the way through the dam cross-section to the front face at 1.56 seconds because the compression spike was probably created by impact as the crack closed.

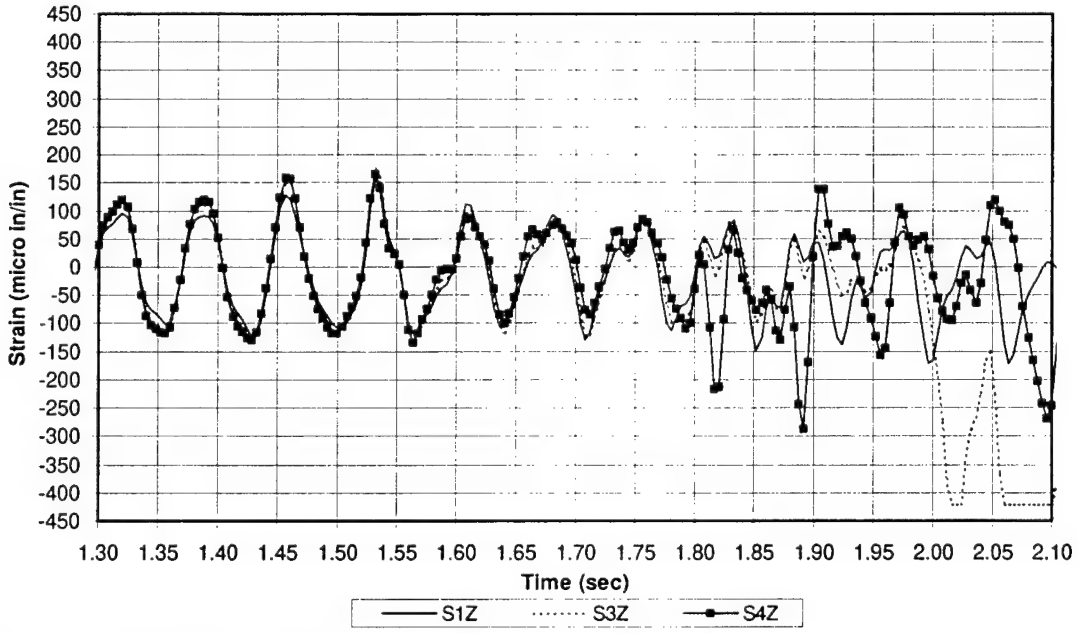

Figure 54. Sine6 strain measurements along the upstream face.

The next tension spike, at 1.61 seconds, has smaller amplitude because tension is now limited by the cracking. However, much greater tension strain is developed at the upstream face gages than downstream because the upstream gages are located about 20 in. (500 mm) above the primary upstream crack surface while the downstream gages are only 1 in. (25 mm) above the downstream crack. The greater distance to the crack allows the development of greater tension strains, including the tension spike related to the compression impact on the downstream face. Table 11 summarizes the progression of failure along the primary crack surface based on the above interpretations of strain gage data. Finally it should be noted that the large compressive strains shown at S3z that be-

gin at 2.0 seconds are not true readings, but rather the result of surface spalling at this location (see Figures 8 and 45). The only sensors that truly exceeded their full-scale range were S15z, S16z, and S17z after complete model cracking and resulting compression spikes shown in Figure 53.

Table 11. Primary crack development and progression based on strain gage and LVDT data.

Time (sec)	Crack Development Description	Evidence for Crack Development
1.27	Crack initiation at the downstream face	Reduction and flattening of tension strains at the downstream face near the front face seen at the S15z and S16z in Figure 53
1.27	Crack initiation at the downstream face	Deformation measurement increase seen at D9z in Figure 59
1.33	Crack appears to begin at the downstream face near the front face	S15z and S16z in Figure 53
1.41	Crack appears to have developed across the downstream face	Reduction and flattening of tension strain oscillations seen at S15z, S16z, S17z and S18z in Figure 53
1.45	Crack opening and impact at the downstream face	Spiked compression strain oscillations on the downstream face shown in Figure 53 and spiked tension strain oscillations on the upstream face shown in Figure 54
1.46	Crack opening and impact at the S9z and S14z front and back face gages near the downstream face	Spiked compression strain oscillations seen at S9z in Figure 56 and S14z in Figure 58, plus flattening of the tension spike at 1.48 sec at these sensors.
1.43 to 1.50	Shift of the neutral axis and center of rotation toward the upstream face	S6z and S11z begin in phase with the upstream gages, then from 1.43 to 1.50 sec, shift to being in phase with downstream gages (see Figures 53, 54, 56 and 58)
1.52	Crack has propagated to the upstream face and opened	Negative deformation (opening) at the D1z LVDT becomes much greater as seen in Figure 60
1.56	Crack has propagated to the upstream face	Spiked compression strain oscillations on the upstream face shown in Figure 54 and on the front (S5z) and back faces (S10z) shown in Figures 56 and 58 respectively
1.72	Crack no longer fully closes	Positive cycle of D1z LVDT in Figure 60
1.83	Portion of the model above the crack is rocking freely	Increased and amplitude compression spikes on the downstream face shown in Figure 53

The strains along the front face (S5z, S6z, S7z, S8z, and S9z) are plotted between 1.3 and 2.0 seconds in Figure 55. The plot in Figure 55 is quite cluttered visually, so Figure 56 plots the most critical S5z, S6z, and S9z data for the time range of only 1.4 to 1.85 seconds. Similarly, strains along the back face (S10z, S11z, S12z, S13z, and S14z) are also plotted between 1.3 and 2.0 seconds in Figure 57. Figure 58 plots the most critical S10z, S11z, and S14z data for the time range of only 1.4 to 1.85 seconds. Like the Sine5 test, during the linear portion of Sine6 the strain gage closest to the downstream face on the back face (S14z)

gives the largest values for this face (see Figure 57), and these measurements are smaller and in phase with the downstream measurements shown in Figure 53. During the linear response in the Sine6 test, the strain gages closest to the upstream face on both the front face (S5z and S7z in Figure 55) and back face (S10z and S12z in Figure 57) are in phase with the upstream face measurements (see Figure 54) and with each other, and they have lower magnitudes than the upstream face. During the linear response of Sine6, and with the exception of the S9z measurements (see previous discussion on linear response, page 53), the strains measured on the front and back faces agree well with the upstream and downstream measurements.

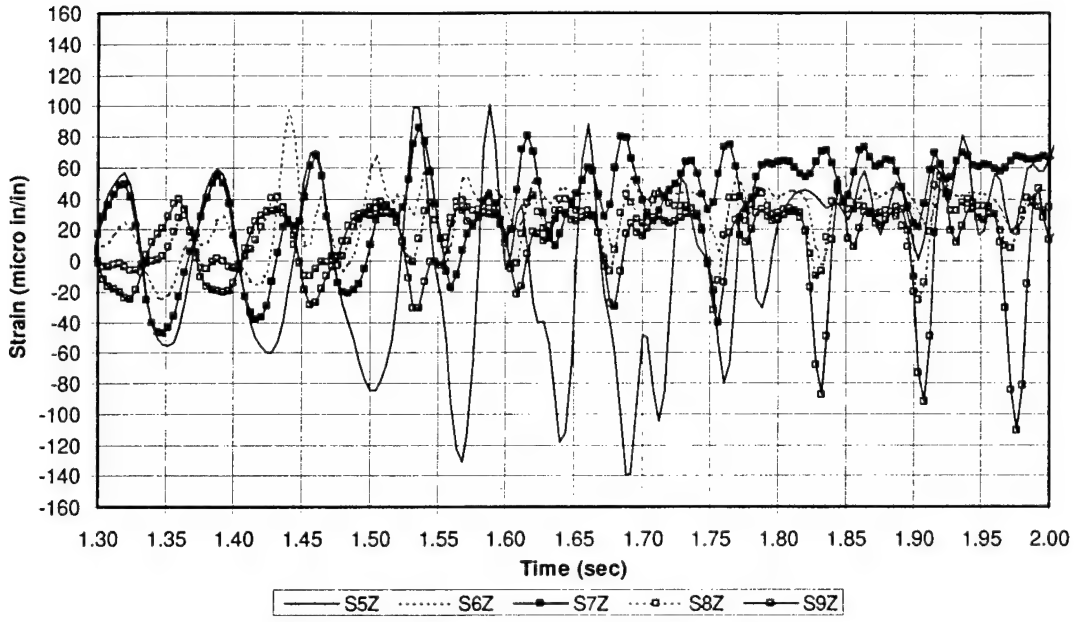

Figure 55. Sine6 strain measurements along the front face for 1.3 to 2.0 seconds.

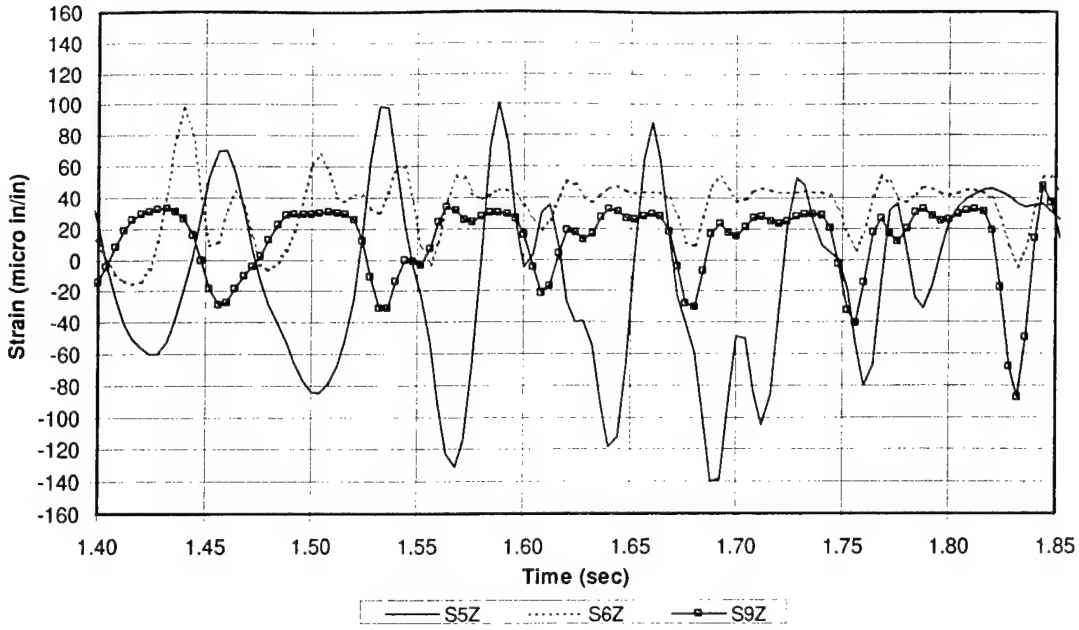

Figure 56. Sine6 front face strains for 1.4 to 1.85 seconds.

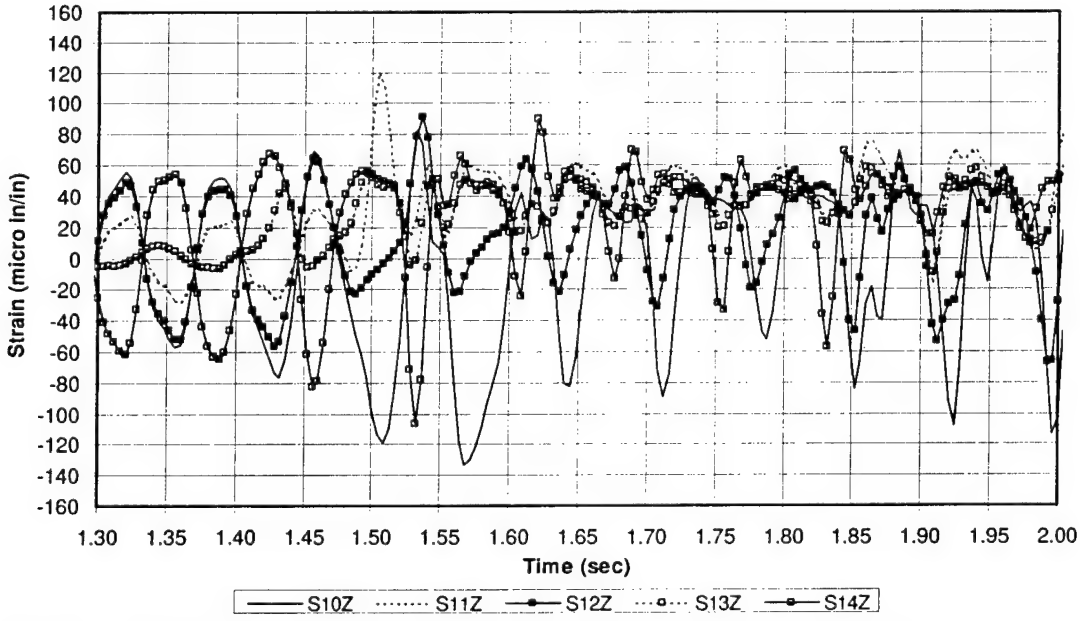

Figure 57. Sine6 strain measurements along the back face for 1.3 to 2.0 seconds.

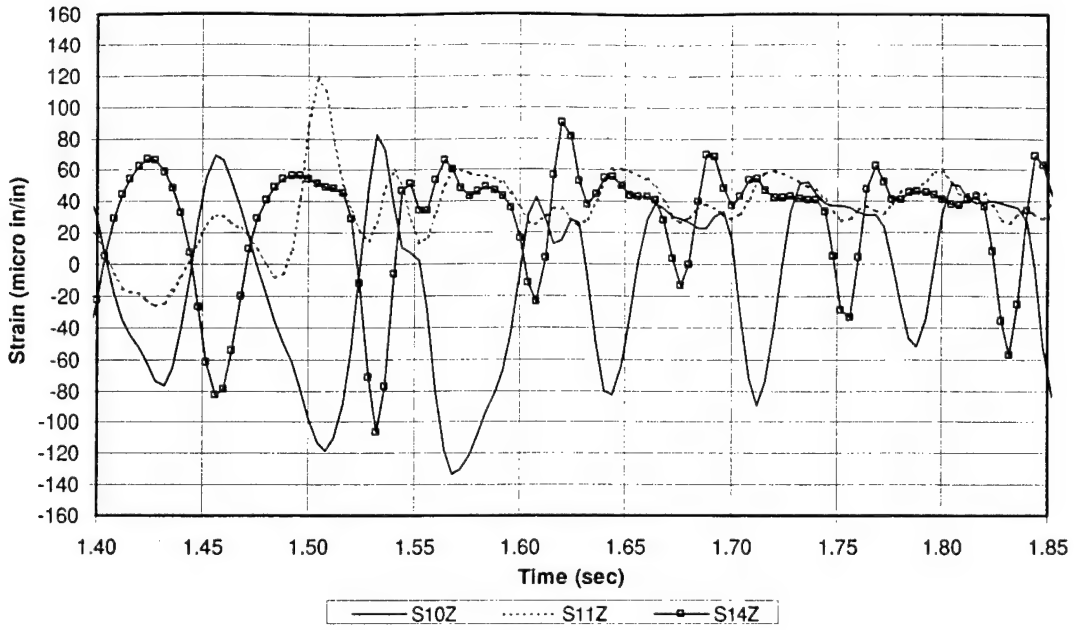

Figure 58. Sine6 back face strains for 1.4 to 1.85 seconds.

The crack propagation can be seen in the strain gage data from the front and back faces, and these observations are consistent with what was seen in the data from the upstream and downstream faces. The S9z strain gage on the front face and the S14z gage on the back face are closest to the location of crack initiation on the downstream face. The primary crack passed approximately 3 in. (80 mm) below the center of these gages on both the front (see Figure 40) and back faces (see Figure 38).[11] Figures 55 and 56 shows a compression spike at 1.46 sec at the S9z sensor, and Figures 57 and 58 shows a compression spike at 1.46 sec at the S14z sensor, indicating crack opening and impact at this time. The tension spike at both S9z and S14z flattens at 1.48 sec, confirming the crack has opened and limited the tension strain. The S6z strain gage is near the center of the model on the front face and the S11z gage is near the center of the back face. The primary crack passes 1 in. (25 mm) above the center of the S6z gage and 1 in. (25 mm) below the S11z gage. The S6z and S11z gage measurements oscillate in phase with the upstream face (S5z and S7z on the front face and S10z and S12z on the back face) during the linear response. This indicates that the center of rotation, or neutral axis, is on the downstream side of the S6z and S11z gages. Then, at 1.43 sec, the center of rotation begins moving to the upstream side of S6z and S11z so that after 1.50 sec these gages are in phase with the downstream face, as

[11] Distances between the primary crack and strain gages were measured from close-up photographs, scaled to the known distances between nearby LVDT mounting blocks (8.0 in., 203 mm) or strain gage dimensions.

measured by the S9z and S14z gages, respectively. Figure 56 clearly shows this phase shift for S6z and Figure 58 shows this shift for S11z, demonstrating the movement of the center of rotation to the upstream side of S6z and S11z. This shift in the center of rotation further demonstrates the complete fracture along the primary crack. The S5z and S10z strain gages are 3 in. (75 mm) from the upstream face on the front and back faces, respectively. The primary crack propagates across horizontally to the upstream face, passing 1.2 in. (30 mm) and 1.8 in. (45 mm) above the S5z and S10z gages, respectively. These gages are much closer to the crack than those on the upstream face (20 in. for the S1z, S3z, and S4z gages). Tension spikes begin to develop in the records for the S5z and S10z gages similar to the way they did for the upstream face. These appear to be caused by the impact and related compression spike on the downstream face. At 1.51 sec the compression amplitude increases and becomes somewhat spiked at these sensors. In the following cycle, at 1.56 sec, the amplitude and sharpness of the compression spike has increased, suggesting that impact has occurred. This is consistent with the compression spike seen along the upstream face at 1.56 seconds in Figure 54. Then, at 1.61 sec at S10z and 1.73 sec at S5z, the tension spike has reduced significantly, demonstrating that the crack has clearly propagated through the cross-section. Finally the compression spikes seen at S9z and S14z near the downstream face reach large amplitudes at 1.83 and 1.53 sec, respectively, as shown in Figures 56 and 58. Table 11 includes summary observations on the progression of failure along the primary crack for the strain gage measurements taken on the front and back faces.

The photographs of the back and front faces (Figures 38 and 40) show vertical secondary cracks near the upstream faces. The portion of the model above the primary crack rocked freely back and forth, opening and closing the primary crack. When the crack closed, the impact would have caused large compressive stresses in the vertical direction. These compressive stresses would have been particularly great near the upstream face due to the diagonal slope of the crack. Microcracks would have developed, particularly near the upstream face, due to the large compressive force. The compressive stress would prevent the cracks from growing horizontally (perpendicular to the stress), but the cracks would be much less restrained from growing vertically. The large compressive force from impact also created a shock wave that propagated to the upstream free surface and reflected back, producing tensile stresses near the free surface. These two phenomena likely contributed to the development of vertical cracks that led to the spalling shown in Figures 44 and 45. Figure 38 shows a large vertical crack approximately 5 in. (125 mm) from the front face, which had propagated both up and down from the primary horizontal crack. Had the Sine6 test lasted longer, the vertical cracking and much larger sections of the upstream face would have spalled. The spalling would eventually have led to loss of vertical support pro-

vided along the horizontal plane of the primary crack at the upstream face. Then the portion of the model above the primary crack would have been free to slide and "walk" down with each cycle of motion, along the primary crack surface in the upstream direction, and eventually fall to the base of the model. This kind of failure would be the equivalent of catastrophic failure in a real dam.

Measured Deformations for Nonlinear Tests

Table 5 and Figures 8 through 11 (see Chapter 3) show the locations of all LVDTs. Each sensor measured the relative deflection between two points 8 in. (200 mm) apart, with the midpoint between each point at the locations shown in Table 5. The deformations on the downstream face were the greatest measured of all faces in both the linear and nonlinear response of the dam model. Figure 59 shows the deformations measured on both the downstream (D9z and D10z) and upstream (D1z and D2z) faces correlating to the linear response recorded in the Sine6 test (0.7 to 1.27 sec). As stated previously, the D9z and D10z LVDTs measured the relative displacements between points 4 in. (25 mm) above and below the change in slope. The D9z LVDT measured slightly greater deformations than D10z during the Sine6 test linear response of the dam model. Figure 59 also shows the deformations at two elevations on the upstream face, with the D1z LVDT at 111.0 in. (2.82 m) and D2z at 130.7 in. (3.32 m). As with the Sine5 test, the linear portion of the Sine6 test produced greater deformations at the D2z LVDT than at D1z. Table 10 provides the time and value of the peak response of the D1z, D2z, and D9z LVDTs prior to cracking. Table 10 also provides the steady-state average deformations for the D1z, D2z, and D9z LVDTs prior to cracking.

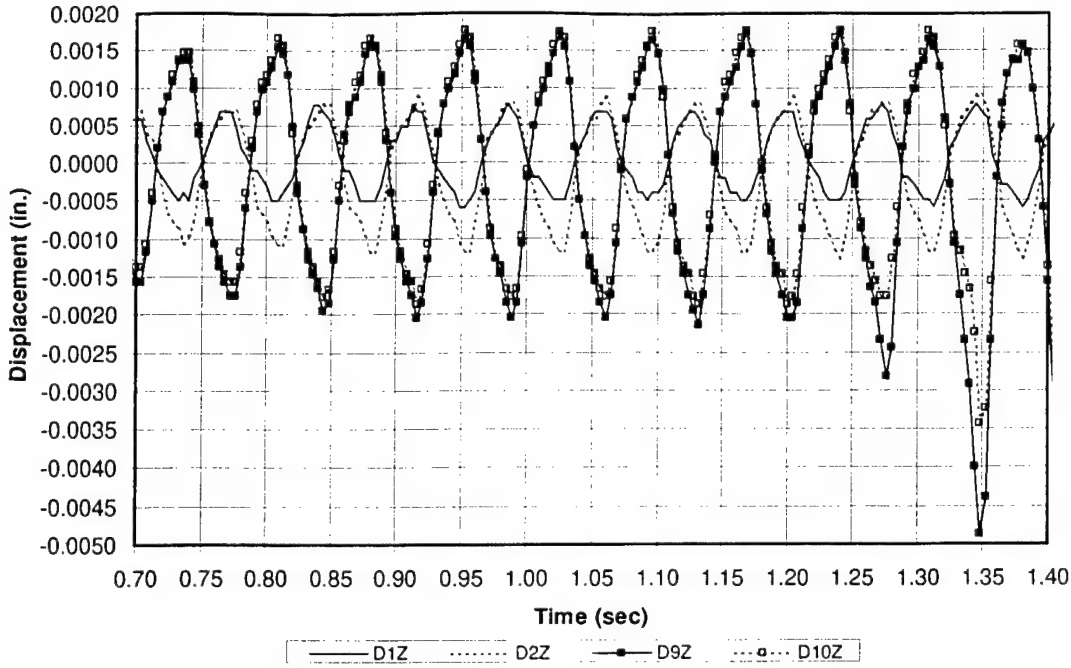

Figure 59. LVDT measurements at both the downstream and upstream faces of the Sine6 test.

Figure 59 shows that the deformations at D9z on the downstream face begin to increase at 1.27 seconds. Negative LVDT measurements indicate that the distance between the LVDT anchor points increases, with the sign convention such that large negative measurements indicate crack opening. The increase first seen at 1.27 sec at D9z agrees with the strain gage measurements on the downstream face (S15z and S16z), where the strains begin to reduce and flatten on the positive (tension) side of the oscillation. In the next cycle, at 1.34 sec, Figure 59 shows the D9z deformations increasing to more than twice the linear values as deformations at D10z also increase. The amplitude of deformations at 1.34 sec shown in Figure 59, an increase of 0.0026 in. (0.066 mm), indicate very minor crack opening at that time. The primary crack forms at the change in slope on the downstream face, halfway between the anchor points of the D9z and D10z LVDTs. Figure 42 shows the downstream face after failure in the Sine6 test, with the primary crack location along with the D9z and D10z LVDTs. Figure A15 shows the position and orientation of the anchor points for the D9z and D10z LVDTs relative to the change in slope on the downstream face. The D9z and D10z LVDTs were oriented parallel to the average of the slope above and below the change in slope on the downstream face. These anchor points were 4 in. (100 mm) vertically above and below the change in slope as shown in Figure A15. Figure 59 also shows that the D9z and D10z measurements at 1.37 sec begin to reduce and flatten on the positive (gage closing) side of the cycle. This suggests that after the crack opened slightly at 1.34 sec, small displaced particles may have prevented complete crack closing.

Figure 60 shows that the crack on the downstream face continues to open more with each cycle, eventually reaching a peak opening of 0.151 in. (3.83 mm) at 1.864 sec. This peak opening was calculated from the average of the peak deformations at D9z and D10z shown in Figure 60. The peak opening should equal the peak deformation once the crack opens (i.e., no correction for the deformation prior to crack development) because the material near the crack will be relieved of stress and strain once the crack opens.

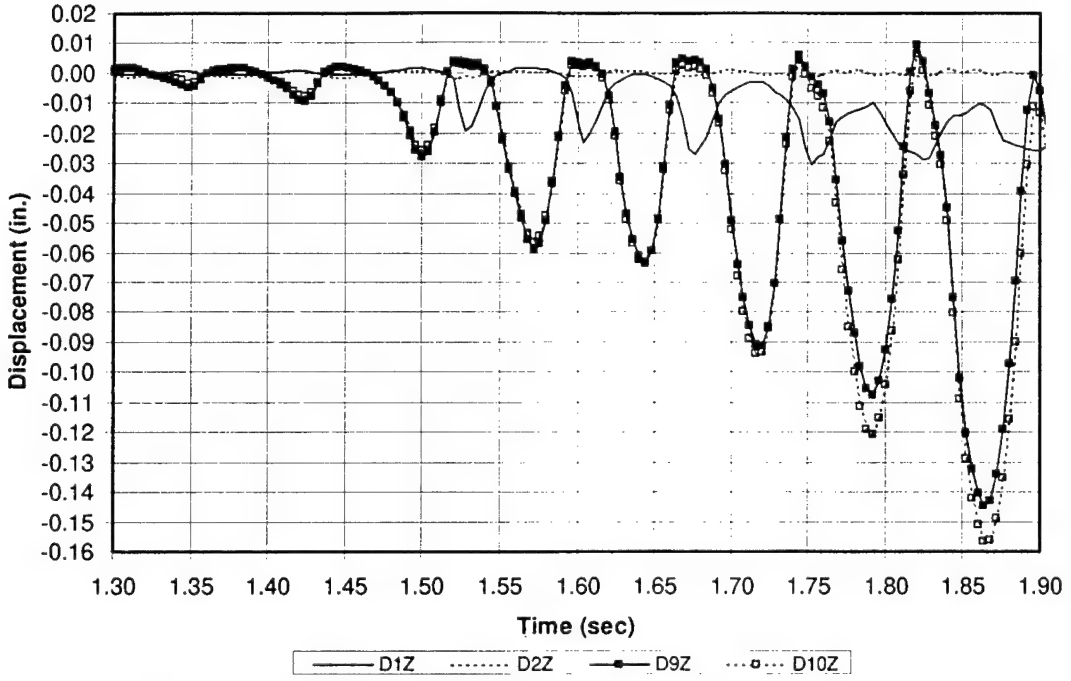

Figure 60. Sine6 LVDT measurements at upstream and downstream faces, 1.3 to 1.9 seconds.

Figures 59 and 60 show that the amplitude of deformation on the upstream face is continually greater at the D2z LVDT than at D1z until 1.52 sec. Then, suddenly at 1.52 sec, the D1z deformation becomes much greater in the negative direction (LVDT opening), indicating crack opening. The photograph of the upstream face in Figure 44 shows that the primary crack passed directly between the anchors for the D1z LVDT so that the sensor directly measured the crack opening. Therefore, Figure 60 provides clear evidence that the primary crack propagated to the upstream face at 1.52 seconds. This observation agrees well with the strain gage data, which showed that the first spiked compression oscillation (indicating impact after crack opening) occurred at 1.56 sec on the upstream face (see Figure 54 and Table 11). The crack opening measured at the D1z LVDT reached -0.0192 in. (-0.49 mm) in the first cycle and then gradually increased more in later cycles, as seen in Figure 60. Figure 60 also shows that the crack on the upstream face never fully closed after three cycles of crack opening at 1.72 seconds. This suggests that small particles began to accumulate in

the crack opening and prevented it from fully closing. Table 11 summarizes the main observations on crack development and progression based on LVDT data.

Figure 61 shows that the D7z LVDT on the front face, just 3 in. (75 mm) from the downstream face, begins to open at 1.34 sec. The time of crack opening agrees with the downstream face D9z and D10z LVDTs. The amplitude of crack opening measured at the D7z LVDT grows with each cycle, reaching a peak amplitude of -0.120 in. (-3.03 mm) at 1.868 sec. This amplitude is consistent with the crack opening on the downstream face, where D9z was closest to the front face and had a peak amplitude of -0.145 in. (-3.68 mm) at 1.864 sec. The opening measured at the D7z LVDT is expected to be less than at D9z because D7z is closer to the center of rotation of the cracked portion of the model. Similar to the upstream face, Figure 61 shows that the amplitude of deformation before cracking was always greater at D4z than D3z. However unlike the upstream face, at 1.52 sec the deformations at both D3z and D4z become much greater in the negative direction, indicating crack opening between the anchors of both the D3z and D4z LVDTs. The primary crack passed through the D3z LVDT, but the photograph in Figure 40 shows that it was a secondary crack that passed through the L4z LVDT. The D3z LVDT is located at the lower left corner of Figure 40 and D4z is located near the top left corner. In this picture only the bottom anchor of the D4z LVDT remains because the top anchor fell off with the portion of the model that spalled, as seen in Figures 40 and 41. While Figure 61 shows that the crack through L4z did form at the same time (1.52 sec) as at L3z, the crack at L4z is still considered secondary because evidence for a crack is not seen on the same elevation on the upstream face, as measured by the D2z LVDT. The spall pattern seen after the test, shown in Figure 40, 41, 44, and 45, shows how the local failure that caused the spall also likely led to the what appears to be a secondary (localized) crack through the D4z LVDT. In other words, the crack measured at 1.52 sec, by the D4z LVDT did not propagate across the entire model cross-section. Figure 61 shows that the local crack measured by the D4z LVDT did continue to grow with later cycles, while the crack measured by D3z did not grow, but instead stayed almost closed after the initial opening at 1.52 sec. Another local vertical crack must have propagated down the model to the level of the D3z LVDT in such a way that the crack through D3z was isolated from opening with each cycle, with the primary crack measured at the D1z LVDT on the upstream face. These observations about the local crack on the front face are further supported by LVDT data from the back face that is more consistent with the upstream face.

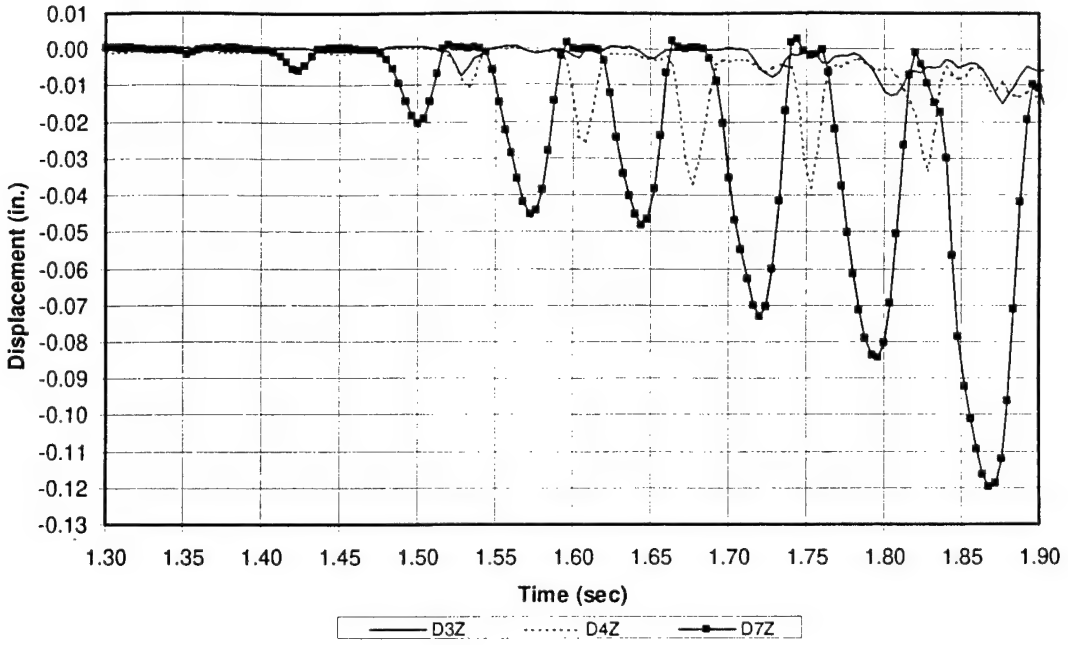

Figure 61. Sine6 LVDT measurements for the front face.

Figure 62 shows that the D8z LVDT on the back face, just 3 in. (75 mm) from the downstream face, begins to open at 1.41 sec. The time of crack opening on the back face is one cycle later than for the front face (1.34 sec). The amplitude of crack opening measured at the D8z LVDT grows with each cycle, reaching a peak amplitude of -0.123 in. (-3.11 mm) at 1.868 sec. Like the front face, this time and amplitude is consistent with the crack opening on the downstream face, where D10z was closest to the back face and had a peak amplitude of -0.157 in. (-3.98 mm) at 1.864 sec. The peak crack opening near the downstream face was slightly greater on the back face (-0.123 in. or -3.11 mm) than the front face (-0.120 in. or -3.03 mm). Again, similar to the upstream face, Figure 62 shows that the amplitude of deformation before cracking was always greater at the D6z than D5z. Like the upstream face, at 1.52 sec the deformations at D5z only become much greater in the negative direction, indicating crack opening between the anchors of the D5z LDVT. The primary crack passes through the D5z LVDT, as seen at the lower right corner of the photograph in Figure 38. A secondary local crack does not form on this face. Figure 62 shows that the primary crack opening measured by the D5z LVDT grew with each cycle while the D6z data remained flat, with no evidence of crack development.

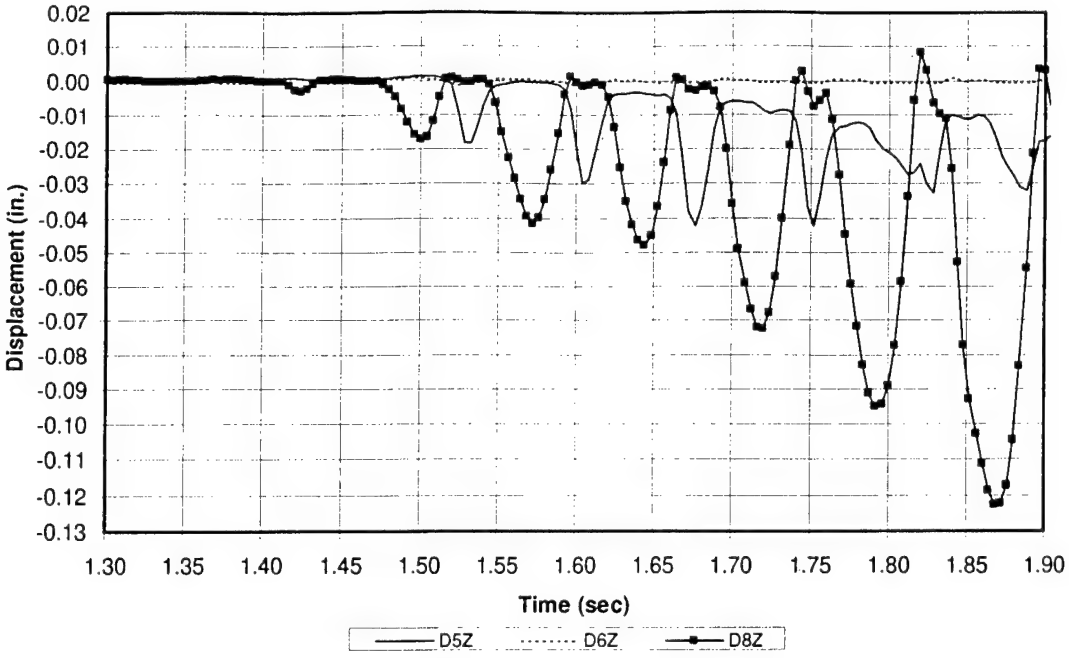

Figure 62. Sine6 LVDT measurements on the back face.

5 Koyna Dam Model Demolition and Core Sample Tests

Demolition Procedures

The Koyna dam model and base beam together weighed about 95,000 lb, far exceeding the capacity of the overhead crane. A method was developed to demolish and remove the model without creating dust that could damage the shake table hydraulics and electronics. Appendix A describes the plans to remove the dam model by breaking it into large sections and then lifting them with the overhead crane. Appendix A describes how inserts were cast into the model that would later be used in lifting the large sections of the model. The Appendix also describes how a test block was cast to test the ability to lift the large section using the inserts and lifting plates. Figure A7 shows the location of these inserts. Appendix A also explains how electrical mechanical tubing (EMT) conduit was cast into the model, designed to be filled with expansive grout to fracture the model into large sections. Figures A8 and A9 show the locations of the EMT tubing. Appendix A also provides details on the demolition plans using the expansive grout, which influenced formwork detailing.

Appendix D provides further demolition plans (beyond those that influenced formwork design). A few days before testing the Koyna dam model an attempt was made to lift the test block with the overhead crane, which was attached to the inserts using the lifting plates. This block was conservatively designed to weigh 16,000 lb (7250 kg), significantly heavier than the portion of the model above the expected crack (14,000 lb, or 6350 kg). The test block material failed around the inserts before the block could be lifted. The failure began with local cracks propagating diagonally up from the inserts at the test block surface. The model material failed at the local stress concentration at the inserts rather than the resistance coming from a more distributed failure surface. Even with this failure, the inserts in the dam model were expected to provide the needed stability during the tests. After the model test an attempt was made to lift the top portion of the model using the inserts and overhead crane. The dam model began to fail locally around these inserts in the same way as the test block. Consequently, large sections of the model had to be lifted using another means. Appendix D explains how these sections were ultimately removed.

Prior to model demolition, the expansive grout was used to try to fracture the test block. The EMT tubes were completely filled with the expansive grout, but after almost 24 hours the test block did not even begin to crack. It appeared that the model material was ductile enough to avoid cracking even though the grout did expand. Therefore, the dam model was demolished without use of the expansive grout. Appendix D explains the actual demolition procedure.

Core Samples

Substantial settlement of the Koyna dam model material took place during casting, and only a limited amount of fibers were seen near the crack surface. This raised the concern that the model material may have been much weaker and less dense near the crack surface than at the base of the model. Therefore, core samples were taken from these locations. Appendix D shows how core samples were obtained to measure actual in-place properties of the model. Cores were taken from near the crack of the model and at the base. These cores were shipped to the GSL at Vicksburg, MS, and materials tests were performed. The core-measured properties are shown in Table 1 (Chapter 2). This table and comments given in Appendix D indicate a very large difference in material properties between the model base and crack surface. This difference in properties should be represented in analytical models whose response is being compared with that of the current physical model. An effort should be made to minimize such differences in future physical experimental models.

6 Summary and Recommendations

Summary

This report provides comprehensive documentation of the construction and seismic testing of a 1/20-scale model of the Koyna dam. The concrete model mix was developed by researchers at GSL. The very weak and fluid concrete material presented several unique challenges for formwork construction and testing. The formwork was designed for the full hydrostatic pressure of the mix, but it still leaked significantly during casting. The material also settled significantly, resulting in much stronger, stiffer, and somewhat denser material at the base of the model than near the major fracture surface. The model was cast on CERL's TESS due to the model's large mass. The formwork leaks led to damage of several control accelerometers in the TESS, so that overturning rotation was not adequately controlled. However, the model was still tested with sinusoidal motions at its natural frequency and it failed in the same location and manner as the actual Koyna dam failed in the 1967 earthquake. The measured accelerations provide both the support motions and dynamic response of the model. Relative displacements were calculated to correct for the overturning rotation at the base of the model. Strains and deformations were measured in the region of expected cracking. Excellent locations were selected for these sensors, so that crack development and progression could be carefully tracked across the model cross-section. This report documents the response of the model subjected to sinusoidal base motions. These results can be effectively compared with analytical models as long as the effects of base rotations and material property variation are properly accounted for.

Recommendations

If future dam models are constructed at 1/20 scale, the formwork must be significantly stiffened and strengthened. Leaks will still occur, but greater formwork stiffness will limit formwork deformation and thereby substantially reduce leaking. Also, two layers of medium-density overlay (MDO) board should be used in an overlapped configuration that will further reduce leaking while increasing stiffness. A sheet of plastic should also be laid between the base beam and shake

table surface to further reduce the potential for water movement into the shake table cavities that contain the control accelerometers.

The model mix also differed from the design and GSL has plans to look at modifying the mix design. In particular, the mix properties differed significantly from the top of the model to the base, and most fibers settled toward the base. This unwanted difference in properties was due to the significant settlement that occurred during model casting.

It is further recommended that a future Koyna dam model be tested using support motions that are scaled from the 1967 earthquake.

References

Chopra, A.K., and P. Chakrabarti, "The Koyna Earthquake and the Damage to Koyna Dam," Bulletin of the Seismological Society of America, Vol. 63, No. 2, pp. 381 – 397, 1973.

Hall, J.F. (1988). "The Dynamic and Earthquake Behavior of Concrete Dams," *Soil Dynamics and Earthquake Engineering*, 7(2).

Harris, D. W., N. Snorteland, T. Dolen, and F. Travers (1999). "Shaking Table 2-D Models of a Concrete Gravity Dam for Computer Code Validation", Technical Report DSO-98-13, Dam Safety Office, Bureau of Reclamation, Denver, CO.

Harris, D. W., N. Snorteland, T. Dolen, and F. Travers (2000). "Shaking Table 2-D Models of a Concrete Gravity Dam", *Earthquake Engineering and Structural Dynamics*, Vol. 29, pp 769-787.

Niwa, A., and R. W. Clough (1980). "Shaking Table Research on Concrete Dam Models", Technical Report UCB/EERC 80-05, Earthquake Engineering Research Center, University of California, Berkeley, CA.

Appendix A: Koyna Dam Model Base Beam and Formwork Design

Base Beam Design

The reinforced concrete base beam was 162 in. (4.11 m) long by 84 in. (2.13 m) wide and 18 in. (0.46 m) high. The base beam was 24 in. (0.61 m) wider than the width of the model to provide a surface for bolting the base beam to the shake table and to anchor the model formwork to the base beam for casting the model. Figure 4 shows the base beam before adding the longitudinal reinforcing steel and before attaching the model formwork. Polyvinyl chloride (PVC) pipes were cast into the base beam to accommodate the bolt hole pattern of the shake table, and bolt inserts were cast into the base beam for anchoring the formwork. Figure A1 (figures appear at the end of Appendix A) is a plan view of the base beam showing the perimeter of the dam model and the shear and longitudinal reinforcement in the base beam. Figure A2 is a base beam cross-section showing both the base beam reinforcement and the reinforcing steel in the bottom 24 in. (0.61 m) of the model. The TESS shake table surface is 144 in. (3.66 m) square, and the base beam was placed on the shake table so as to minimize the offset between the center of gravity of the model and center of shake table vertical actuators. Although no vertical acceleration is needed in this test, the vertical actuators provide vertical force to lift the model and shake table (no vertical acceleration was needed in this test), plus provide overturning resistance. The base beam is bolted to the shake table such that the upstream edge of the base beam is even with the shake table and the downstream edge extends 18 in. (0.46 m) beyond the edge of the shake table surface. The longitudinal (upstream/downstream) center of gravity of the combined dam model and base beam is 63 in. (1.60 m) from the edge of the shake table, resulting in the center of gravity being offset 9 in. (0.23 m) from the center of the shake table. This offset results in slightly greater loading of the vertical actuators near the upstream face, but still well within their capacity.

The dam model will respond in both flexure and shear, and loads will be concentrated near the upstream and downstream ends of the model. The load path will carry the longitudinal forces through the base beam in shear and into the shake

table by friction. Some of the shear load may transfer toward the outside of the beam in shear, where the bolts will concentrate the clamping force to the shake table. The base beam was conservatively built 18 in. high (0.46 m) with longitudinal reinforcement to resist the small bending forces where the base beam overhangs the shake table at the downstream face. Shear reinforcement was provided to aid in the transfer of forces to the clamped surface near the hold-down bolts. The primary purpose of the reinforcement was to tie the dam model to the base beam and ensure that no slippage takes place along this surface. A fairly dense grid of small stirrups was used to provide a large surface area of contact in the weak dam material and minimize stress concentrations in the weak concrete against the reinforcing steel. The longitudinal steel in the dam model further increased this surface area. The actual Koyna dam contained no reinforcing steel, so the steel was located in only the bottom 24 inches (0.61 m), where no model failure would be expected. The presence of this steel does not modify the model behavior as long as no cracks form in the region.

Formwork Design

The formwork was designed to resist the full hydrostatic pressure of the concrete model material. Table A1 defines the dimension of the dam regions shown in Figure 3. The formwork faces consisted of 0.75 in. (19 mm) medium density overlay (MDO) board with the overlay on both sides. MDO board is often used for concrete formwork due to its strength and resistance to water penetration. The MDO board was braced with 2 x 4* and 4 x 4 vertical ribs approximately 11 in. (0.28 m) on-center. Figure A3 is a detailed drawing of the front face of the dam model formwork showing the MDO board and vertical ribs. The 2 x 4s are stud grade Spruce Pine Fir and the 4 x 4s are treated Yellow Pine.

The vertical ribs were supported by horizontal walers, which were in turn supported by ties and corner connections. The pressures, moments, stresses, and deflections were calculated for the MDO board at the level of each waler. Table A2 shows these values at the elevation of each waler. The MDO board spans approximately 11 in. between the vertical 2 x 4 and 4 x 4 ribs. The maximum stresses in the MDO board occur at the lowest wood waler, where negative moment is applied near the vertical ribs, and this stress is conservatively calculated to be 1728 psi (11.9 MPa) (see Table A2). However, during casting of the model,

* Measurements are nominal, in inches.

numerous leaks led to formwork saturation at penetrations that weakened and softened the MDO board. This decreased MDO board capacity and substantially increased deflections.

Table A1. Dimensions of the dam model regions shown in Figure 3.

Dam Model Region	Unit Weight (pcf)	Height (in.)	Width (in.)	Depth (in.)	Weight (lb)
A	150	72.0	29.1	60.0	10918
B	150	72.0	11.0	60.0	2061
C	150	76.8	3.2	60.0	640
D	150	130.7	40.1	60.0	27285
E	150	130.7	94.9	60.0	32307
				Model Weight =	73209
Base Beam	150	18.0	162.0	84.0	21263
				Total Weight =	94472

Table A2. Formwork pressures, loading, stresses, and rib deflections.

Elevation Above Base Beam (in.)	Waler Vertical Spacing (in.)	Pressure (psi)	Vertical 2 x 4 Spacing (in.)	MDO Board Moment (lb-in)	MDO Board Stress (psi)	MDO Board Defl (in.)	Vertical 2 x 4 Moment (lb-in)	Plywood /2 x 4 Stress (psi)	Plywood /2 x 4 Defl (in.)
202.71		0.00	11						
160.71	42	3.65	11	37	393	0.004	5902	879	0.023
130.71	30	6.25	11	63	673	0.006	5160	769	0.010
104.71	26	8.51	11	86	915	0.009	5274	786	0.008
82.71	22	10.42	11	105	1121	0.011	4623	689	0.005
57.71	25	12.59	11	127	1354	0.013	7214	1075	0.010
34.71	23	14.59	11	147	1569	0.015	7074	1054	0.008
17.71	17	16.06	11	162	1728	0.017	4255	634	0.003
0	17.7	17.60	11	177	1893	0.018	5059	754	0.004

The MDO board was screwed to the vertical ribs with drywall screws, so that the MDO and ribs together would act as a composite member in spanning between the horizontal walers. Because the ribs are continuous across the walers, the maximum moment occurs at the walers. Table A2 shows the calculated moment, stresses, and deflections of the MDO board and vertical ribs ("Vertical 2 x 4" in Table A2). Actual deflections were somewhat greater due to high moisture levels in the MDO board and ribs during casting.

A mirror image configuration of the formwork shown in Figure A3 was used for the back face. Similar MDO board and vertical ribs were used for the upstream and downstream faces. Figure A4 shows this formwork for the upstream face. The vertical ribs on this face are yellow pine 2 x 8s, in place of the 2 x 4s. These were used so that they could be cut on a slope on the bottom 76.8 in. (1.95 m) to accommodate the slope of the model along the upstream face and still remain

vertical. This surface slopes in 3.2 in. (81 mm) from the base beam up to the 76.8 in. (1.95 m) elevation (see Figure 1). Therefore, the 2 x 8 vertical ribs were cut down to 4.05 in. (103 mm) deep at the base of the model and sloped to their full width (7.25 in., 184 mm) at the 76.8 in. (1.95 m) elevation. From this level the model upstream surface was vertical up to the top of the dam. The front and back faces were more critically loaded than the upstream face, so the same design was used on the upstream face and calculations are not repeated here.

The downstream face has a less steep slope (see Figure 1), where the top 72.0 in. (1.83 m) portion slopes down steeply and the remaining lower portion slopes more gradually. The forms for the top portion and lower portion of this face were constructed separately and bolted together at their intersection. The upper portion of this formwork was constructed with 0.75 in. (19 mm) MDO board and 2 x 4 ribs. Figure A5a shows the upper section of this downstream face and Figure A5b is an elevation side view showing the beveled lumber cuts of the MDO board and 2 x 4 ribs. Figure A5b also shows the location and size of the holes used to bolt the upper and lower faces of this formwork to each other. The lower portion of this formwork was constructed with ¾ in. (19 mm) MDO board and treated yellow pine 4 x 4 ribs. The heavier ribs were used on this face because they had to resist the additional uplift force along the sloped surface and transfer a small portion of the vertical load in tension to a bolted connection to the horizontal angle at the base beam of this face. Due to the slope of this face, the 4 x 4 ribs also spanned a greater distance between horizontal walers. Figure A6a shows the lower section of the downstream face and Figure A6b is an elevation side view showing the beveled lumber cuts of the MDO board and 4 x 4 ribs. Figure A6b also shows the location and size of the holes used to bolt the upper and lower faces of this formwork to each other. The downstream face is more severely loaded than the front face, but use of 4 x 4 ribs results in smaller stresses and deflections in the MDO board and 4 x 4s.

Horizontal walers on all four faces were made of two yellow pine 2 x 10s with a 1.5 in. (38 mm) gap between them (see Figure A7). These walers were also centered at the joints in the MDO board on the front and back face. Every other waler along the lower portion of the downstream face also had a 4 x 6 (Douglas Fir, Grade II) screwed to the lower of the two 2 x 10s so as to act in composite. These walers were inserted into an opening in vertical L4 x 3.5 x 0.25 angles so the top surface of the waler bears against the angle opening. This angle was bolted to the horizontal angle around the base of the model so the angle provides the vertical holddown force needed for the waler to resist the vertical uplift pressure. The vertical angle is oriented so the edge of the 3.5 in. leg rests against the MDO board and a vertical 4 x 4 is inside the angle and also against the MDO face. The 4 in. wide leg of the angle was then bolted to the horizontal angle.

The gap between the walers was needed to overlap the walers on the front and back face with the walers on the upstream and downstream faces. Coil ties were also installed through the formwork within this gap between the 2 x 10s. Figure A7 shows the waler and tie locations of the front face formwork. This figure also shows a cross-section of the downstream walers. The walers on the downstream face were cut on a bevel so their edges could bear against the 2 x 4s of the upper portion and 4 x 4s of the lower portion of this face. Figure A7 also shows how the walers overlap each other at the model corners. At these corners vertical 2 x 4s (sloped along the downstream face) are screwed to the walers to tie them to each other at the corners. The walers are then supported at each end and at one-third points by coil ties for the three lower walers, and near the center for the next two walers. The walers were sized so no coil ties would be needed near the predicted fracture surface — the change in slope — so that they would not interfere with the development of this failure surface during testing. Table A3 shows the calculated distributed load, waler span, moments, stresses, and deflections at each elevation of the front and back face walers. The walers are conservatively assumed to be simply supported at the corners and tie locations. The maximum waler stresses occur at the lowest wood waler, which has a value of 1412 psi (9.74 MPa) (see Table A3). Table A3 also shows the same calculations for the L5 x 5 x 3/8 angle around the perimeter of the formwork at the base of the model. These angles were bolted to inserts cast into the base beam. Figure A8 shows the walers, ties, and corners on the upstream face, plus the cross-section for the walers on the front and back faces. Figure A9 shows an elevation view of the downstream face, showing the walers, ties, and corners. Table A3 also shows the calculated loads applied to the coil ties that support the walers. The maximum load is conservatively calculated to be 7254 lb (32.3 kN). The selected ties (B-1 heavy coil tie from Dayton Superior) have a safe working load of 6750 lb (30.0 kN), including a factor of safety of 2, which indicates adequate capacity.

Table A3. Front and back face waler distributed load, moments, stresses and deflections.

Elevation Above Base Beam (in.)	Waler Vertical Spacing (in.)	Pressure (psi)	Dist Load on Waler (lb/in)	Model Total Width (in.)	# Ties	Waler Span (in.)	Waler Moment Mw (lb-in)	Waler Size	Waler Moment of Inertia (in^4)	Waler Section Modulus (in^3)	Waler Stress (psi)	Waler Defl (in.)	Tie Load (lb)
202.71		0.00	19	29	0	29	1622	1.5 x 9.25	99	21.4	76	0.001	
160.71	42	3.65	131	31	0	31	16164	3 x 9.25	198	42.8	378	0.002	
130.71	30	6.25	175	40	0	40	35161	3 x 9.25	198	42.8	822	0.009	
104.71	26	8.51	204	60	1	30	22670	3 x 9.25	198	42.8	530	0.003	3804
82.71	22	10.42	245	76	1	38	44328	3 x 9.25	198	42.8	1036	0.010	5824
57.71	25	12.59	302	95	2	32	37776	3 x 9.25	198	42.8	883	0.006	5973
34.71	23	14.59	292	112	2	37	50953	3 x 9.25	198	42.8	1191	0.011	6816
17.71	17	16.06	279	125	2	42	60396	3 x 9.25	198	42.8	1412	0.016	7254
0.00	17.7	17.60	156	138	3	35	23249	L5x5x3/8	8.74	2.42	9607	0.005	3365

The dam model was expected to fail by cracking across the cross-section, beginning at the change in slope on the downstream face. Once the crack propagates through the cross-section, this segment will rock back and forth as motions con-

tinue. This section would weigh about 14,000 lb (6350 kg) and could fall onto the shake table actuators below, especially if the slope of the crack surface were very steep, and cause a substantial amount of damage. To prevent such an occurrence, inserts were cast into the model 24 in. (0.61 m) below the top of the model, which is at least 48 in. (1.22 m) above the predicted failure surface (see Figure A7). Lifting plates were attached to these inserts and attached to shake table's overhead crane using slack fabric straps. Because the model is very massive and must be demolished on the shake table, additional inserts were cast into the model well below the anticipated failure surface so it could be broken into large sections (20,000 lb, or 9100 kg each) and lifted off the shake table using the insert lift points. The capacity of the inserts cast into the weak dam model material was unknown, so a test block was cast on the same day as the model and the same inserts were attached to the test block formwork in the same configuration as the model. The test block was conservatively designed to weigh 16,000 lb (7250 kg). It also had the same width as the model in the cross-stream direction (60 in. or 1.52 m) and the inserts were installed at an elevation determined to create a similar critical fracture surface as on dam model, so the behavior of the inserts would be similar. If the test block could successfully be lifted with the overhead crane, greater assurance would be provided that the crane could stabilize and, if necessary, suspend the section of the model above the predicted fracture surface. However, even if the inserts have inadequate capacity to lift the section of the model above the crack, the overhead crane could still provide lateral support to prevent this section from toppling or sliding along the fracture surface. After removing the model section above the crack, demolition plans call for breaking the model into two 20,000 lb sections. Each of these sections would be lifted by four inserts, so the load per insert would be less than the critical section or the test block. Figure A10 shows the test block formwork before casting. Figures A11 and A12 are front and back elevation views of the test block, showing details of the formwork, including the locations of the inserts on the front and back faces.

The model was instrumented with accelerometers, linear variable differential transformers (LVDTs), and strain gages. The accelerometers and LVDTs were not directly adhered to the model because the model material was extremely weak and likely fail along the adhesive surface. Therefore, small steel plates were cast into the model by attaching plates with elevator bolts to the inside of the formwork. Figure A7 shows the location of LVDT plates on the front face of the formwork. Figures A8 and A9 shows the location of accelerometer and LVDT plates on the upstream and downstream faces, respectively. Figure A13 shows elevation cross-section views of the accelerometer plates on the upstream and downstream faces. Each of these drawings shows wood wedges that are installed on both the interior and exterior sides of the formwork to hold the accelerometer

plates in a vertical orientation, where the formwork is on a slope. This orientation will facilitate the installation of instrumentation in all the three orthogonal directions. The elevator bolts each have a very large head that further tie the accelerometer plates to the model. These bolts will force a large critical failure cone surface, which will prevent failure during seismic testing. Figure A14 shows a detailed front view of the instrumentation plates used for attaching both accelerometers and LVDTs. Each LVDT sensor measures the relative displacement between two LVDT plates installed 8 in. (203 mm) apart. Most of the LVDTs are oriented vertically, so both plate surfaces are also installed vertically. However, the LVDTs installed on the downstream surface are on a sloped surface, across the change in slope. The plate surfaces that support these sensors must be parallel to each other at a slope equal to a straight line between the two locations of the plates. Figure A15 shows an elevation cross-section view of these plates, illustrating the needed orientation and size of wood wedges so the plates are parallel to each other and a straight line between them.

The Koyna dam model was expected to fail during seismic testing at the change in slope on the downstream face. This section would then be removed as a single piece to avoid creating the dust and safety hazards that would arise from trying to remove it in small pieces. The remaining model and base beam would still weigh considerably more than the capacity of the overhead crane (80,500 lb versus 40,000 lb, or 36,500 kg versus 18,100 kg). Additional model material must be removed, down to an elevation of 27 in. (0.69 m) above the base beam, to bring the base beam and remaining model total weight down to the 40,000 lb (18,100 kg) crane capacity. Plans were made to remove an additional 41,000 lb (18,600 kg) of material in two pieces by fracturing the model using expansive grout. This was to be done by casting two layers (4 conduit for each level) of 1.5 in. Electrical Mechanical Tubing (EMT) (actual outside diameter was 1.875 in., or 48 mm) in the upstream/downstream direction. The top layer of EMT conduit sloped down from an elevation of 69 in. (1.75 m) on the downstream face to 65 in. (1.65 m) on the upstream face (see Figures A8 and A9). These conduits were 61 in. (1.55 m) below the predicted failure surface, ensuring that they would not interfere with the performance of the dam model. The conduit were also oriented in the upstream/downstream direction rather than cross-stream so as to minimize any influence on the dynamic behavior of the model. With this slope, the upstream end of the conduit could be plugged and the fluid expansive grout poured into the downstream end. The upstream end plug would have a small air hole to let air escape and the upstream end would be gradually plugged so that the conduit would be completely filled with expansive grout. Similarly, the lower layer of EMT conduit sloped down from an elevation of 29.5 in. (0.75 m) on the downstream face to 24.5 in. (0.62 m) on the upstream face. The conduits were cut at their ends to follow the slope of the inside face of the formwork. They were held

in place during casting by placing coil ties inside the conduit, with rubber plugs at the ends of the conduit and holes cut in the rubber through which the ties penetrated and the coil bolts were inserted. These coil bolts supporting the coil ties were kept relatively loose so they would not load the outside faces of the MDO board when these expanded during the pressure of casting.

TESS Protection Frame

A protection frame was constructed to both protect the Triaxial Earthquake and Shock Simulator (TESS) shake table from leaks during casting and from falling sections of the model during seismic testing. This protection frame was designed to serve both as a "moat" during casting and an impact-absorbing surface during testing. During seismic testing, the model was expected to crack across the entire cross-section, beginning at the change in slope on the downstream face. The overhead crane attached to the section above this crack should stabilize it and prevent it from falling on the shake table. However, a remote possibility still remained that this entire 14,000 lb (6350 kg) portion of the model could break free from the insert connections and fall in the upstream direction 13 ft (4.0 m) down to the TESS actuators. It was also possible that smaller portions of the model could fall in other directions. Therefore, the protection frame was constructed around the perimeter of the TESS platform, but with the greatest energy-absorbing surface along the upstream edge (right side of Figure 7). Figure A16 shows the protection frame covered with plastic sheets and drop cloths to protect the TESS hydraulic systems from potential dust created by falling material. Figure A17 shows a plan view drawing of the entire protection frame. Figure A18 shows a more detailed plan view of the north portion of the protection frame, and Figure A19 provides cross-section views at the indicated locations. Details A and B of Figure A19 provide the details of the portion of the protection frame designed to absorb energy below the upstream face of the model. This portion consists of a heavy L8 x 8 x 1 angle iron with a wood sandwich panel. Impact energy can be absorbed by crushing of the sandwich panel and significant yielding of the angle. Similarly, Figure A20 shows a detailed plan view of the east portion of the protection frame, and Figure A21 provides cross-section views at the indicated locations. Finally, Figure 22 shows a detailed plan view of the south portion of the protection frame and Figure A23 provides cross-section views at the indicated locations.

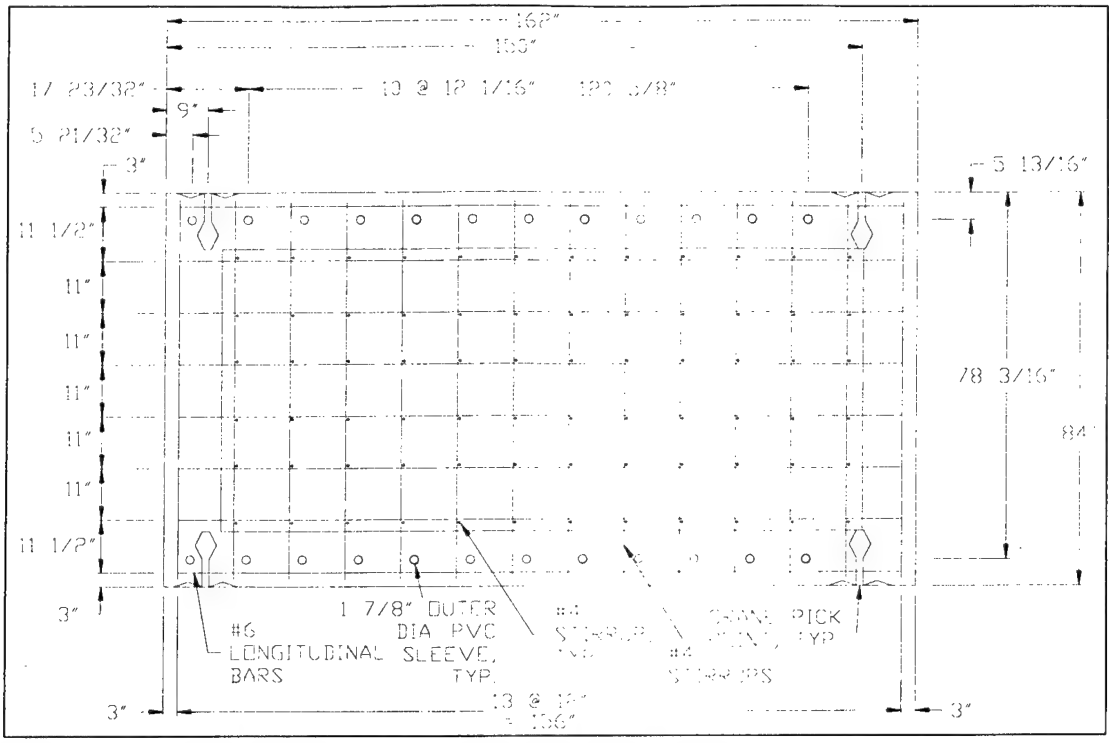

Figure A1. Plan view drawing of Koyna dam model base beam.

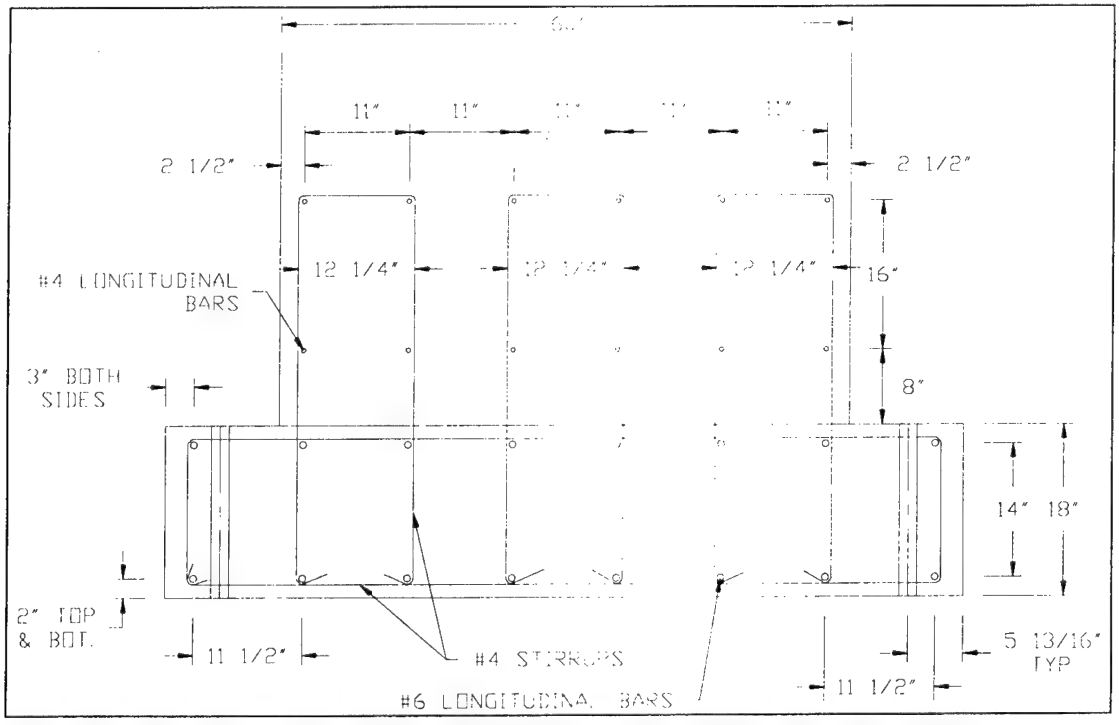

Figure A2. Base beam cross-section including dam model reinforcing steel at base.

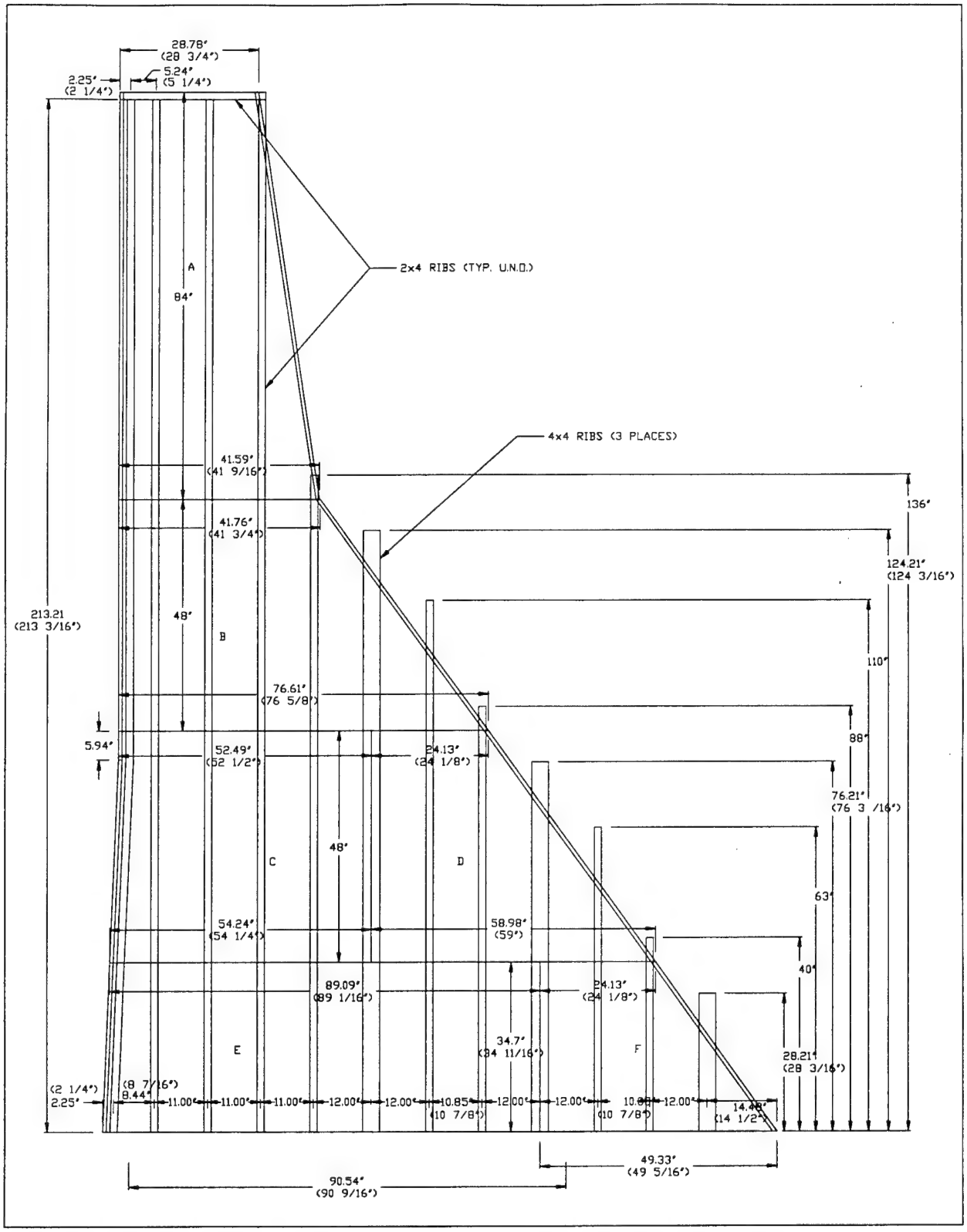

Figure A3. Front face drawing of model formwork showing MDO board and vertical ribs.

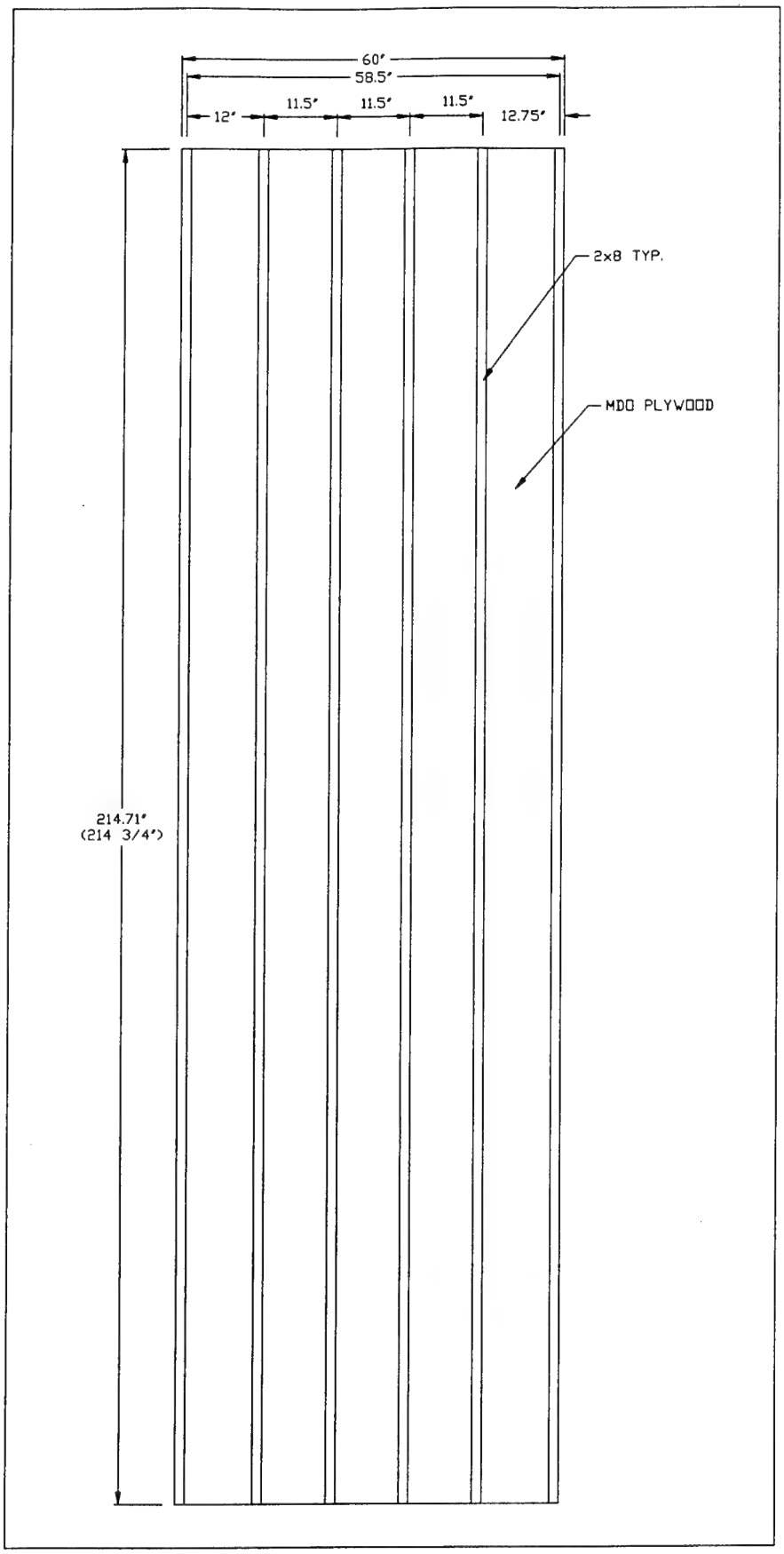

Figure A4. Drawing of upstream face formwork showing the MDO board and 2 x 8 vertical ribs.

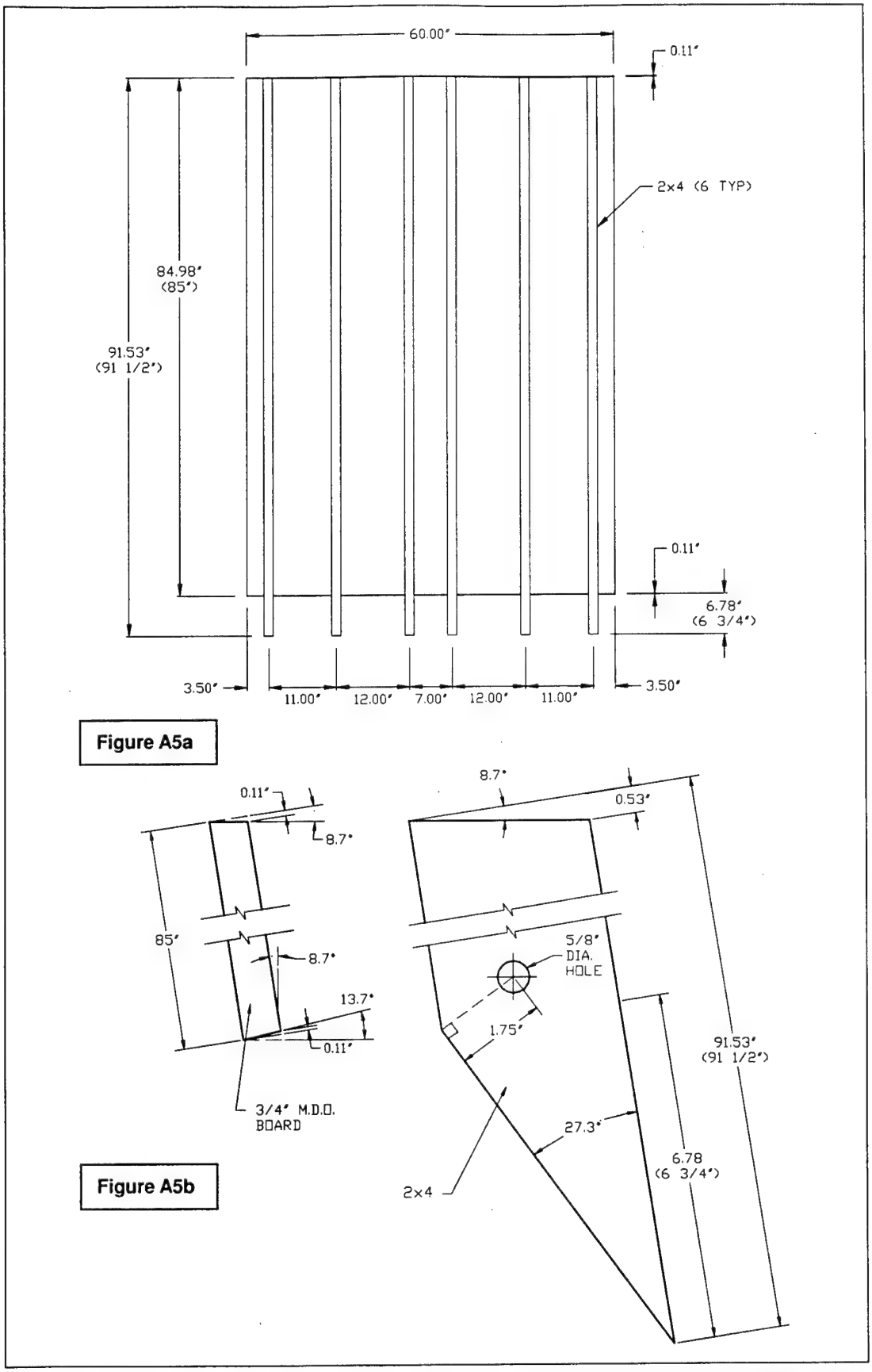

Figure A5. Upper downstream face drawing of (a) dam model formwork and (b) elevation view showing details of the MDO board ribs, and bolt hole locations.

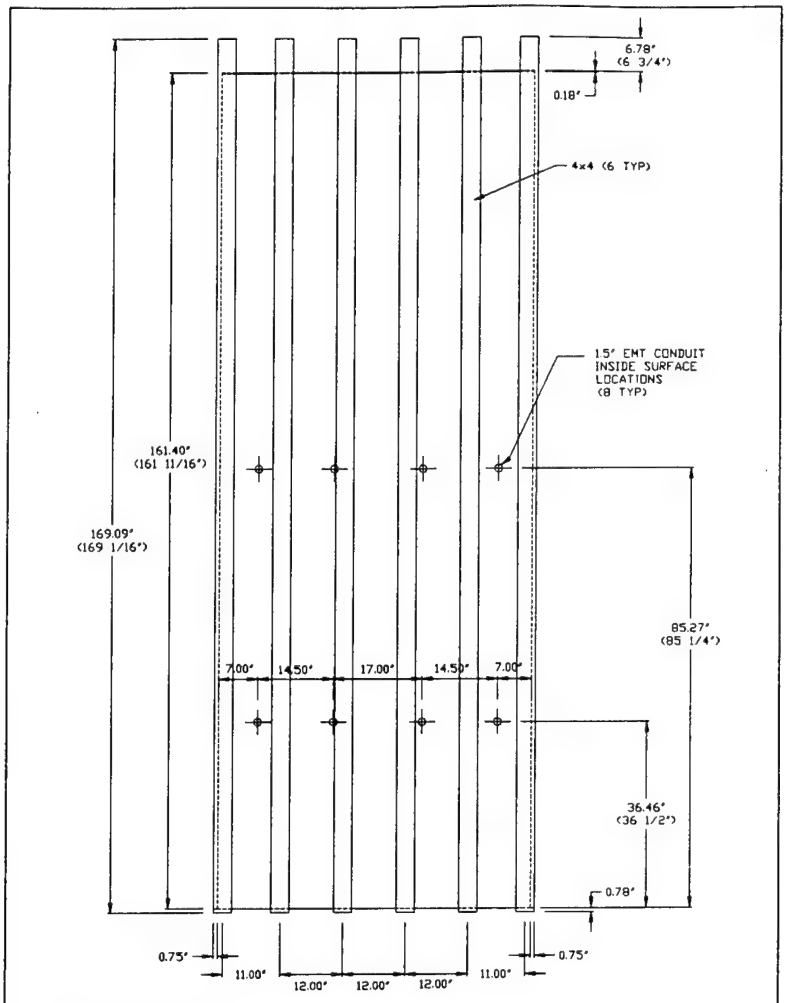

Figure A6a

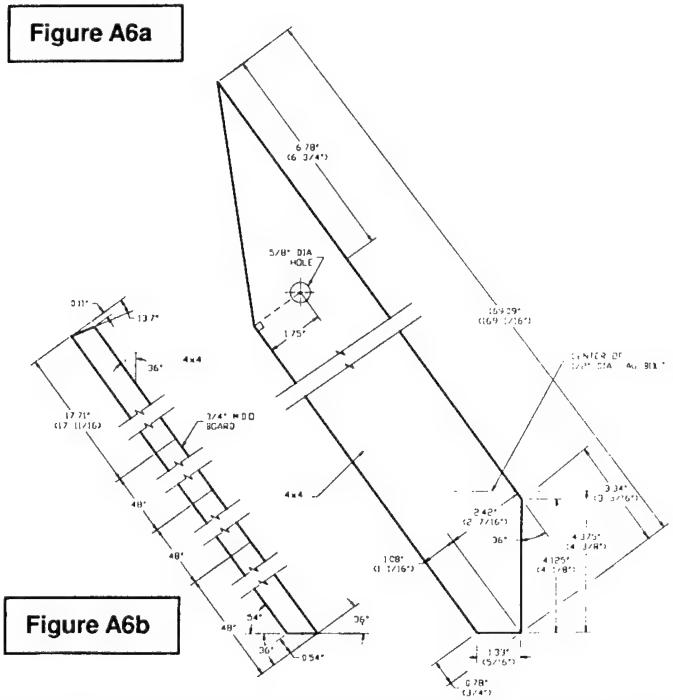

Figure A6b

Figure A6. Lower downstream face drawing of dam model formwork (a) showing MDO board and ribs and (b) elevation view showing details of the MDO board, ribs, and bolt hole locations.

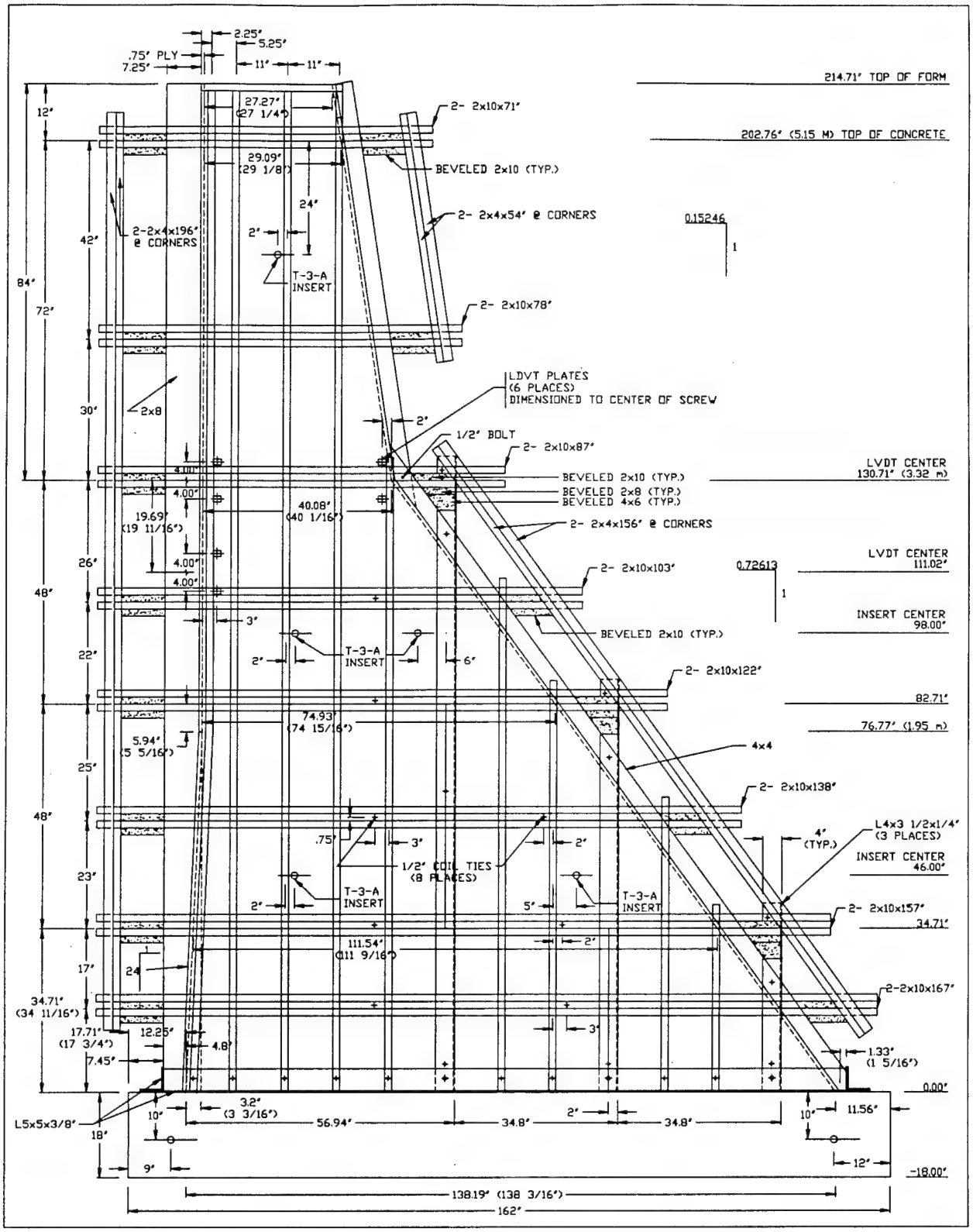

Figure A7. Front face formwork showing front walers, corners, a cross-section of the upstream and downstream walers, plus location of coil ties, inserts, and instrumentation plates.

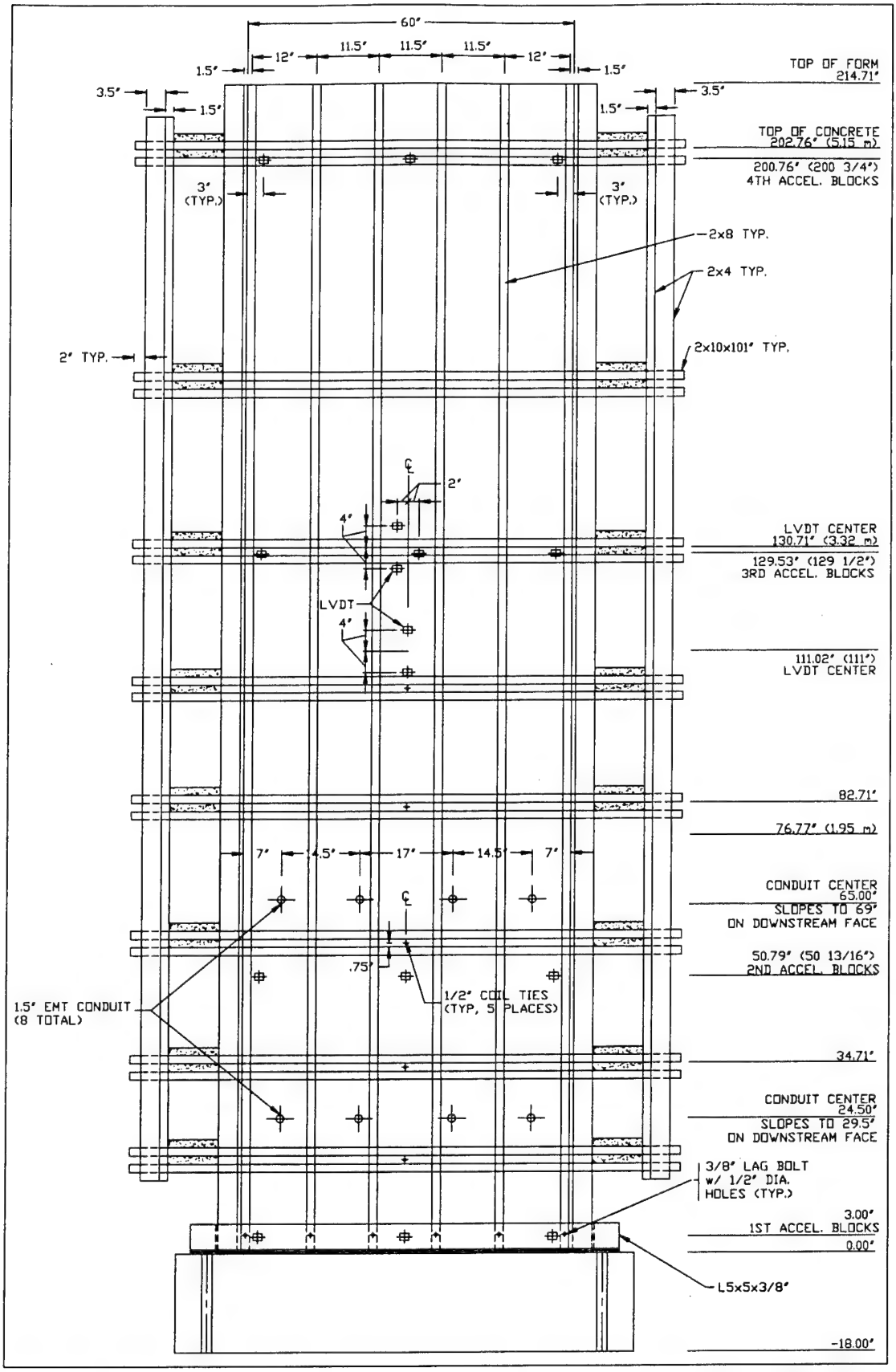

Figure A8. Upstream face formwork showing the walers, corners, and the location of ties, EMT conduit, and instrumentation plates.

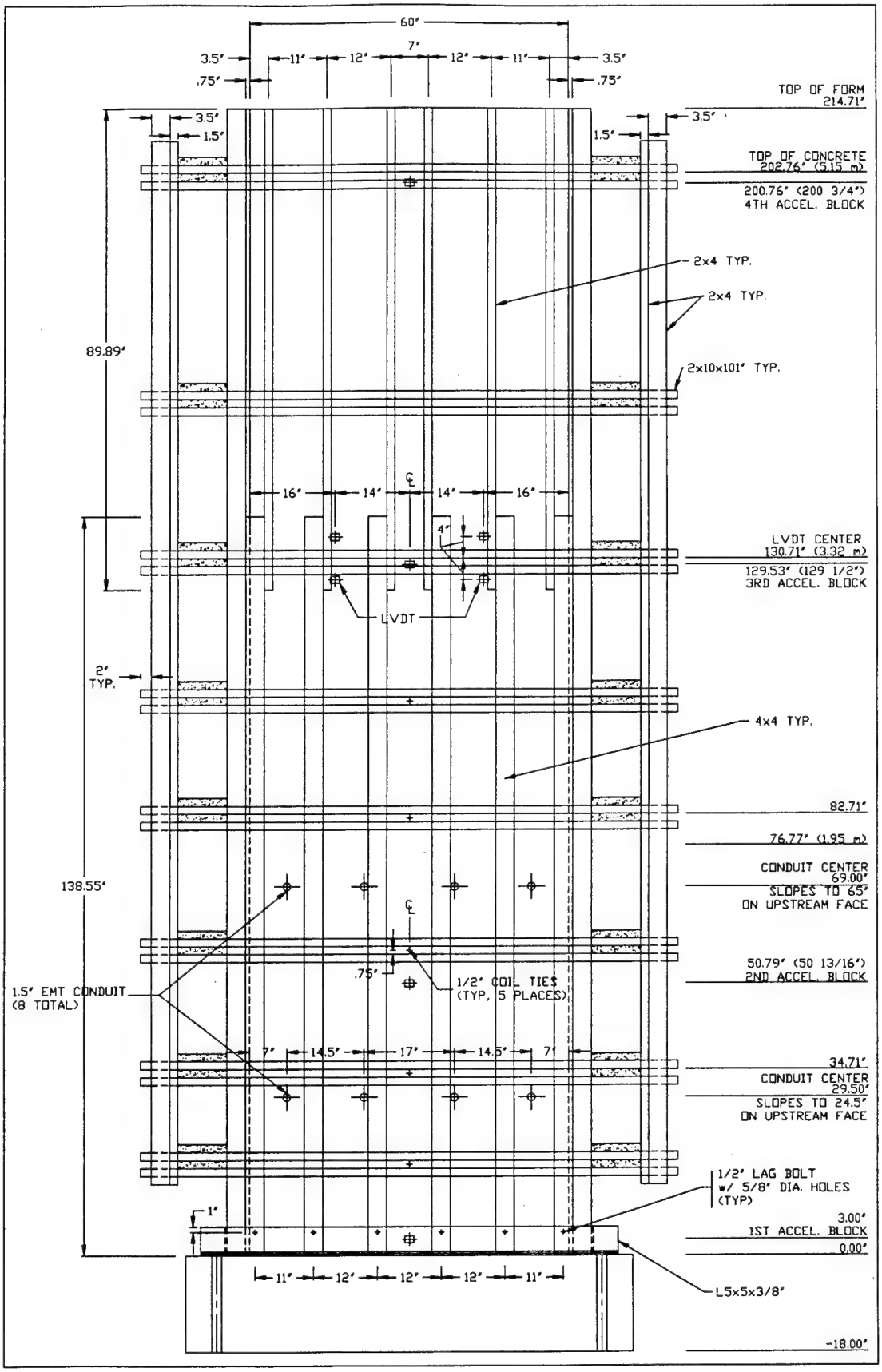

Figure A9. Downstream face formwork showing the walers, corners, and the location of ties, EMT conduit, and instrumentation plates.

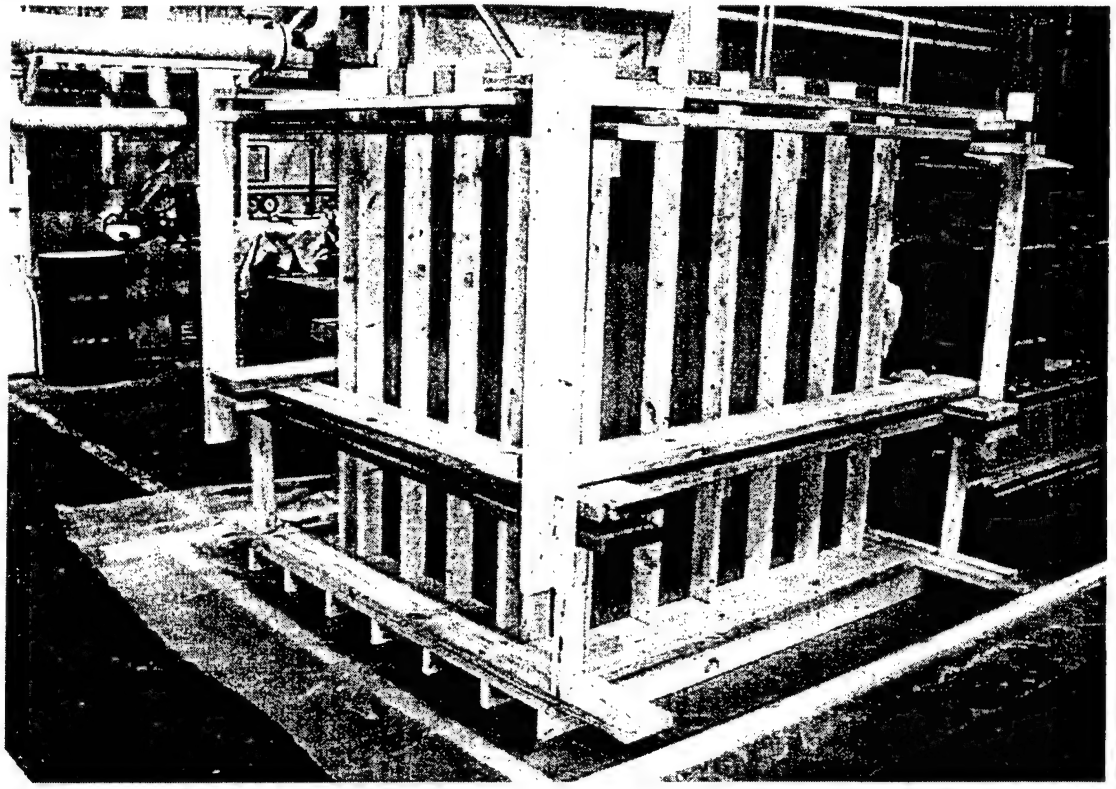

Figure A10. Test block formwork before casting.

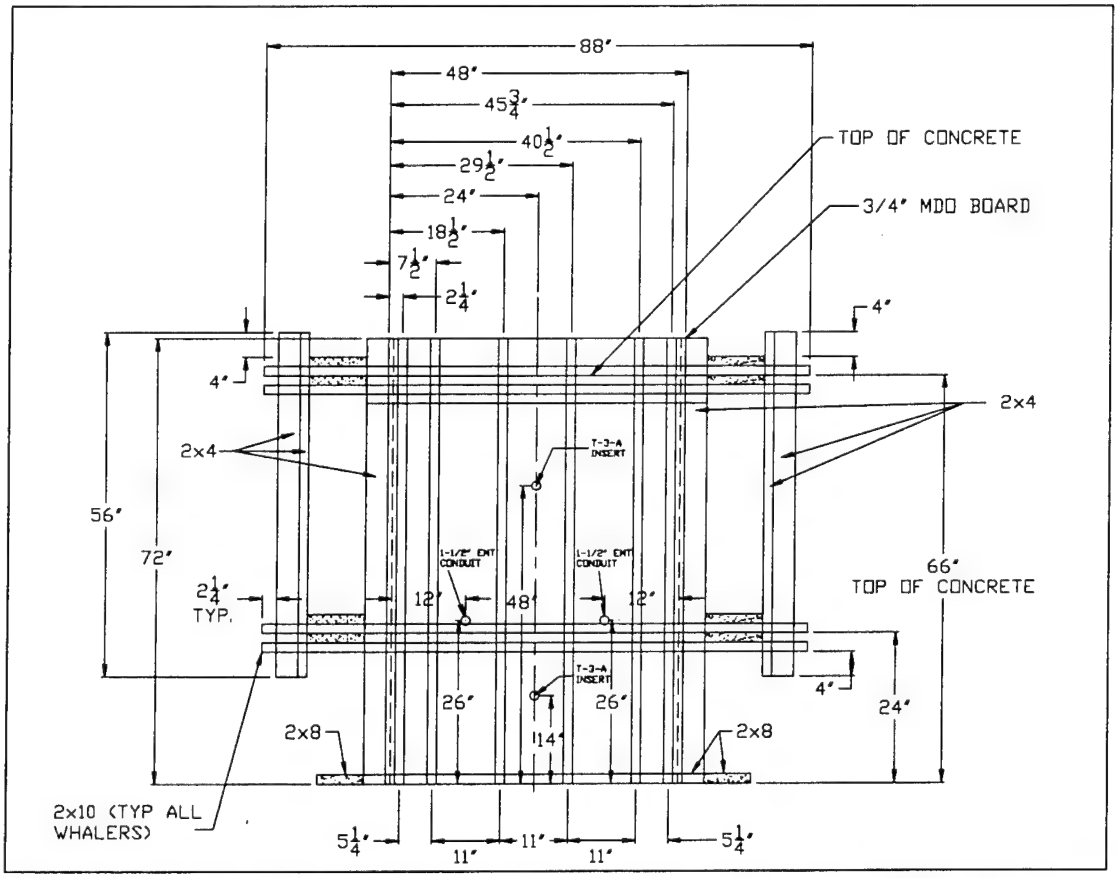

Figure A11. Front elevation view of test block formwork, including insert and EMT locations.

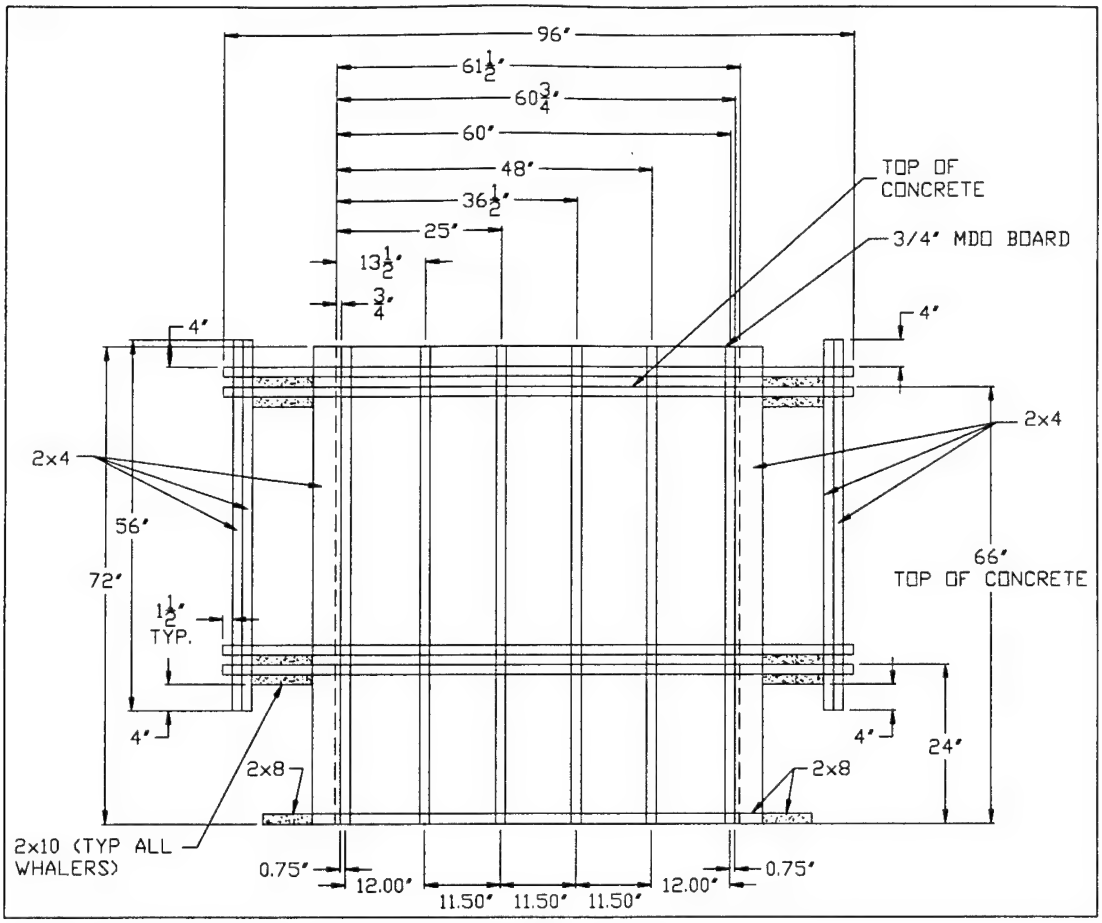

Figure A12. Side elevation view of the test block formwork.

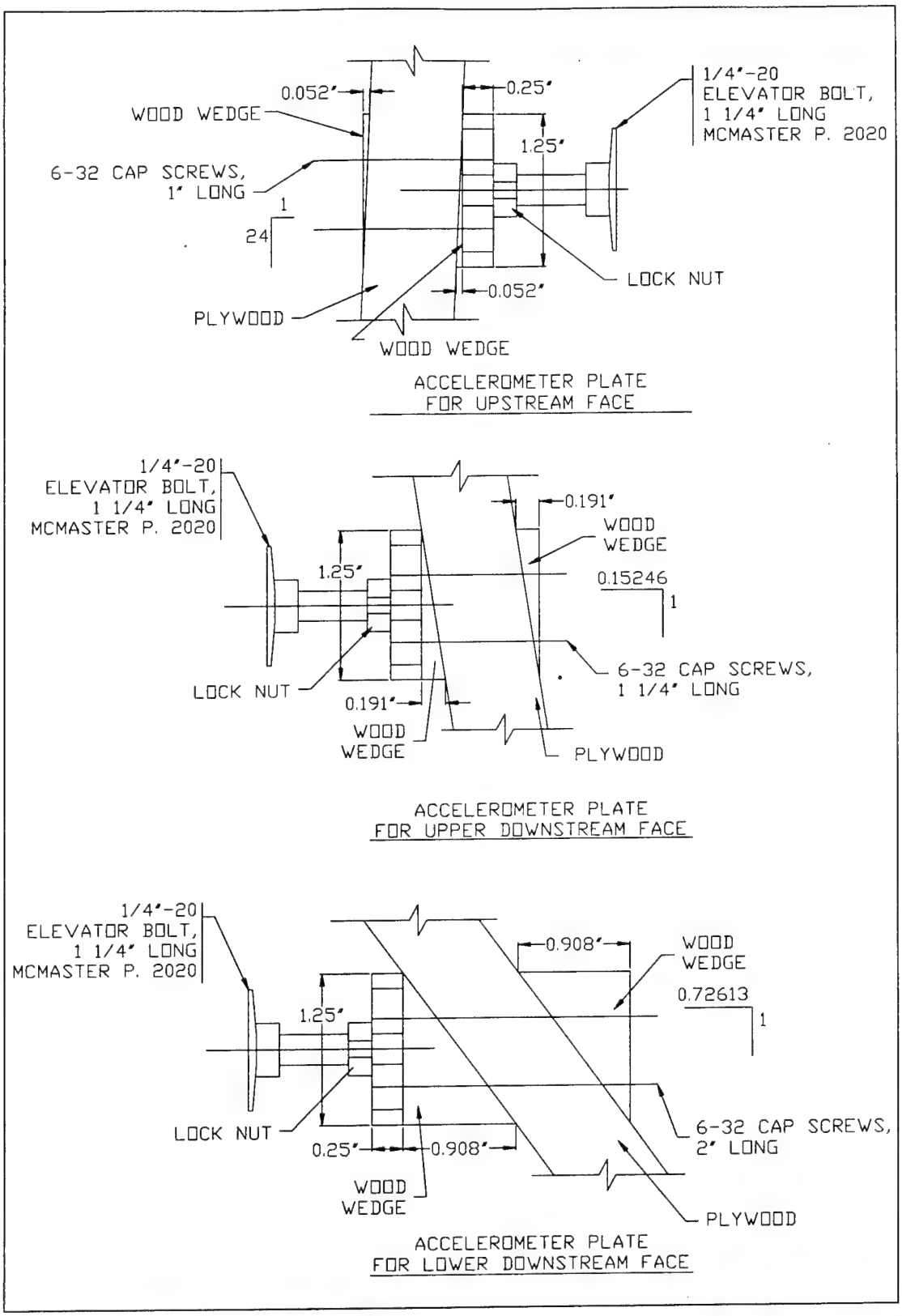

Figure A13. Elevation cross-section views of accelerometer plates for the upstream and downstream faces.

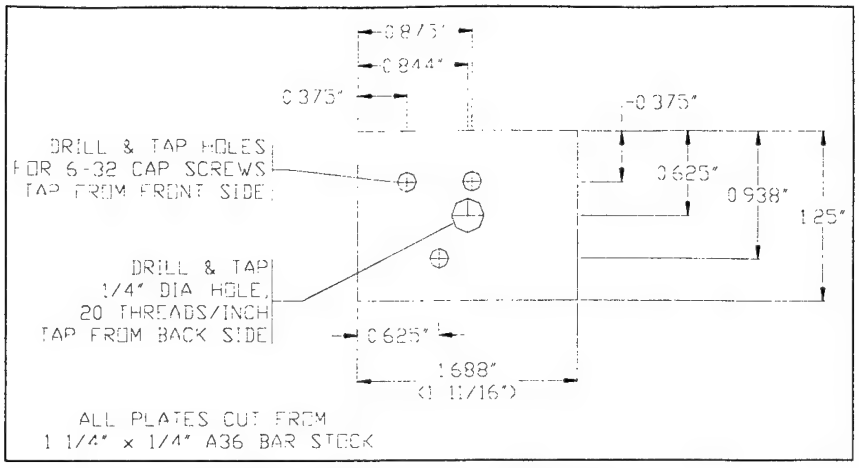

Figure A14. Details of accelerometer and LVDT plates.

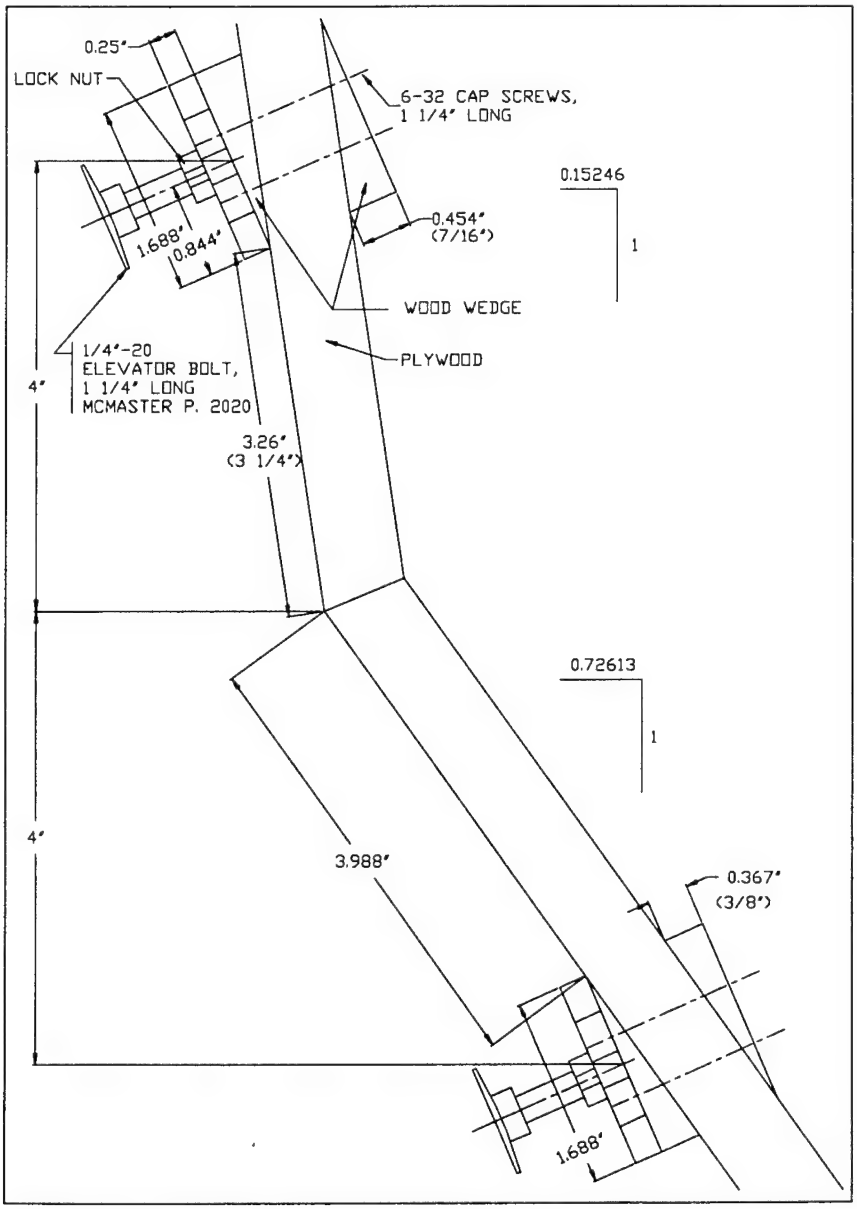

Figure A15. Elevation cross-section view of LVDT plates at change in slope, downstream face.

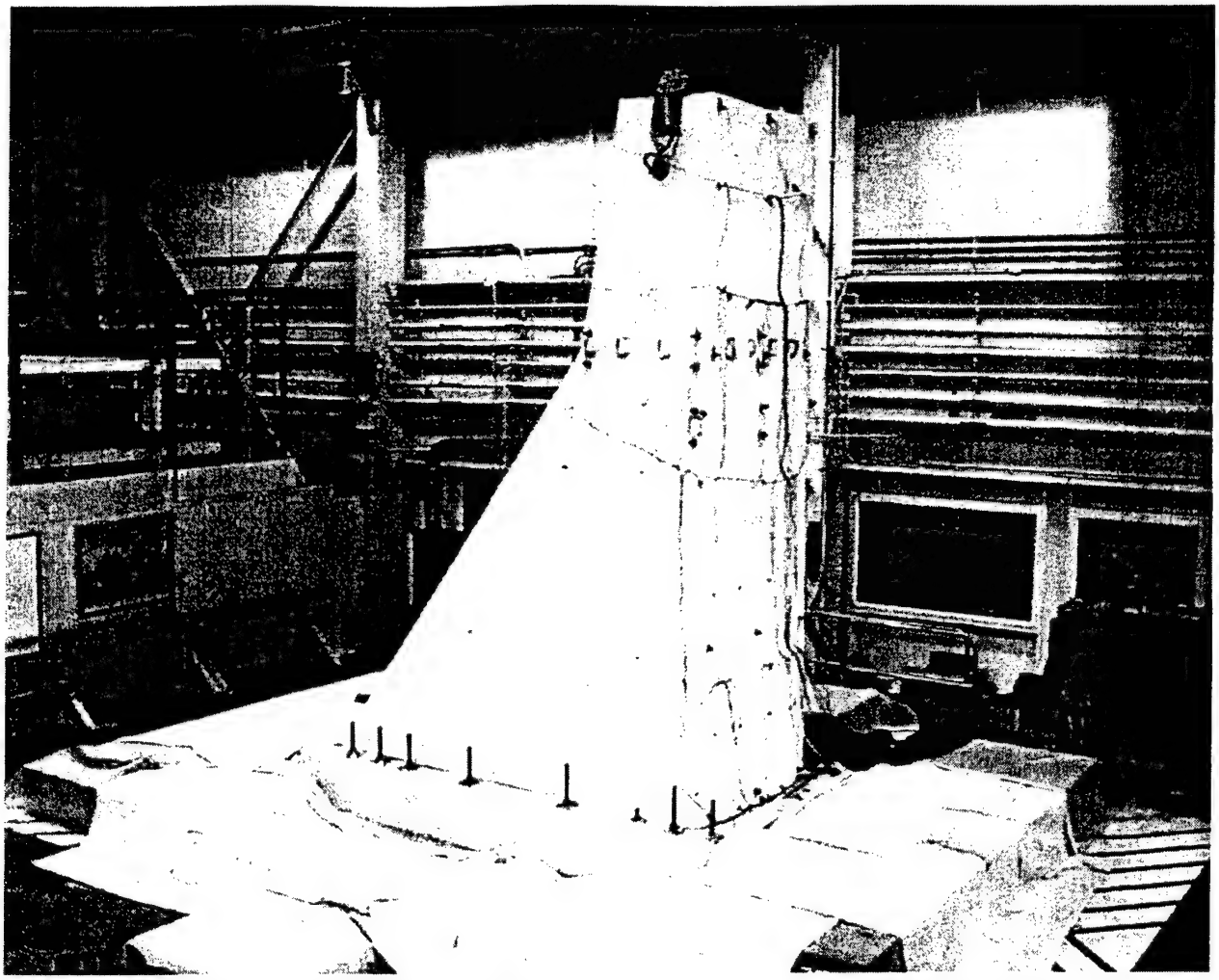

Figure A16. Model before testing showing TESS protection fame covered with plastic sheets and dropcloths.

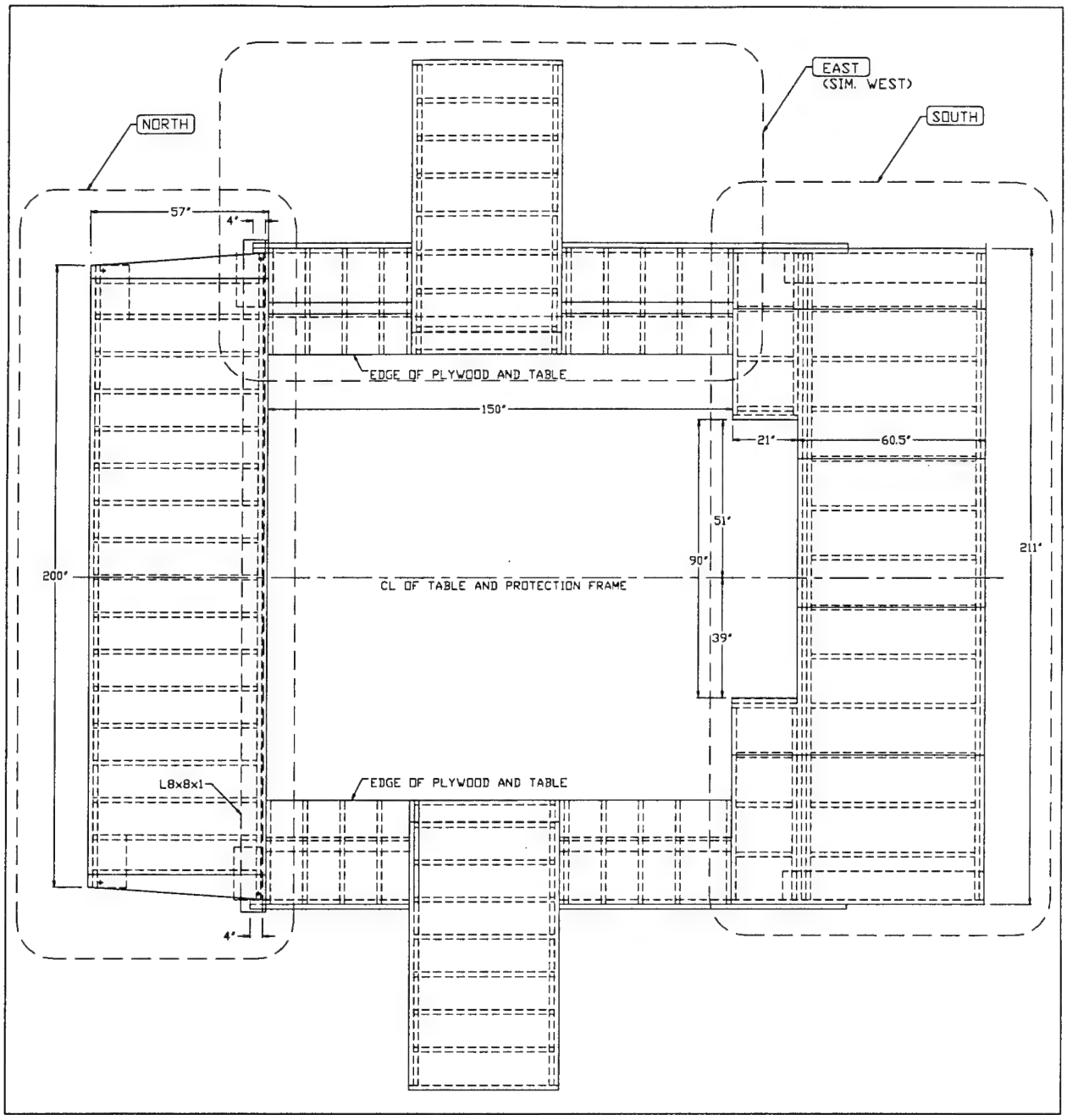

Figure A17. Plan view of the entire TESS protection frame.

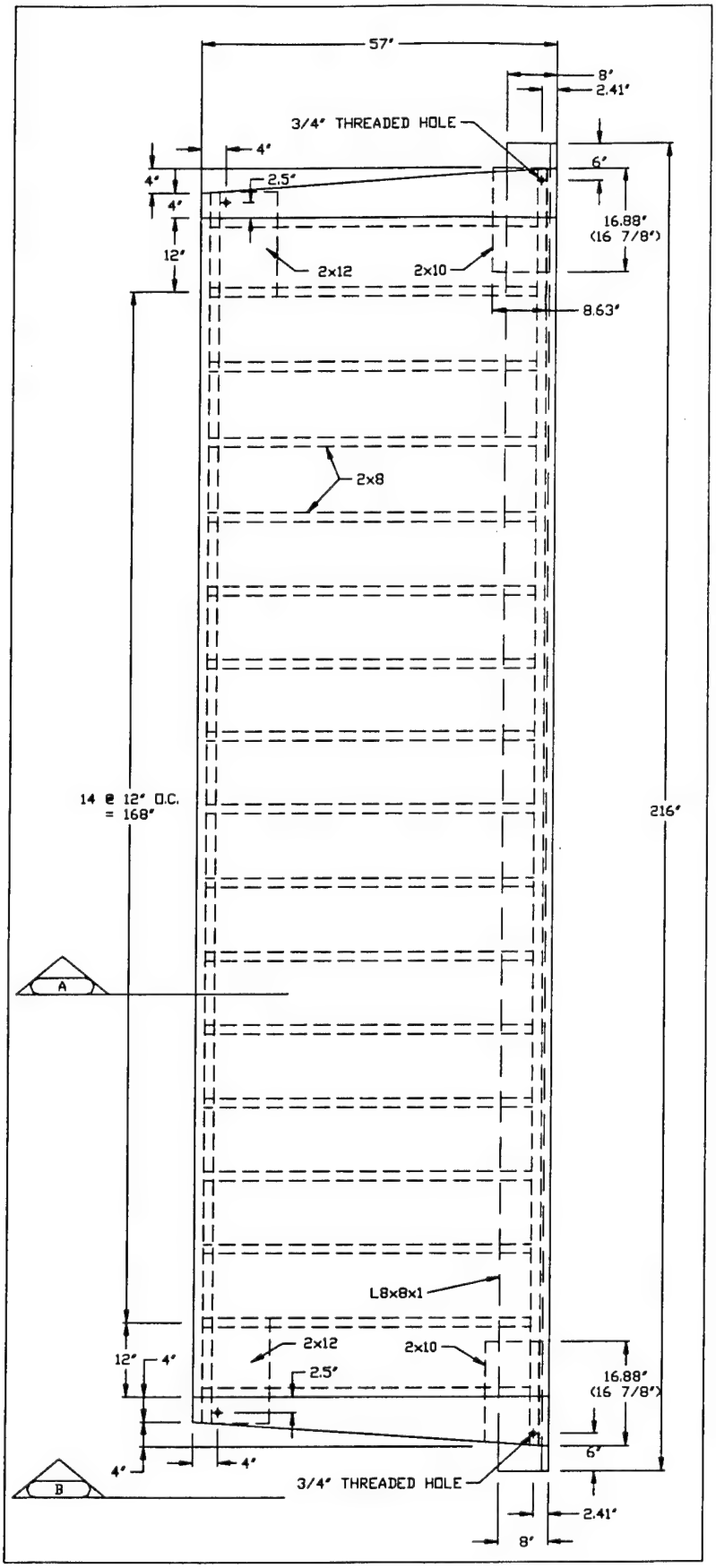

Figure A18. Plan view of north portion of the TESS protection frame.

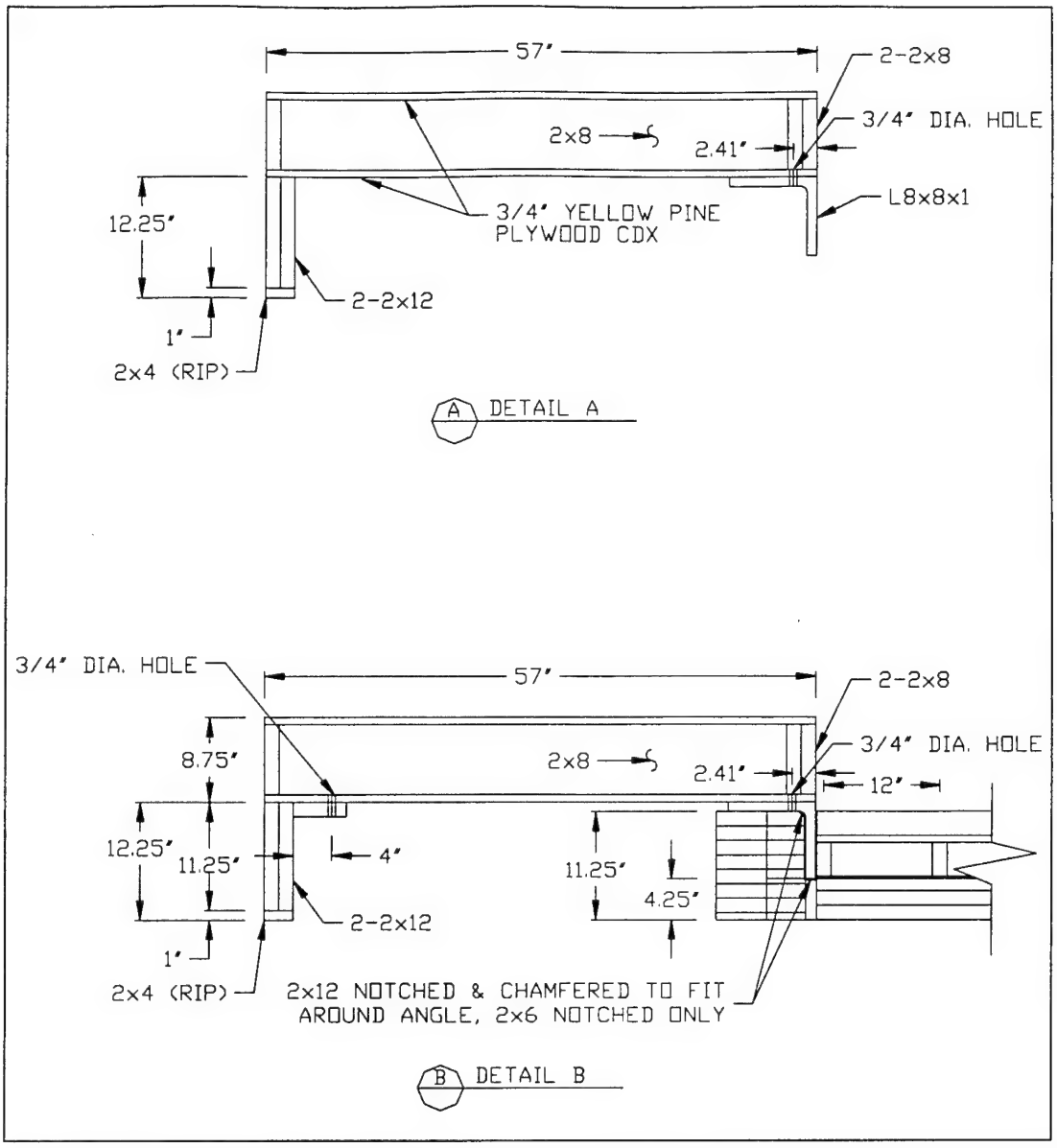

Figure A19. Cross-section views for north TESS protection frame.

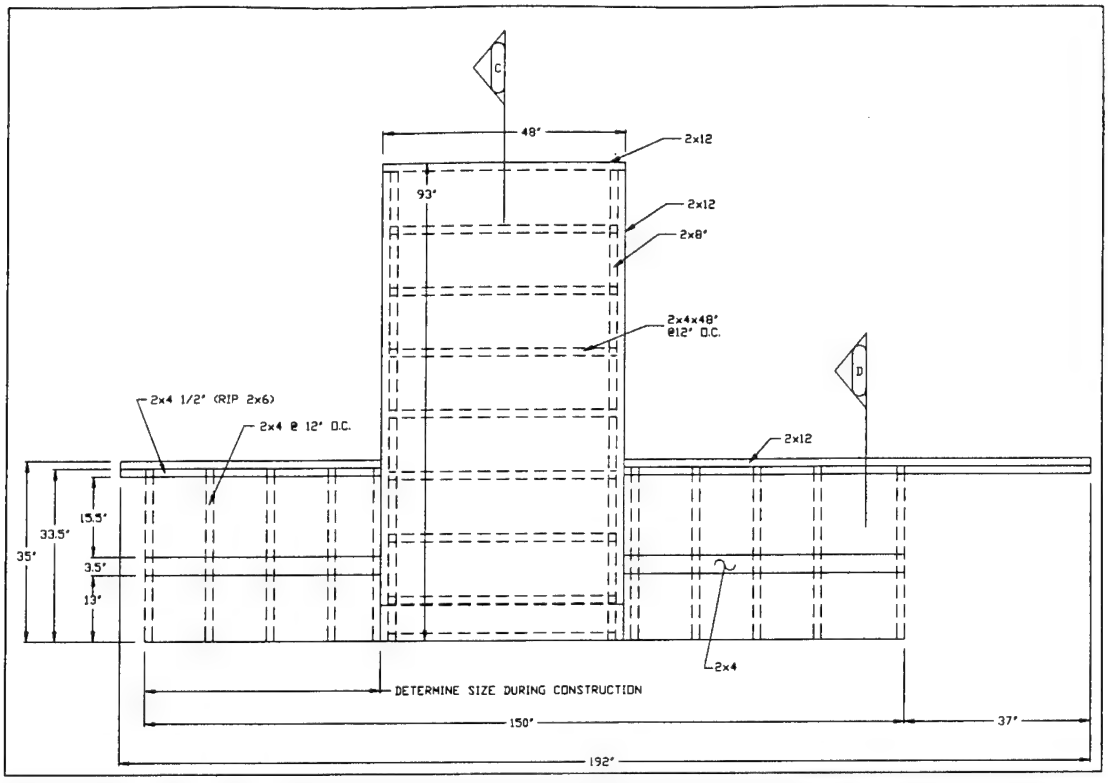

Figure A20. Plan view of the east portion of the TESS protection frame (west is mirror image).

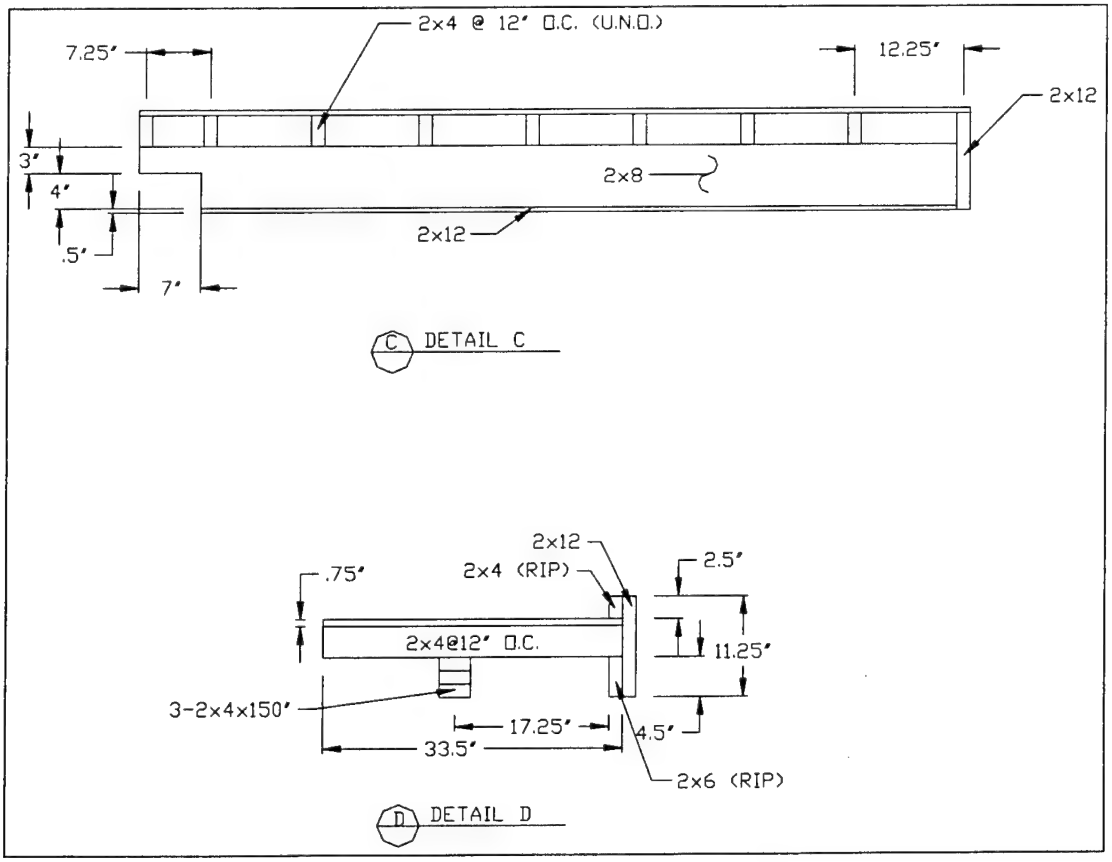

Figure A21. Cross-section views for east TESS protection frame.

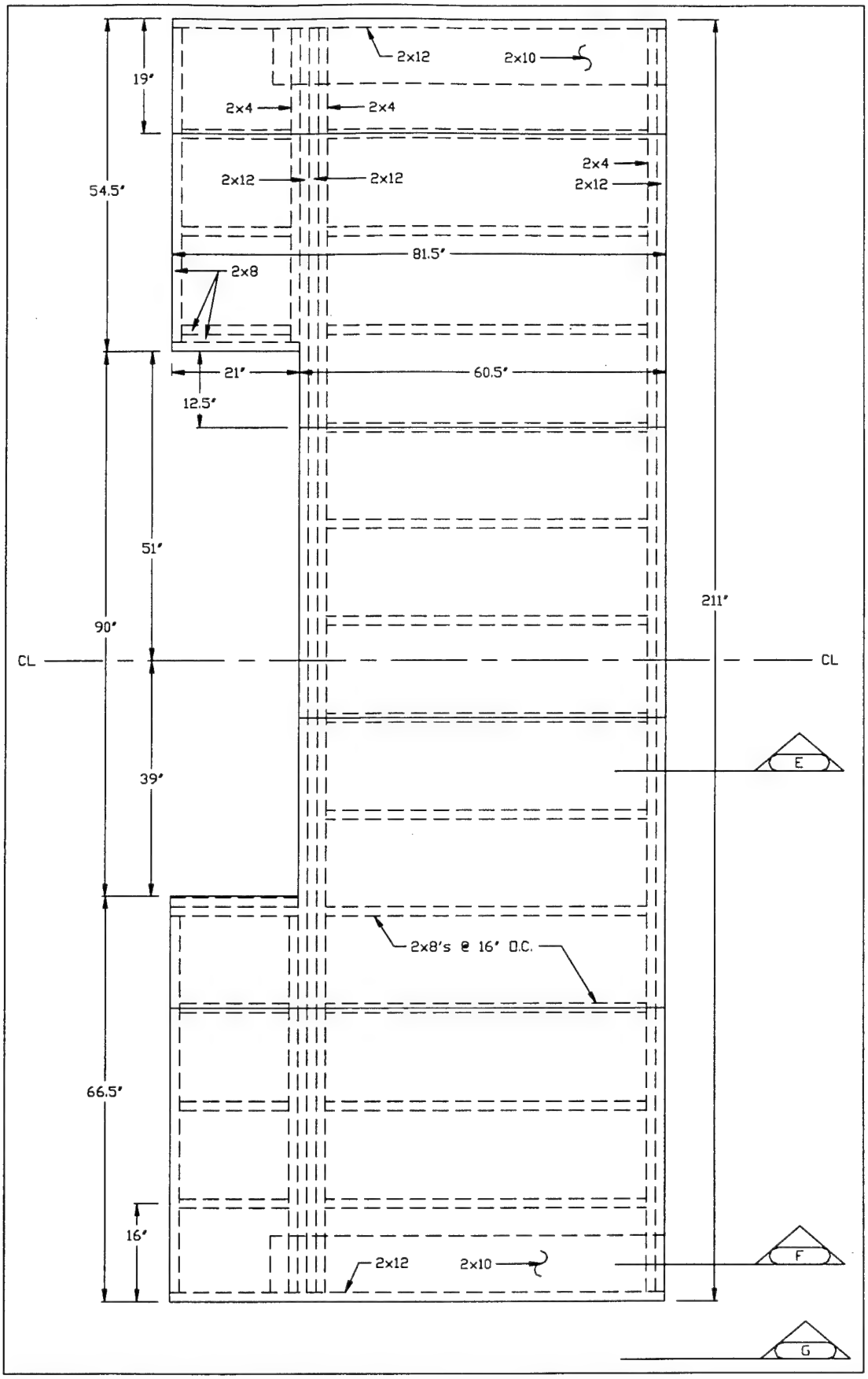

Figure A22. Plan view of the south portion of the TESS protection frame.

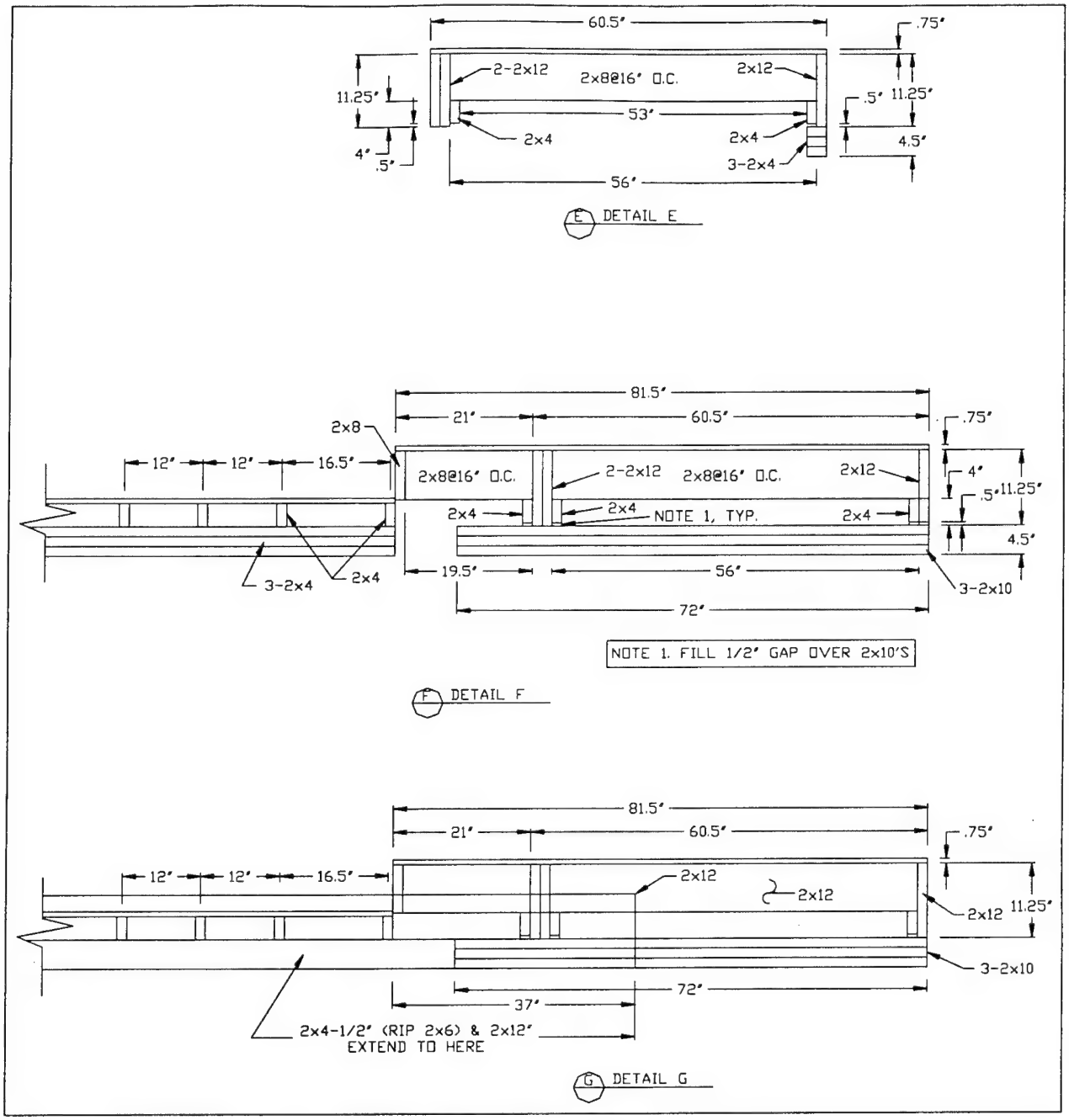

Figure A23. Cross-section views for south TESS protection frame.

Appendix B: Model Materials, Casting, and Surface Preparation

Table 1 (see Chapter 2, page 15) shows that the 1/20-scale Koyna dam model material design requires a very weak material (200 psi, 1.38 MPa) with a low modulus of elasticity (200 ksi, 1380 MPa), normal ultimate compressive strain (0.0025), and normal density (150 pcf, 2400 kg/m^3). Personnel from the Concrete and Materials Division of GSL developed the mix design shown in Table B1 to achieve these properties, based on laboratory testing. The principal component of this mix is Baroid API drilling-grade barite[12] (fine 200 mesh[13]) with a specific gravity of 4.25. This material is used in the oil well drilling industry. The barite was delivered to the ready-mix plant[14] in 2508 lb (1138 kg) "super sacks." These large nylon sacks have a chute at the bottom, and they were placed on wood pallets and sealed with a plastic shrink wrap.

Model Material Batching Process

The material was batched in ready-mix trucks, with 7 cu yd (5.35 m^3) per truck. On the morning of the batching (18 October 1999) the water content of the moist sand was measured and the quantity of water and weight of moist sand was adjusted so that the resulting mix would match the values shown in Table B1. Batching was done outside using a scale and conveyer system.

[12] Supplied by Cimbar Performance Minerals, a division of Baroid Drilling Fluids, which is a division of Halliburton Energy Services.

[13] A material with a specification of 200 mesh indicates that 97% of the material passes through a mesh with 200 openings per inch.

[14] Prairie Central, located in Champaign, IL provided batching services.

Table B1. Koyna Dam model mix proportions and quantities.

Material	Quantities of Materials per the Following		
	1 Cubic Yard	7 Cubic Yard Ready Mix Truck	28 Cubic Yard Total
Type I Portland Cement	285 lb	1995 lb	7980 lb
Natural Concrete Dry Sand	360 lb	2520 lb	10,080 lb
Baroid API Drilling Grade Barite	2508 lb	17,556 lb	70,224 lb
Water	839 lb	5873 lb	23,492 lb
3M Polyolefin 25/38 Fibers	7.7 lb	53.9 lb	215.6 lb
Total Weight	4000 lb	27,998 lb	111,992 lb

The batching of each 7 cu yd truck proceeded as follows:

1. All but 50 gallons of water was placed in the ready-mix truck.
2. Half of the required sand was weighed in the scale.
3. The sacks of barite were lifted by a forklift and emptied into a front-end loader. The loader then dumped the barite into the scale, and this process was repeated for 3 sacks.
4. The fourth sack of barite was emptied into the loader and approximately half of the Portland cement (11 bags at 94 lb each = 1034 lb = 514 kg) was added. Together these were dumped into the scale.
5. The material in the scale was conveyed into the ready-mix truck.
6. The remaining sand was weighed in the scale.
7. Two more super sacks of barite were placed in the scale.
8. A seventh sack of barite was emptied into the loader and the remaining Portland cement (10 bags at 94 lb each plus 21 lb = 961 lb = 436 kg) was added. Together these materials were dumped into the scale.
9. The material was conveyed into the ready-mix truck.
10. The polyolefin fibers came taped in 2 in. diameter bundles, and had earlier been broken free and weighed out in 5 gallon buckets. These fibers were slowly dropped into the truck, as the material was mixed, so as to prevent the fibers from balling up.[15]

[15] In retrospect it appears that the fibers should have been left in their bundles to ensure that they would not ball up and would be uniformly distributed. Because of the lack of large aggregate, there was a concern that the bundles may not break-up, so the tape was removed. However, the mixing time was very long, and this would have ensured that the tape dissolved. If the tape had not been removed, the bundles would have been thrown in the truck individually, which would have ensured uniform distribution and no balling up of the fibers.

11. The batch was mixed for at least 10 minutes. Then the mix consistency was visually checked and the density was measured. The water content was adjusted to achieve the desired mix density.
12. The ready-mix truck continued to mix the material while making the 10-minute trip to CERL.

Personnel from the Concrete and Materials Division of GSL performed all quality control activities related to defining the material properties of the concrete. This included ensuring the correct batching procedure at the ready-mix plant, checking and correcting the material density, and casting test cylinders and beams. Figure B1 shows the casting of test cylinders and illustrates the fluidity of the material.

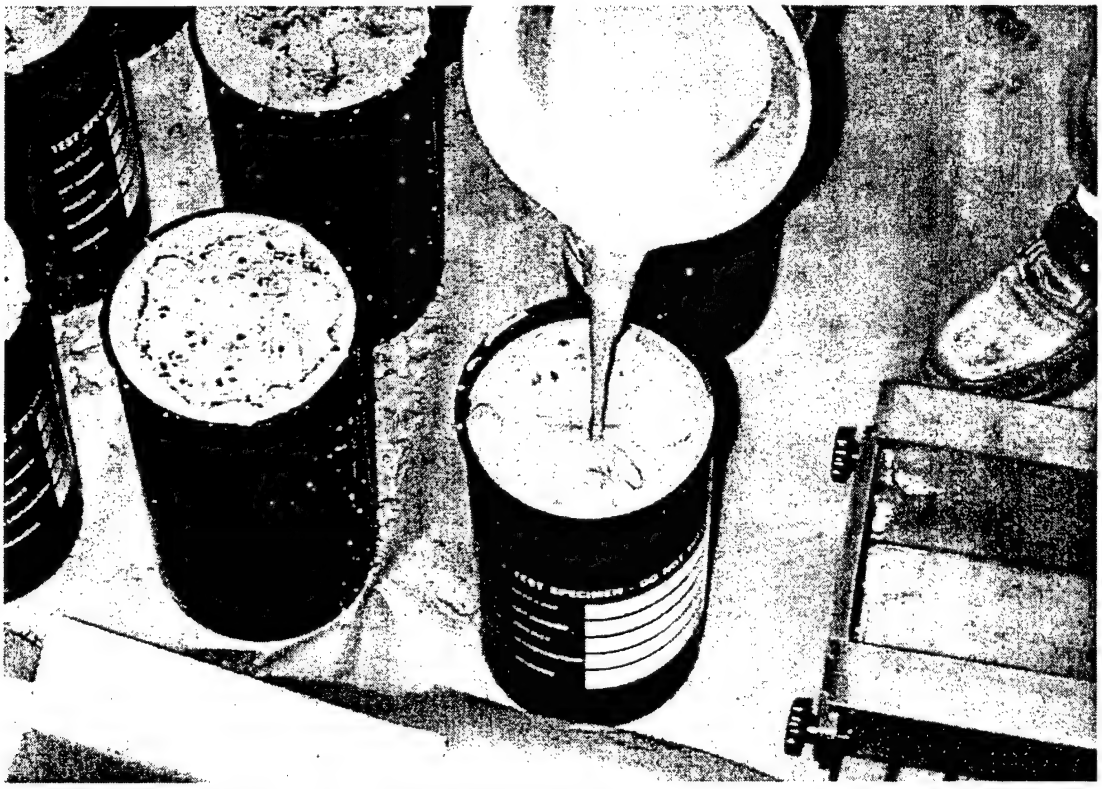

Figure B1. Casting Koyna dam model test cylinders with the very fluid experimental mix.

Casting the Model

The model was cast on 18 October 1999. The ready-mix trucks delivered the material to CERL and discharged into a pump with a boom and a 5 in. (127 mm) line. The end of this line had a 4 in. (102 mm) diameter, 12 ft (3.66 m) long rubber pump hose so that the material could be discharged near the bottom of the model and test block formwork. The boom was gradually raised so that the hose

remained just below the surface of the material as it was poured. This approach prevented the material from dropping which would have lead to material separation and additional pressure on the formwork. Figure B2 shows the rubber hose discharging into the model formwork, looking down into the formwork and showing an interior view of much of the hardware. On the left side of Figure B2 is one of the top bolt inserts, located 24 in. (0.61 m) below the design elevation of the top of the model and 36 in. (0.91 m) below the top of the forms. This picture shows other inserts, formwork coil ties, instrumentation plates with elevator bolts attached, and EMT conduit. Almost immediately the material began to settle, and clear water rose to the surface (see Figure B2).

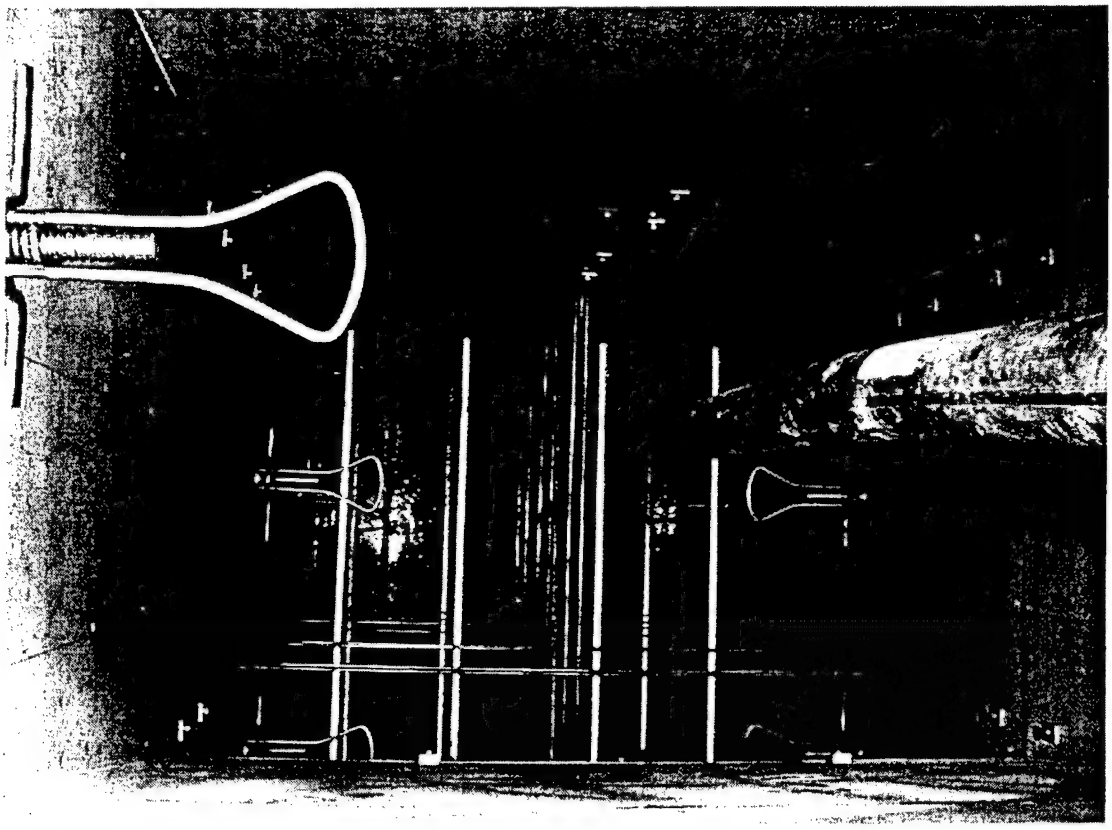

Figure B2. The rubber hose discharging material into the model formwork.

During the pumping of the second truckload of concrete the formwork began to leak around ties and other penetrations (see Figures B3 and B4). Initial leaks were essentially clear water, where the water had settled out of the mix, but later the material itself began to leak, as seen in Figures B3 and B4. The leak shown in Figure B3 is on the downstream face where a coil-tie bolt, used to support an EMT conduit, penetrates the formwork. Figure B4 shows a leak on the downstream face where a coil-tie bolt, used to support a waler, penetrates the formwork. These leaks were plugged using rags and wood scraps that were screwed into the formwork. Leaking became much worse as the elevation of ma-

terial and resulting pressures increased. During the pumping of the third truck, the elevation passed the change in slope on the downstream face by about 1 ft. At that point considerable leaking took place, and pumping was stopped while the leaks were plugged. The formwork MDO board began to absorb moisture along its penetrations and soften as a result, so that the formwork became more flexible. Also, the horizontal walers on the downstream face were not, initially, wedged tight against the bearing edges of the vertical angles. The lack of tight bearing allowed the downstream formwork to lift about 1/8th in. (3 mm), which further increased leaking. Blocking installed between the downstream 4 x 4s, and between the MDO board and L5x5x3/8 angle, limited this leaking. The MDO board that had absorbed moisture deflected at least 1/8th in. (3mm) between vertical ribs. The walers on the downstream face also began to deform noticeably.

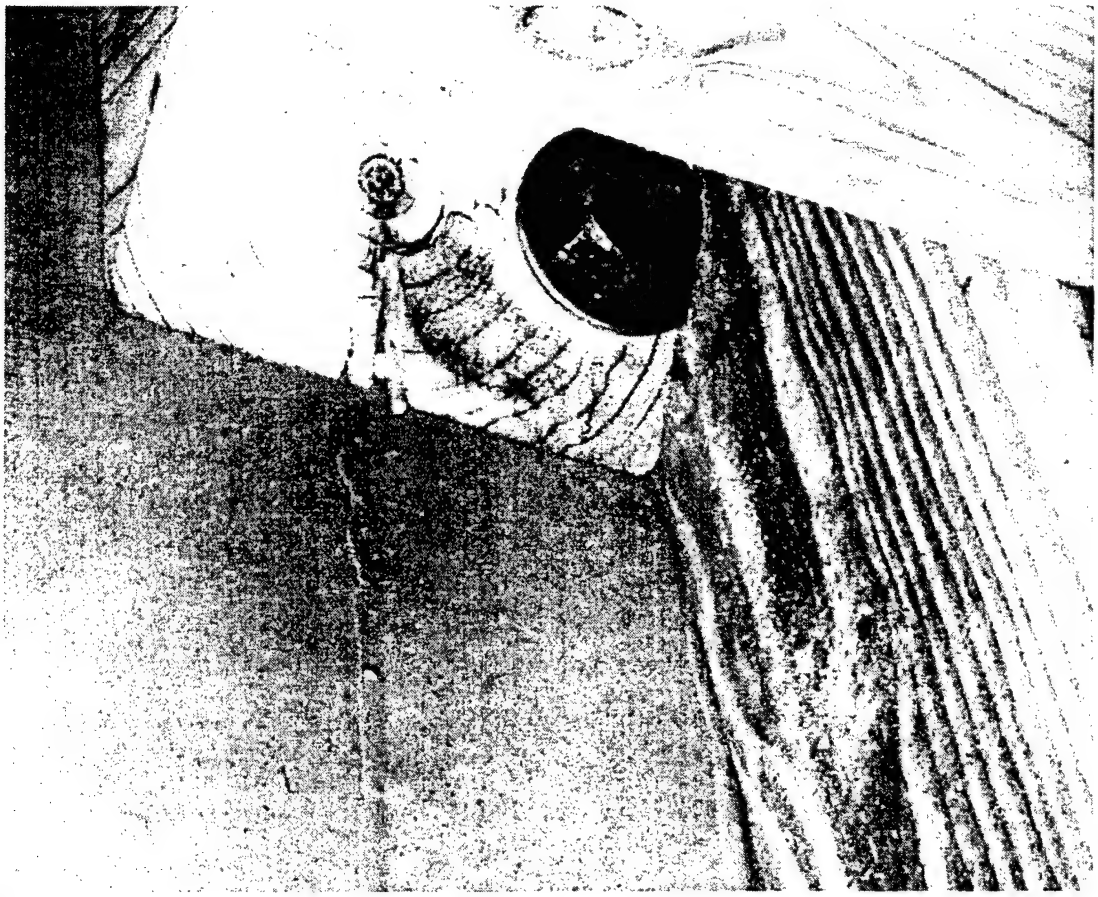

Figure B3. Leaks on the downstream face where a coil-tie bolt penetrates the formwork.

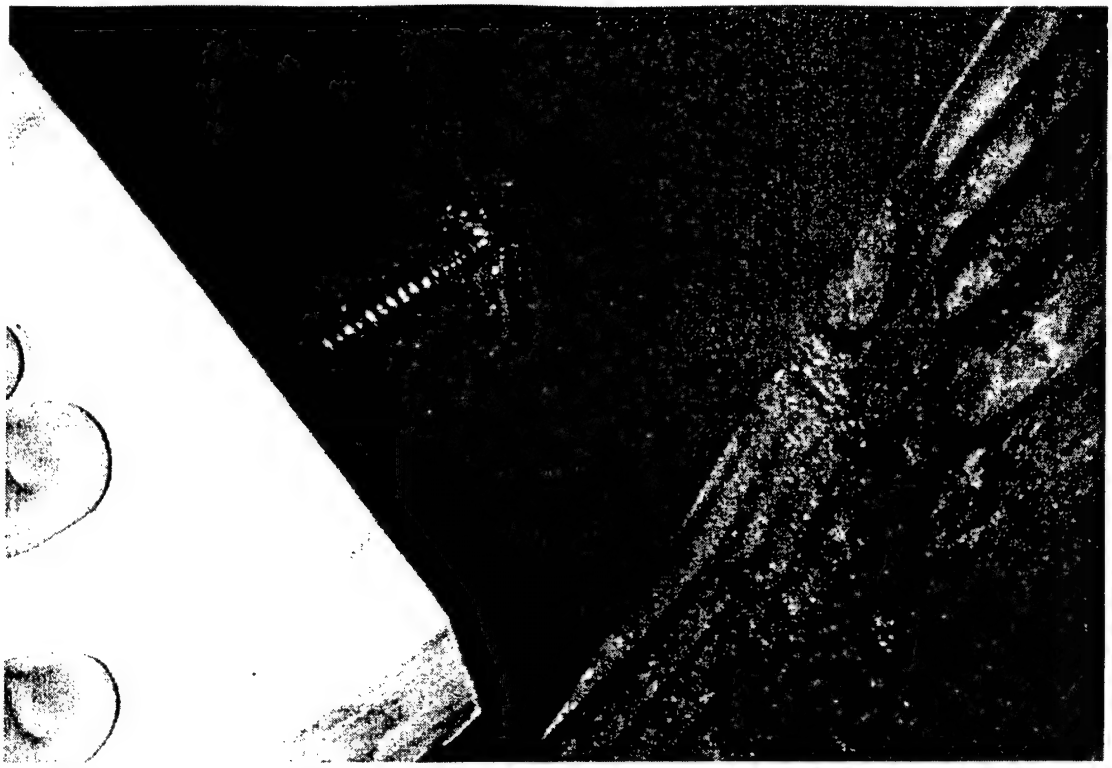

Figure B4. Leak on downstream face where coil-tie bolt for waler support penetrates formwork.

After leaking was stopped, the remaining material in the third truck was pumped into the test block. Further pumping of the material was postponed for about 3 hours, so as to stabilize the leaks that had been plugged. Then the material from the fourth truck was pumped into the formwork in approximately 12 in. (0.3 m) lifts, with a 30-minute delay between lifts. This process continued until the material reached an elevation of about 4 in. (0.1 m) above the design elevation. The only leaks to occur after the 3 hour pumping delay were of essentially clear water and these were easily plugged. Still, because of concerns about leakage and the moist, heavily loaded formwork, it was decided to not cast the model to the top of the formwork, which would have been 12 in. (0.3 m) above the design elevation. As expected, the material continued to settle, with about 9 in. (0.2 m) of clear water on the top surface. Therefore, the final elevation of the model top was 4.8 in. (0.12 m) below the design elevation.

Immediately after casting, the formwork for future models was redesigned to greatly reduce leaking and to stiffen and strengthen it. These improvements will be incorporated into the formwork for any future Koyna dam models that may be cast.

Model Curing, Formwork Removal, and Surface Preparation

The materials experts who developed the mix said that the model surface must not be allowed to dry at all, or else large cracks would form. Therefore, the exposed top surface of model and test block were kept moist initially with standing water and later with saturated burlap. About 30 layers of burlap were placed on the top of the dam model and they were kept saturated using a 5-gallon bucket with a very small hole drilled into it. The formwork continued to leak slowly and this slow flow of water ensured that the model remained moist on all surfaces.

Plans were made to test the model at 28 days after casting. Because of the extremely weak model material, the formwork was left on to support the model as long as possible. However, the formwork had to be removed in time for surface preparation and sensor installation. Test cylinder tests were scheduled for 7 and 14 days after casting, so it was decided to remove the model formwork after receiving the 14-day cylinder test results to confirm that sufficient material strength had developed. The test block formwork was stripped first, at 14 days after casting (1 November 1999). Its surface was immediately painted with two coats of a clear curing compound.[16] At 16 days after casting (3 November 1999), the Koyna dam model formwork was stripped. Two coats of the same curing compound were applied to every surface of the model on the same day that the formwork was removed. It was important that any cracks developing during testing be easily seen. Therefore, all surfaces of the model and test block were painted with two coats of whitewash (a lime and water mixture). Cracks that develop could be easily seen because the white surface would contrast well with the darker gray model material. Because the whitewash is brittle, it will crack itself when the model cracks, thus not masking crack development.

While the model cured and the surface was prepared, construction of the TESS protection frame was completed. Figure B5 shows the Koyna dam model after the application of curing compound but before whitewash application.

[16] VOCOMP-20 Water-Emulsion Acrylic Curing and Sealing Compound.

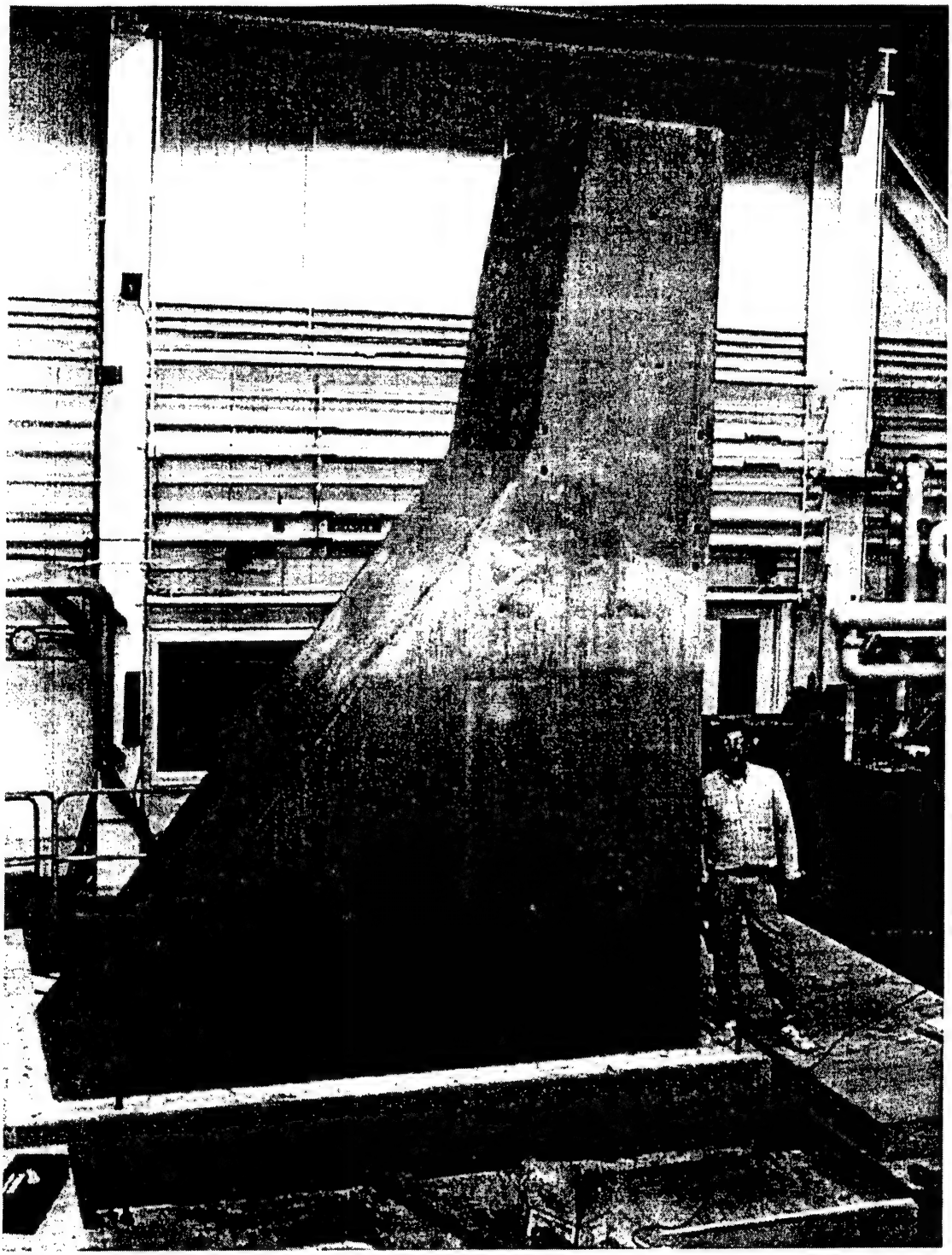

Figure B5. Back face of Koyna dam model after the application of curing compound, but prior to whitewash application.

Appendix C: Detailed Test Plan

[Note: The text below is the test plan used as the basis for all shake table tests of the Koyna Dam model. It has been lightly edited to remove typographical errors.]

The following tests will be conducted on the first Koyna dam model. All tests will be conducted on the Triaxial Earthquake and Shock Simulator (TESS).

1. Attach a 50 lb modal shaker, provided by Geotechnical and Structures Laboratory (GSL), to the top center of the upstream face of the dam model. This will be the driving point for low-level modal tests conducted by GSL.

2. Determine the natural frequencies, mode shapes, and damping of the primary mode in the X-direction (transversal) using the 50 lb modal shaker. Then drive the model with random motion and measure the response on a grid pattern on the upstream face of the model. The data generated from these tests can be compared to the analytical models.

3. The dam model is expected to have fairly high damping so it may be difficult to define the frequencies accurately by the random-motion testing. Therefore, sine sweep tests at a slow sweep rate may be performed in each of the three directions. The amplitude of these sine motions will begin at 0.002 g and may be increased if needed. Sine sweep tests will begin at 4 hertz and will sweep up to 64 hertz (4 octaves) initially. The sweep rate will be 12 octaves per minute for a total duration of 20 seconds (i.e., 5 seconds per octave). Assuming the model natural frequency is 13 hertz, this sweep rate will result in approximately 33 cycles of amplified response for 5 percent critical damping. Figure C1 shows the response of a single-degree-of-freedom oscillator to harmonic motion at 2, 5, and 10 percent critical damping. From this figure the gross assumption is made that amplified response from a sine sweep record will occur when the transmissibility from harmonic motion is above 3, which occurs over half an octave shown in Figure C1. It takes 2.5 seconds to sweep half an octave, which results in 33 cycles for a 13 hertz oscillator. It is expected that the model response will be amplified approximately 3 to 5 times that of the support motions at the natural frequency of the model, assuming damping of 5 to 10 percent. Therefore, the sweep rate of 12 octaves per minute should provide significant amplified response to define the natural frequencies of the model without overexciting it.

4. The second Koyna dam model[17] will be tested with time history motion in the X direction that has been scaled from the 1967 earthquake. Figure C2 shows the unscaled motions recorded in the transversal direction. Figure C3 shows the same record scaled for the test model. This record was created by multiplying the time step by 1 over the square root of the reciprocal of the model scale, i.e., $1/\sqrt{20}$. There is a concern that the second model tested in the X-direction according to the motion shown in Figure C3 could excite a response in the Y-direction, which would be restrained in the actual dam. To evaluate this concern, the first Koyna dam model[18] was to be tested with a low percentage (2 percent) of the record shown in Figure C3. This level was to be increased as needed to excite a clear response in the model. The Y-direction response was to be compared with the X-direction response, based on the recorded accelerations at the top of the model (A10x versus A10y). Figure C4 shows response spectra for the scaled Koyna record (Figure C3) at 2, 5, and 10 percent damping. The response of the Koyna dam model can be estimated based on this plot for the first natural frequency of the model in the X-direction.

5. Finally, the model will be excited with sinusoidal motions in the X-direction just above the natural frequency of the model. In the modal testing, the measured natural frequency was 13.2 hertz. If the TESS modal tests yield a similar natural frequency, the model will be tested with sinusoidal motions at 15 hertz. Figure C1 shows that a single-degree-of-freedom oscillator at 13.2 hertz with 5 percent damping, excited with 15 hertz harmonic support motion, will respond at 3.2 times the support motion. Alternatively, if this same oscillator were excited with 14 hertz support motion, it would respond at 6.15 times the sinusoidal support motion. These motions will begin with a peak amplitude of 0.005 g and duration of 7 seconds. These tests will be repeated at higher amplitudes with an increment in amplitude of 0.005 g. The sinusoidal records will ramp up linearly in 1 second, maintain a constant peak amplitude for 5 seconds, then ramp down in 1 second. After each test the model will be visually inspected for signs of cracking. Any cracks will be marked. Selected data channels will be inspected to observe model behavior.

6. If it appears that damage may have occurred, resonance tests will be repeated to determine the new resonance frequency.

---

[17] Testing of a second dam model was part of the original testing concept, but no final plans for this have been made.

[18] The "first" model is the one that was tested and documented in this report.

7. Additional sinusoidal tests will be conducted above the new resonance frequency of the damaged model.

8. Sinusoidal tests will continue, by repeating steps 6 through 8 until ultimate failure of the dam model.

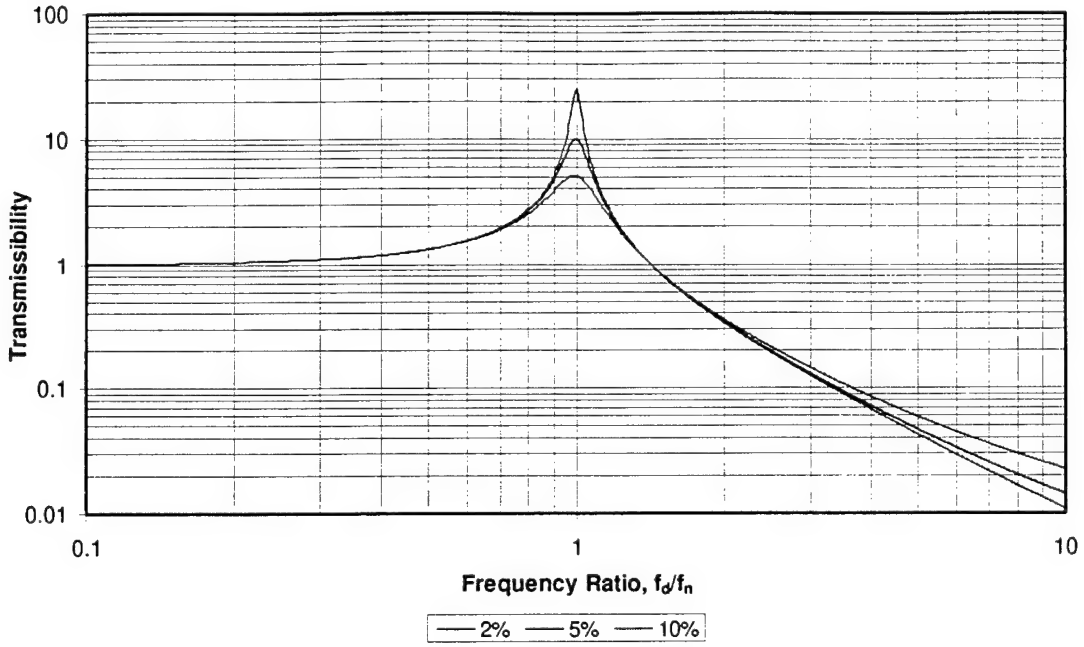

Figure C1. The response of a 13.2 Hz SDOF oscillator to harmonic motion.

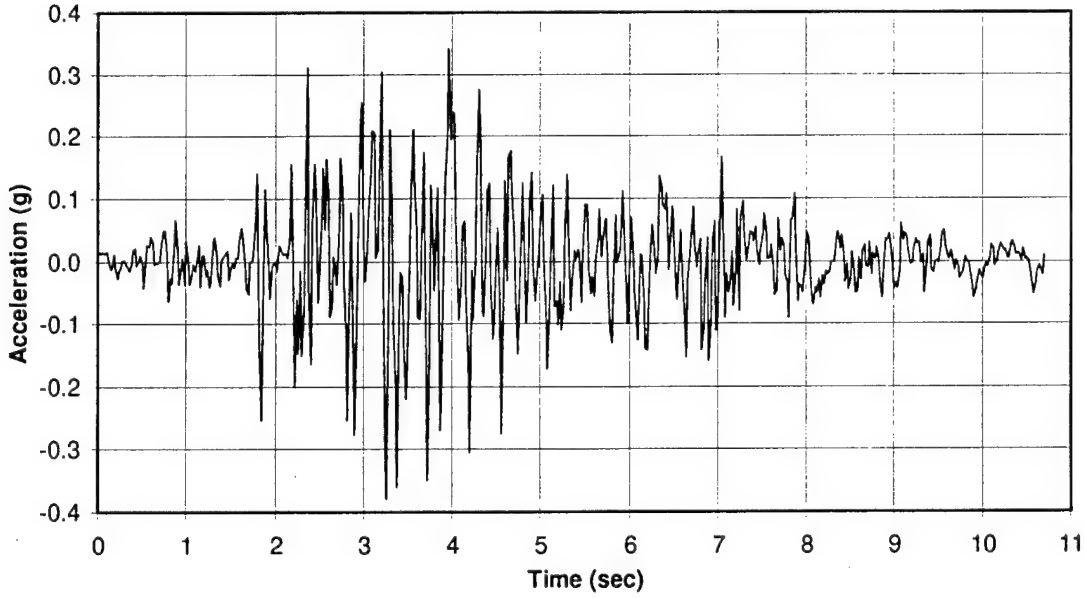

Figure C2. 1967 earthquake motions recorded in the transverse direction.

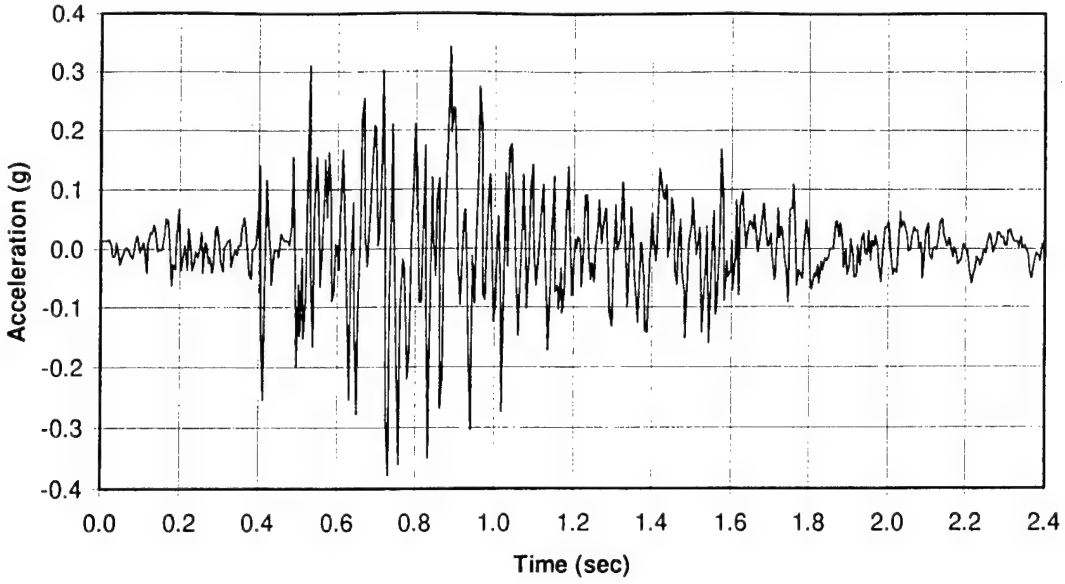

Figure C3. Scaled motions for the 1/20 scaled dam model in the transverse direction.

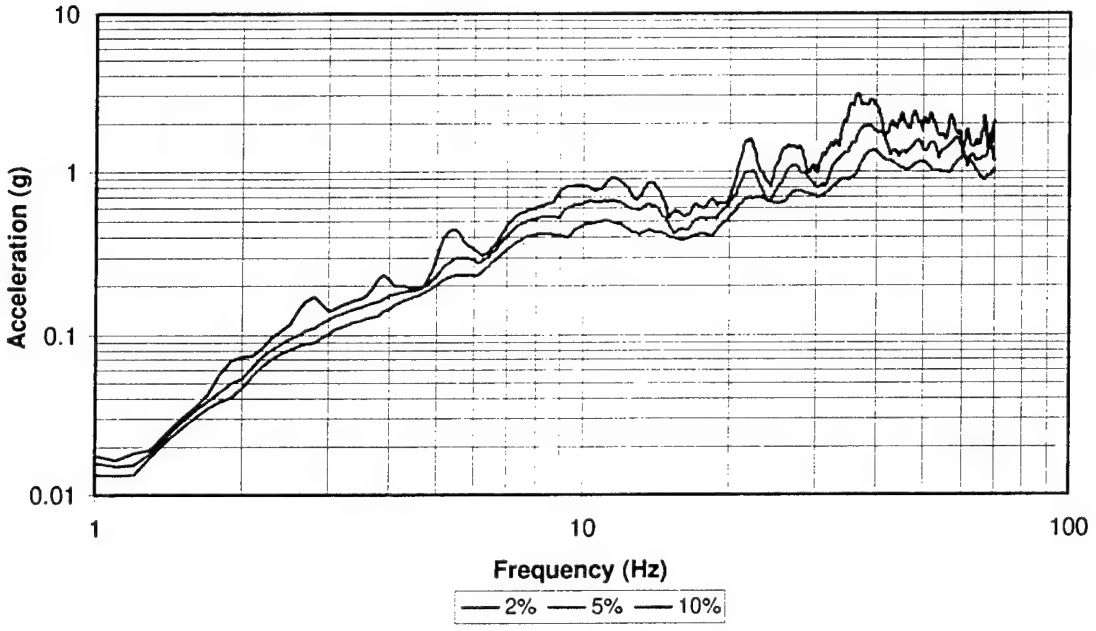

Figure C4. The response spectra for the scaled Koyna record.

Appendix D: Model Demolition and Core Samples

Demolition Plan

The Koyna dam model and base beam together weighed about 95,000 lb, exceeding the 40,000 lb capacity of the overhead crane. An effort was made to find a large enough mobile crane to lift the 95,000 lb specimen. The mobile crane would need to fit through the shake table overhead door also, and such a crane could not be found at a reasonable cost. Therefore, the model could only be removed by demolishing it on the shake table. A method of demolition was needed that would minimize dust because of the close proximity of the shake table hydraulics and electronics, so extensive use of a jackhammer or other impact devices was not acceptable. The use of impact drills or saws also would create dust and were therefore undesirable. Consequently, plans were made to demolish the model on the shake table by breaking it into large sections using expansive grout. Appendix A explains demolition details that influenced formwork detailing. An expansive grout material called Bristar 100 was purchased from Demolition Technologies, Greenville, AL. The Bristar 100 material is simply mixed with water and poured into a hole. Normally holes are drilled, but Demolition Technologies recommends that the holes be created by casting thin steel pipes into the temporary structures. Casting pipes into the model would also eliminate the dust created by drilling holes, so electrical mechanical tubing (EMT) was cast into the dam model at the locations shown on the formwork drawings in Figures A8 and A9. The EMT conduit was used because it has thin walls and will easily yield as the grout expands and fractures the concrete.

Actual Demolition Procedure

The expansive grout proved ineffective in cracking the test block, so a different method was used to break up the dam model. This method also had to avoid creating much dust. The first task was to remove the portion of the model above the crack. As explained in Chapter 5, this section could not be lifted by the inserts and overhead crane alone. Instead, a large-bucket tractor (15,000 lb, or

6800 kg capacity) was used to lift this section in conjunction with the overhead crane. A lifting ledge was created by removing about a 5 in. (130 mm) deep portion of the model material from the upstream face below the primary crack using a small pneumatic hammer. Figure D1 shows how the lower lip of the bucket was inserted below this ledge. The bucket was rotated, so as to come in contact with the upstream face. Then chains were wrapped around this section of the model to hold it against the bucket. Then the bucket was gradually rotated, as the overhead crane lifted the model section so that the bucket eventually held the section with the overhead crane still attached. The photograph in Figure D1 was taken soon after the rotation began, as can be seen by the greater opening on the downstream face. This section of the model and the remaining ones were removed from the direction of the upstream face so that they passed over the highest-strength section of the TESS protection frame (in case the section failed at the ledge and fell).

The next section of the model had fractured along the EMT tubing, but without use of the expansive grout. Large high-strength steel rods (1.25 in. or 32 mm diameter) were inserted 36 in. (0.91 m) into the top set of EMT tubes on the upstream face. A small I-beam was placed against the upstream face below the steel rods. The overhead crane was attached to the I-beam. A wood 4 x 4 was placed below the I-beam also against the upstream face. Then the lip of the bucket of the tractor lifted against the 4 x 4 while the crane lifted the I-beam, so that a total force of 55,000 lb was available to pry up on the steel rods on the upstream face of the model. Prior to lifting, the pneumatic hammer was used to create about a 1 in. (25 mm) deep groove between the EMT tubes on both the upstream and downstream faces. This groove was intended to increase the stress concentration, which would cause a tension crack to begin at the upstream face. Figure D2 shows the lifting configuration right after failure along the top set of EMT tubes. Once the crack began on the upstream face, it immediately propagated across the model cross-section along the EMT tubes. Next the failed section was blocked up and two chains were inserted below this section. Figure D3 shows the lifting of this section with the overhead crane.

The next section was similarly failed along the EMT tube. However, the fracture surface was greater at this lower level. A problem arose in that the overhead crane and the tractor lifted with enough force to raise one side of the remaining model and shake table. This could have been avoided if the shake table hydraulics were turned on so the vertical actuators could resist the lifting force. Rather than turning on the shake table, the model was further weakened by using a saw to cut around the model perimeter at the elevation of the EMT tubes. Then a sledgehammer was used to hit the model near the elevation of the EMT tubes. Both these steps created a greater stress concentration, and model eventually

cracked along the lower set of EMT tubes. Failure along the lower set of EMT tubes was more difficult for four reasons: (1) larger fracture surface; (2) less lifting resistance because of the reduced mass of the remaining model; (3) location of the fracture surface directly above the reinforcing steel coming up from the base beam; and (4) greater strength of the concrete near the base of the model (as determined later by analyzing core samples).

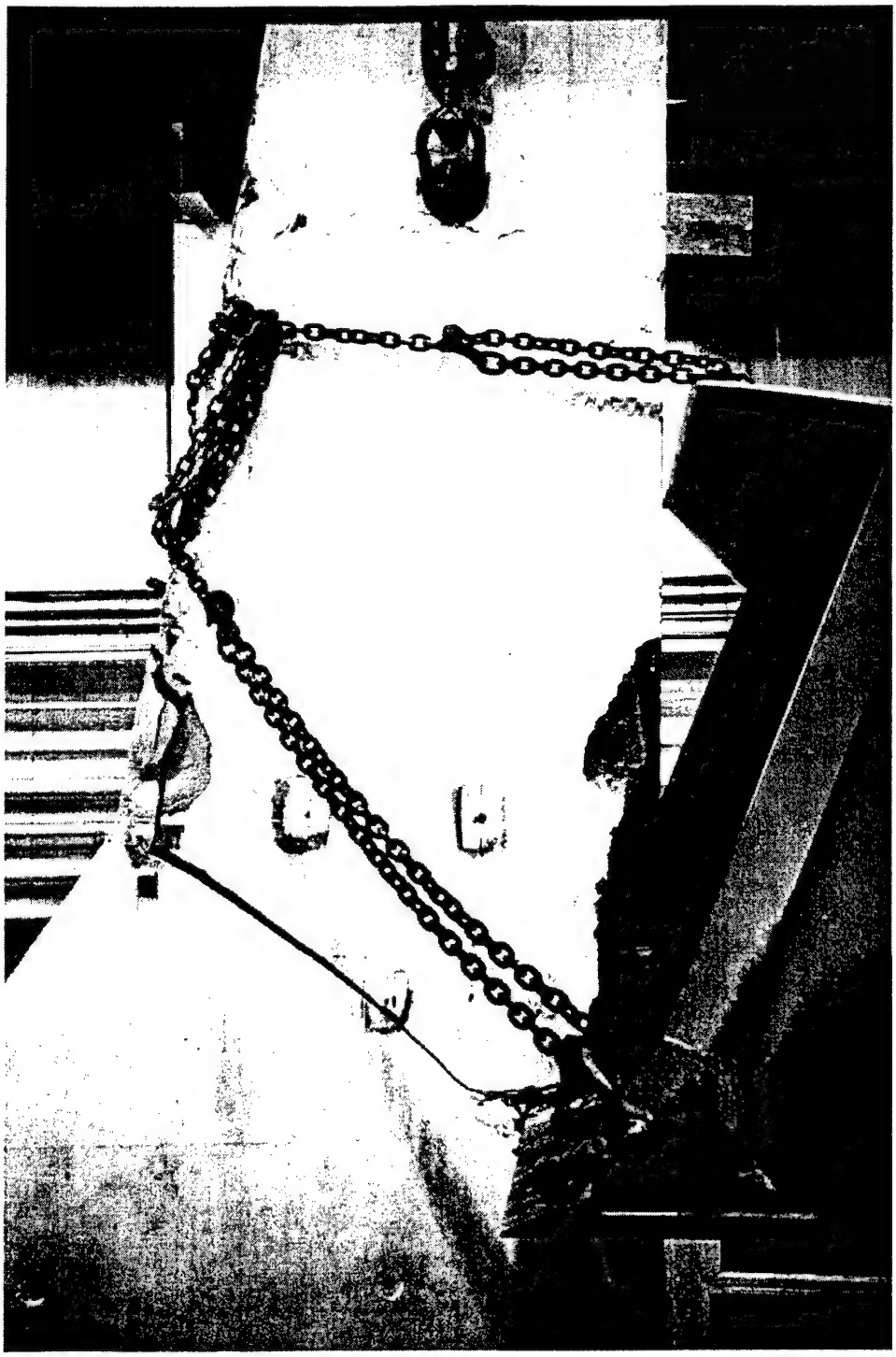

Figure D1. Removing top section of model with tractor and overhead crane.

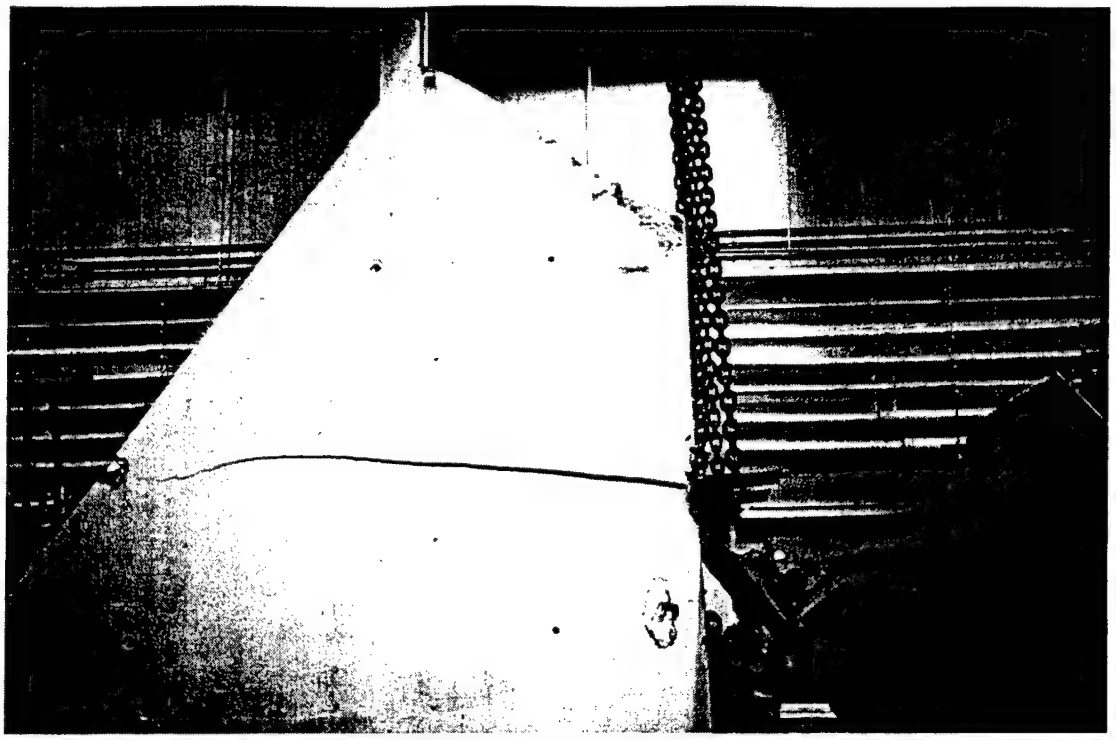

Figure D2. Lifting configuration for cracking along the top set of EMT tubes.

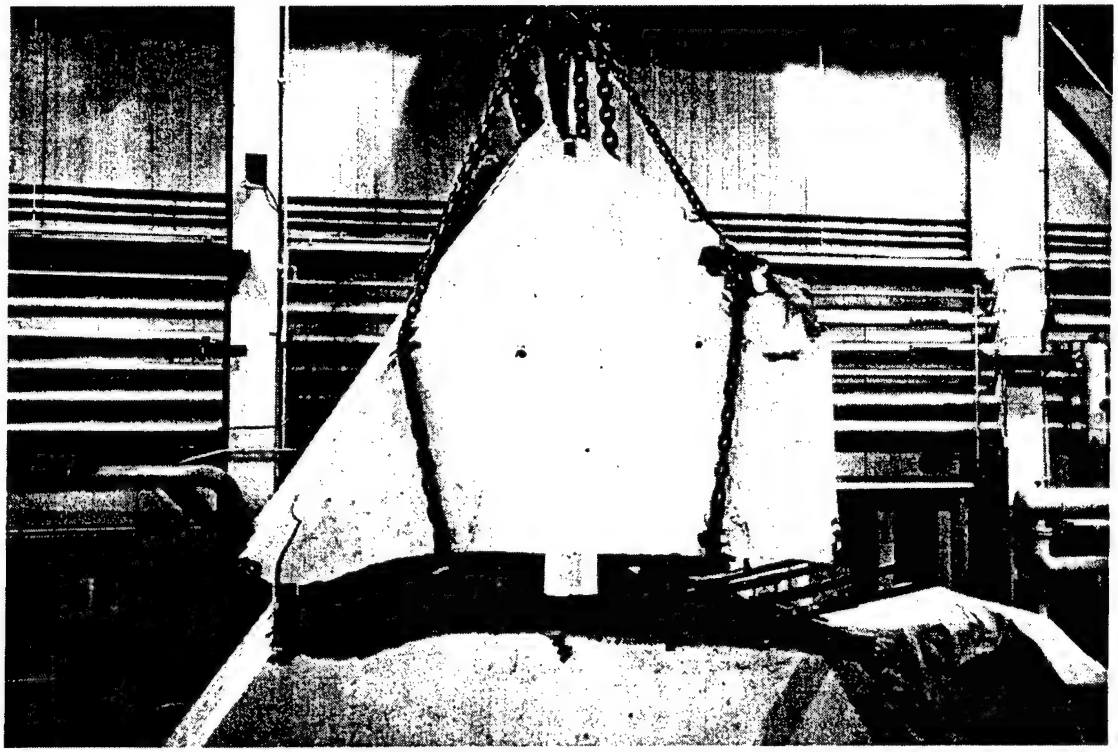

Figure D3. Lifting of the failed section of the model with the overhead crane.

Extraction and Testing of Core Samples

The substantial settlement of the Koyna dam model material during casting and the limited amount of fibers near the fracture surface raised a concern that the material may be much stronger and denser near the base than near the fracture surface. Therefore it was decided to take core samples from near the crack surface and near the base of the model. A local contractor was hired to drill multiple core samples from both the base of the model and out of a section of the model that was saved from near the primary crack surface against the downstream face of the model. All cores were 4 in. (100 mm) in diameter. Figure D4 shows the drilling of a core sample from near the base of the model. Figure D5 shows a 16 in. (400 mm) long core taken from the base of the dam model. The section from the cracked surface was much smaller and more fragile than the section at the base. Figure D6 shows the drilling of a core sample from the section near the primary crack. The cores taken from near the crack were only about 7 in. (180 mm) long while those taken from the base were about 16 in. (400 mm) long. The model section from near the crack was very fragile and was developing multiple cracks, which limited the length of cores that could be extracted.

The cores were carefully packed and shipped to GSL for testing. The date tested (10 February 2000) was 115 days after casting the model (18 October 1999). The materials expert at GSL stated that the material properties would change very little after 28 days, so the 115-day properties should represent 28-day properties. The average material properties for the cores taken from both the base of the model and near the crack are given in Table 1. The materials expert further noted the following:

> *Fibers were visibly present and numerous in specimens identified as coming from near the base. However, only a few fibers were visible in specimens identified as coming from near the crack. Some specimens identified as being from near the crack were too short to test. All specimens were tested in their as-received moisture condition.*

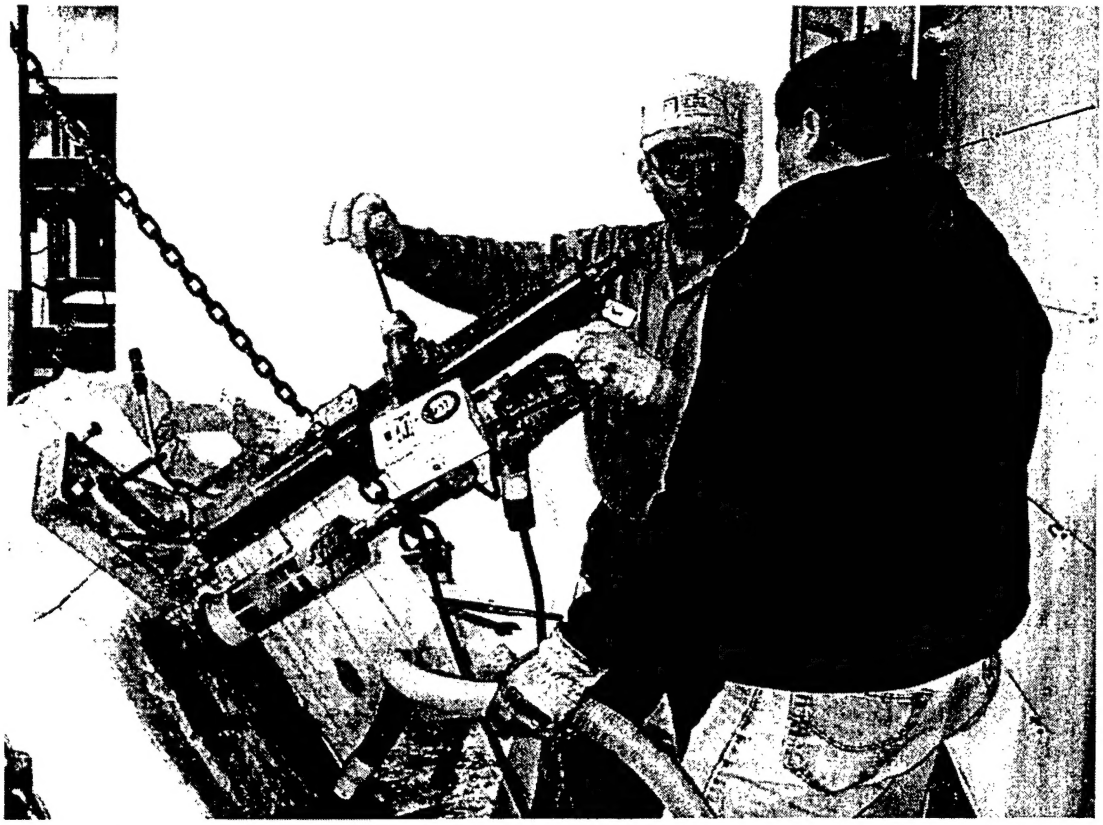

Figure D4. Drilling core samples near the base of the model.

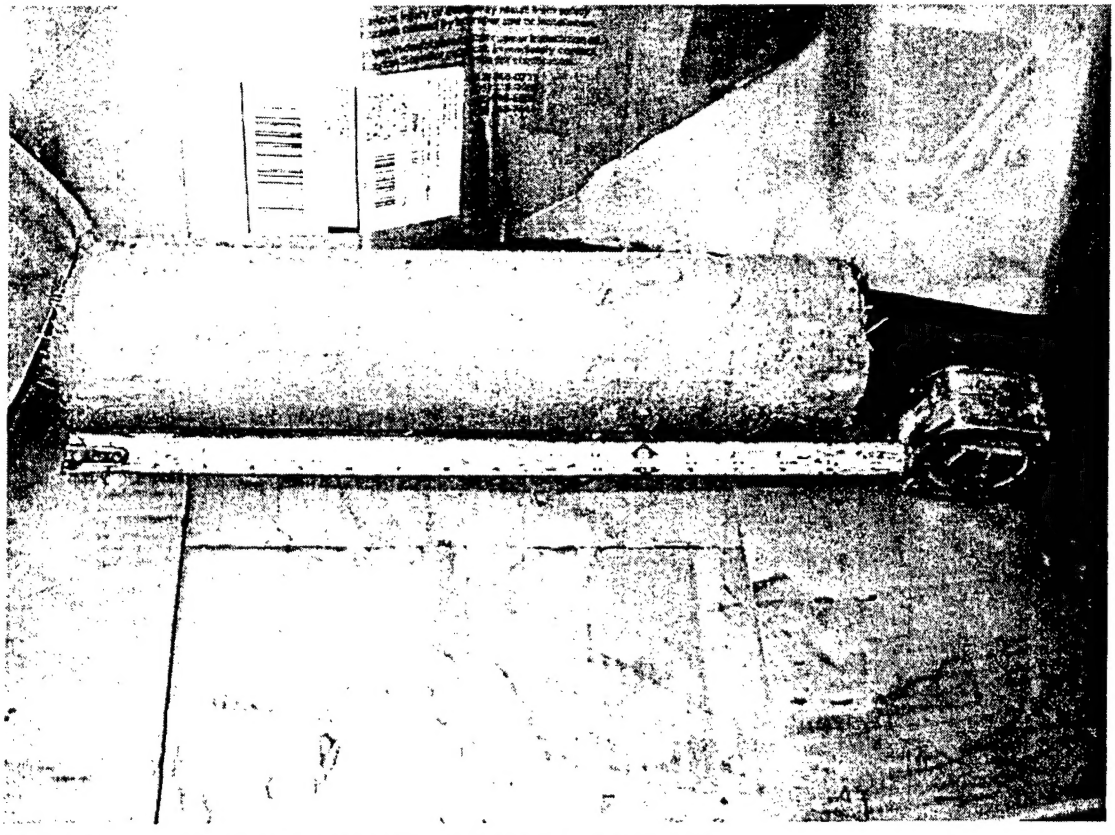

Figure D5. A core sample taken from the base of the dam model.

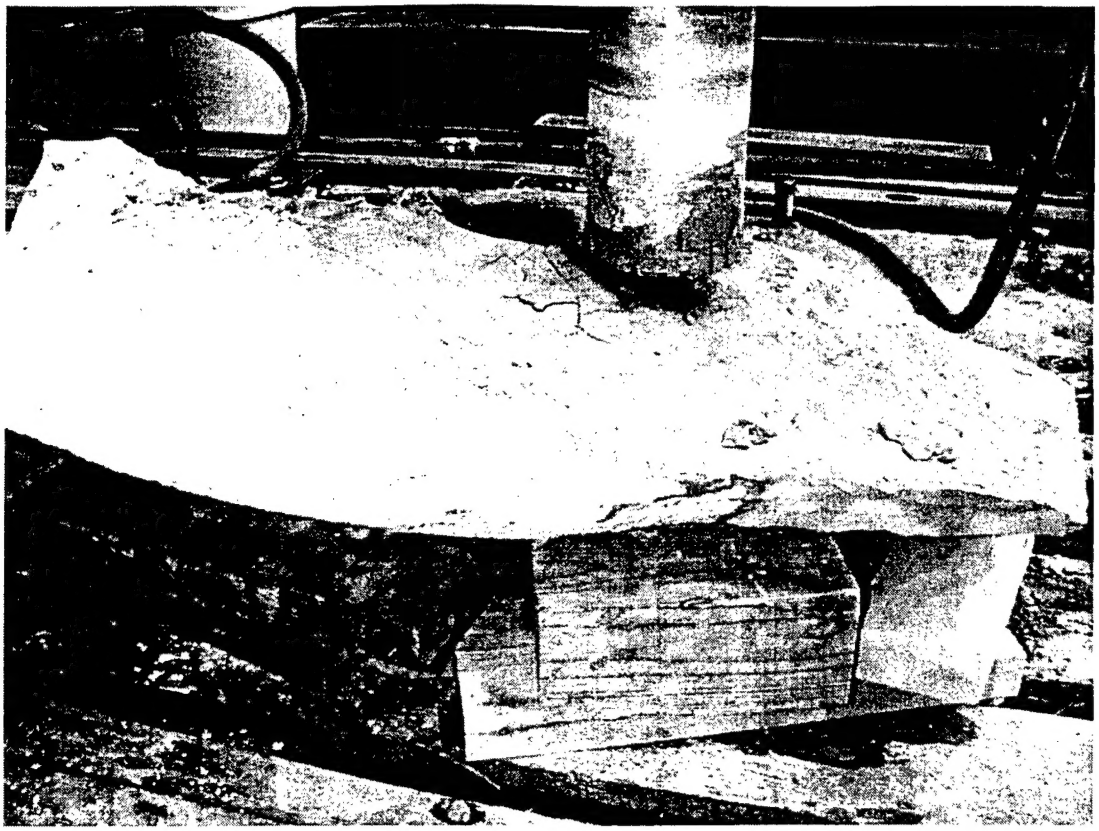

Figure D6. Drilling core samples from a section near the primary crack.

CERL Distribution

Chief of Engineers
ATTN: CEHEC-IM-LH (2)
ATTN: CEERD-SS-A

Engineer Research and Development Center (Libraries)
ATTN: ERDC, Vicksburg, MS
ATTN: Cold Regions Research, Hanover, NH
ATTN: Topographic Engineering Center, Alexandria, VA

Defense Tech Info Center 22304
ATTN: DTIC-O

7
3/01

REPORT DOCUMENTATION PAGE

Form Approved
OMB No. 0704-0188

1. REPORT DATE (DD-MM-YYYY)	2. REPORT TYPE	3. DATES COVERED (From - To)
11-2001	Final	

4. TITLE AND SUBTITLE
Seismic Testing of a 1/20 Scale Model of the Koyna Dam

5a. CONTRACT NUMBER

5b. GRANT NUMBER

5c. PROGRAM ELEMENT NUMBER

6. AUTHOR(S)
James Wilcoski, Robert Hall, James Gambill, Enrique Matheu, and Mostafiz Chowdhury

5d. PROJECT NUMBER
MIPR

5e. TASK NUMBER

5f. WORK UNIT NUMBER
33013

7. PERFORMING ORGANIZATION NAME(S) AND ADDRESS(ES)
U.S. Army Construction Engineering Research Laboratory (CERL)
P.O. Box 9005
Champaign, IL 61826-9005

8. PERFORMING ORGANIZATION REPORT NUMBER
ERDC TR-01-17

9. SPONSORING / MONITORING AGENCY NAME(S) AND ADDRESS(ES)
U.S. Army Corps of Engineers
441 G Street NW
Washington, DC 20314-1000

10. SPONSOR/MONITOR'S ACRONYM(S)
CECW-EW

11. SPONSOR/MONITOR'S REPORT NUMBER(S)

12. DISTRIBUTION / AVAILABILITY STATEMENT
Approved for public release; distribution is unlimited.

13. SUPPLEMENTARY NOTES
Copies are available from the National Technical Information Service, 5285 Port Royal Road, Springfield, VA 22161.

14. ABSTRACT

In 1967, the Koyna mass concrete dam in India was seriously damaged by a magnitude 6.5 earthquake. The event is unique because the Koyna Dam is the only concrete dam to be significantly damaged due to ground shaking, and accelerometers at the site recorded time histories of the entire occurrence. The event provides researchers a classic problem for experimental studies and validating numerical procedures used to predict the seismic response of concrete gravity dams.

This report comprehensively documents the construction and seismic testing of a 1/20-scale model of the Koyna dam, the largest scale model of the dam ever to be so tested. The model was tested to failure using sinusoidal motions, and the results can be effectively compared with analytical models as long as the effects of base rotations and material property variations are properly accounted for.

The results of the sinusoidal wave test program are available for incorporation into possible future tests using scaled records from the 1967 earthquake. Additional formwork strengthening and stiffening is recommended for models used in any future testing conducted with a 1/20 scale model. Specific recommendations are offered to improve formwork integrity, model quality, and protection of test equipment and instrumentation.

15. SUBJECT TERMS

concrete gravity dams	earthquake testing	modeling
materials testing	Koyna Dam	seismic testing

16. SECURITY CLASSIFICATION OF:			17. LIMITATION OF ABSTRACT	18. NUMBER OF PAGES	19a. NAME OF RESPONSIBLE PERSON
a. REPORT	b. ABSTRACT	c. THIS PAGE			Jim Wilcoski
Unclassified	Unclassified	Unclassified	SAR	137	19b. TELEPHONE NUMBER (include area code) 217-352-6511